Studies on Enhancement of Stability, Rheology, and Mechanical Performance of 3D Printable Foam Concrete

A Thesis Submitted

in Partial Fulfilment of the Requirements

for the Degree of

Doctor of Philosophy

by

Boddepalli Uday

Department of Civil Engineering

Indian Institute of Technology Guwahati

Guwahati-781039, India

August, 2024

भारतीय प्रौद्योगिकी संस्थान गुवाहाटी
Indian Institute of Technology Guwahati

Dedicated

To My

Parents, Wife, Son, and

Well Wishers

भारतीय प्रौद्योगिकी संस्थान गुवाहाटी
Indian Institute of Technology Guwahati

Indian Institute of Technology Guwahati

Department of Civil Engineering

Statement

I, hereby declare that the content embodied in this thesis entitled ***"Studies on Enhancement of Stability, Rheology, and Mechanical Performance of 3D Printable Foam Concrete"*** is the result of investigations carried out by myself at the Department of Civil Engineering, Indian Institute of Technology Guwahati, Guwahati, India.

In keeping with the general practice of reporting scientific observations, due acknowledgements have been made wherever the work described is based on the findings of other investigators.

Date:

Place: IIT Guwahati

Boddepalli Uday

भारतीय प्रौद्योगिकी संस्थान गुवाहाटी
Indian Institute of Technology Guwahati

Certificate

This is to certify that the thesis entitled ***"Studies on Enhancement of Stability, Rheology and Mechanical Performance of 3D Printable Foam Concrete"*** by Boddepalli Uday (Roll No: 196104104), to the Indian Institute of Technology Guwahati, India, for the award of Doctor of Philosophy, is a record of bonafide research work carried out by his under our guidance and supervision. The work embodied in this thesis has not been submitted for any other degree or diploma. In our opinion, the thesis is up to the standard of fulfilling the requirements of the doctoral degree as prescribed by the regulations of this Institute.

Date:

Place: IIT Guwahati

Dr. G. Indu Siva Ranjani

Assistant Professor

Department of Civil Engineering

Indian Institute of Technology Guwahati

Guwahati-781039, Assam, India

Dr. Biranchi Panda

Assistant Professor

Department of Mechanical Engineering

Indian Institute of Technology Guwahati

Guwahati-781039, Assam, India

भारतीय प्रौद्योगिकी संस्थान गुवाहाटी
Indian Institute of Technology Guwahati

Acknowledgements

This thesis is the culmination of the collaborative efforts of numerous individuals who have supported me, both directly and indirectly, throughout my extensive PhD journey. Over the course of this challenging endeavour, I have acquired valuable lessons in perseverance. Without the guidance, encouragement, and contributions of these individuals, completing this thesis would not have been possible. I am deeply grateful to all those who assisted me during my research, and it is with great privilege that I acknowledge their invaluable support.

I express my sincerest gratitude and respect to my thesis advisors, Dr. Indu Siva Ranjani Gandhi and Dr. Biranchi Panda, for their unwavering belief in my abilities. Their guidance, continual assistance, insightful feedback, and invaluable suggestions have been instrumental in my academic journey. I am particularly thankful to Dr. Indu Siva Ranjani Gandhi for her dedicated support, unwavering encouragement, and uplifting presence during challenging times throughout my PhD Her pursuit of excellence has left an indelible mark on me, which I believe will resonate in my future endeavours. Working alongside her has been an enriching experience, and I am grateful for her role in shaping and guiding my research from its inception. I also express my deep appreciation for the contributions of Dr. Biranchi Panda, whose dedication, expertise, and willingness to share his knowledge have greatly enhanced my PhD experience. His wealth of experience in the field of 3D printing, coupled with his generous investment of time and ideas, has played a pivotal role in the success of my research endeavours.

I extend my heartfelt gratitude to the members of my Doctoral Committee: Prof. Ajay Kalamdhad, Prof. G. Pugazhenthi, and Dr. Abhishek Kumar. Their insightful suggestions, encouragement, and timely assistance were invaluable throughout the various stages of my research work.

I extend my gratitude to the head of the Civil Engineering Department (former and present), faculty in-charge of Infrastructure Engineering and Management laboratory and Structural laboratory (former and present), faculty in-charge of Sustainable Resources for Additive Manufacturing (SReAM) laboratory, and staff members viz. scientific officer Dr. Arun Ch. Borsaikia, technical superintendent Mr. Pranab Hazarika, Junior technician Mr. Saurabh Kr. Mudoi and Mr. Mitu Ali for helping me in extensive physical work for providing uninterrupted

help accomplishing the PhD work. I also would like to would like to acknowledge the support provided by Central Instruments Facility (CIF), Department of Civil Engineering, and Department of Mechanical Engineering, IIT Guwahati.

My heartfelt thanks go to my labmates, colleagues, and seniors, including Dr. Smrati Jain, Dr. Selija Khwairakpam, Dr. Arya Anuj Jee, Dr. Jyotish Kumar Das, Dr. Jnyanendra Kumar Prusty, Mr. Sathishraj Mani, Mr. Leela Sai Rangarao Maradani, Mr. Chandrashekhar Wagh, Mr. Abhishek Kamisetty, Ms. Nicola Thounaojan, Mr. Srinivas Dodda, Mr. Dhruthiman Dey, Ms. Syed Bustan Fatima Warsi, Mr. Rahul Das, Mr. Amit Sahu, Ms. Nafisa Nazneen Choudhury, Mr. Rahul, Ms. Reena Bisht, Mr. Simranjeet Singh Batra, Mr. Akhil Charak, Mr. Divyesh Sharma, Mr. Rhijul Sood, Ms. Nandini Sharma, Ms. Adyasha Priyadarshini and Mr. Siddartha Khashyap. Their stimulating discussions and collaborative efforts, even during late-night sessions before deadlines, greatly enriched my research experience.

A special expression of gratitude is reserved for my friends Mr. Innamuri Jaya Satya Sandeep and Mr. M. Leela Sai Rangarao for their invaluable guidance and feedback on my research throughout my PhD journey.

I am deeply grateful to all my friends at IIT Guwahati who have made my time here truly memorable, especially Mr. Venkata Naga Chandra Guntakala, Mr. Tholeti Venkata Satya Aditya, Mr. Sreekanth Yadav, Dr. Rohit Sangineni, Mr. Satish Cilaveni, Mr. Anil Kumar Mekala, Mr. Pilli Rajashekar Reddy, Mr. Ravi Kiran Dokala, Dr. Krishna Chaitanya Maturi, and Mr. Bhaskar.

Finally, and of utmost importance, I wish to express my deepest gratitude to my parents, wife, sister, and other family members for their unwavering love and encouragement. I owe everything to them. Their constant moral support, encouragement, and motivation have been instrumental in helping me achieve my goals.

Boddepalli Uday

Abstract

Multifunctional properties are a requirement due to the increasing need for the thermal resistance, acoustic insulation, fire resistance, and etc. for the modern construction. Nevertheless, the material must be both mechanically sound and porous in order to fulfil these requirements. One such concrete that satisfies the demands of modern building is foam concrete (FC). FC is a cellular concrete produced using binder, fine aggregate or filler, foam and water as ingredients. Proper control in dosage of foam can result in wide range of densities ranging from 300 to 1800 kg/m^3. FC is a unique, non-structural and low-cost light weight concrete with special properties such as low density, high acoustic insulation, low thermal conductivity, high energy absorption capacity, good fire resistance, and good freeze and thaw resistance. The aforementioned properties of FC are mainly dependent on the microstructure of FC which is influenced by the foam production parameters (air pressure, type of foam generator), foam stability (drainage, density, size, shape, and etc.) and surfactant characteristics (type of surfactant, viscosity, surface tension, and etc.). FC has an extensive spectrum of demands to satisfy an array of applications.

Adopting the new-era construction methods for FC structures accelerates the construction simultaneously lowering costs and labour demands. Extrusion-based 3D printing is the most popular approach for additive manufacturing despite the fact that there are other methods as well. 3D concrete printing (3DCP) is a technology that can build the structure layer by layer by extruding through the nozzle. Further, to design the 3D printable foam concrete (3DP-FC) mixture, dimensional stability plays an important role. During and after printing, extrusion of highly flowable materials like FC presents numerous challenges. High flowability restricts the buildability whereas the more stiffness leads to collapsing of the foam bubbles. The stability of foam concrete mixes is highly dependent on the volume of the foam added to the mortar, stability of the lamella around air bubble and spacing between the air bubbles. These parameters may vary with type of foaming method (mixed or pre-foaming method), surfactant characteristics, rheology of the paste surrounding the bubble and pressure applied during the extrusion process. Hence, there is a need to address these issues from 3DCP perspective.

This research proposes to improve the stability and buildability of 3DP-FC through enhancing the surfactant characteristics, rheology of the air voids and paste content. A two-stage enhancement was carried out. First one is improving the stability of 3DP-FC by improving the surfactant

characteristics. Whilst the other is to improve the rheology via adopting various admixtures. In stage 1, the influence of surfactant characteristics on extrudability and stability of 3DP-FC is studied. Different studies on fresh state related, printability and air void characterization have been carried out for two different surfactants (natural and synthetic based) along with different foam stabilizers. Based on the experimental outcomes it can be suggested that the surfactant solution with viscosity above 5 mPa.s and surface tension less than 31 mN/m can result in stable 3DP-FC mixes. Further, the volume of foam in the mix is found to have significant impact on printability characteristics. Unlike traditional foam concrete, the variation in stabilizer concentration and density of concrete for the stable mixes studied, did not show much impact on the fresh state related characteristics (slump, slump flow and static yield stress) and air void microstructure. Furthermore, the structural build-up achieved is restricted to 15 and 10 layers for 1300 and 1000 kg/m^3 respectively. Therefore, to improve the structural build-up of 3DP-FC, rheology of the paste should be improved.

In stage 2, study was conducted to improve the buildability and mechanical properties of 3DP-FC through replacement of the sand with fly ash (FA) and addition of polyvinyl alcohol (PVA) fibers. The results shows that FA improved the buildability, however, reduced the stability of 3DP-FC. Fibers, on the other hand helped in improving the stability. Moreover, the addition of FA improved the compressive and flexural strengths of 3DP-FC, compressive being the dominant improved property. Interestingly, strength improvement beyond 28 days was found to show insignificant improvement. Microstructural studies were conducted to understand the limited pozzolanic reaction after 28 days and these results are in line with the obtained compressive and flexural results. This is due to the low water to solids ratio adopted for achieving the buildability causing the unavailability of calcium dissolute (pore water) to react with FA. Further, addition of PVA fibers reduced the thermal conductivity for all the mixes. But for mixes with FA replacing sand, thermal conductivity increased due to the bubble breakage. However, this was compensated by the addition of PVA fibers which resulted in reduction in the dry densities of 3DP-FC mixes. Nonetheless, density has significant impact on water absorption characteristics of 3DP-FC as observed from experimental results mixes. It is to be noted that increase in air content and the reduction in solid content in concrete mixes resulted in decreased inter-void thickness and closer proximity of air voids subsequently enhancing the likelihood of interconnection among entrained air voids. Addition of FA as a sand replacement reduced water absorption due to the bubble breakage. Additionally, fiber

addition to sand replaced mixes has reduced the water absorption due to the pore refinement in the matrix surrounding the fiber.

Key Words: 3D Printable Foam Concrete; Surfactant; Drainage; Fresh Density; Air Void; Image Analysis; Fly Ash; Fibers; Rheology; Static Yield Stress; Mechanical Properties; Dry Density; Viscosity; Buildability; Extrudability; Thermal Conductivity; Sorption; Water Absorption.

भारतीय प्रौद्योगिकी संस्थान गुवाहाटी
Indian Institute of Technology Guwahati

Table of Contents

List of Figures

भारतीय प्रौद्योगिकी संस्थान गुवाहाटी
Indian Institute of Technology Guwahati

List of Tables

Abbreviations/ Notations

3DCP	3D Concrete Printing
3DP-FC	3D Printing of Foam Concrete
C_3S	Tricalcium Silicate
C_2S	Dicalcium Silicate
C_3A	Tricalcium Aluminate
C_4AF	Tetra-calcium Aluminoferrite
C10	Irregular air void
C50	Median circularity
C-S-H	Calcium Silicate Hydrate
CMC	Carboxymethyl Cellulose
D50	Median air void
D90	Bigger size air void
EDS	Energy Dispersive X-ray spectroscopy
F	Foam
FA	Fly Ash
FC	Foam concrete
G	Gypsum
H	Hingot
HPMC	Hydroxypropyl Methyl Cellulose
i	Cumulative volume absorbed per unit area of inflow surface
IFD	Initial Foam Density
L	Larnite
LWC	Light weight concrete
M	Mullite
OPC	Ordinary Portland Cement
PCE	Polycarboxylate Ether
PVA	Polyvinyl alcohol
Q	Quartz
SF	Silica Fume
SiC	Silicate Carbide
SLS	Sodium Lauryl Sulfate

SP	Super Plasticizer
TGA	Thermogravimetry Analysis
VMA	Viscosity Modifying Agent
W/S ratio	Water to solids ratio
XG	Xanthan Gum
XRD	X-ray Diffraction

Chapter 1

Introduction

1.1 General

Now-a-days modern construction prefers the use of multifunctional materials because of its special attributes such as light weight, thermal insulation, acoustic insulation, fire resistance, freeze-thaw resistance, etc. in addition to its mechanical characteristics. Considering these special properties, the multifunctional materials finds its use commonly in panels and blocks for partition walls, false walls, suspended false ceilings, external environmental infills and light weight slabs (Falliano et al., 2019a). Foam concrete (FC) (a type of cellular concrete) could be considered as the material of right choice for the above-mentioned applications because of its unique attributes.

1.2 Cellular concrete

American concrete institute (ACI) in 523 defines cellular light weight concrete as "a mixture of cement, water and preformed foam". The need of foam is to provide air entrainment in the concrete to produce a porous solid (Chica and Alzate, 2019; Panesar, 2013). The classification of cellular concrete is shown in Figure 1.1.

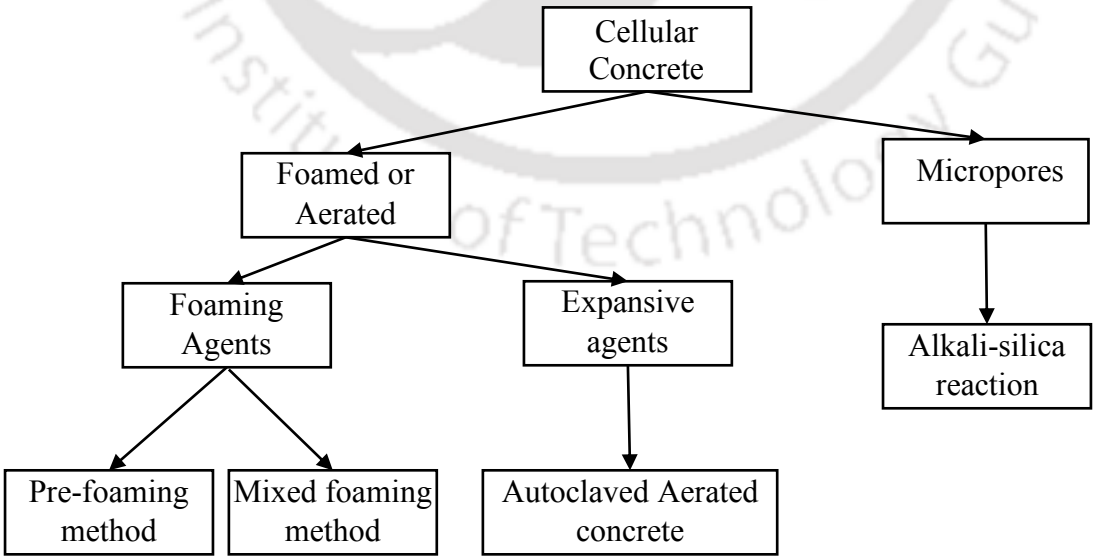

Figure 1.1: Classification of cellular concrete (Chica and Alzate, 2019)

The foam generated could be through expansive agents like aluminum powder or through entraining the air bubbles using the foaming agents (could be natural or artificial foaming agents). The advantage of foam generated using foaming agents over expansive agents is its flexibility of using for both onsite and precast productions.

1.3 Foam concrete

Foam concrete is a cellular concrete produced using binder, fine aggregate or filler, foam and water as ingredients. Proper control in dosage of foam can result in wide range of densities ranging from 300 to 1800 kg/m^3 (Ramamurthy et al., 2009). FC is a unique, non-structural and low-cost filler material with special properties such as low density, low thermal conductivity, high acoustic insulation, good fire resistance, good freeze and thaw resistance and high energy absorption capacity (Gandhi et al., 2023; Singh Batra et al., 2023; Wagh et al., 2021). The aforementioned properties of FC are mainly dependent on the microstructure of FC which is influenced by the foam production parameters (air pressure, type of foam generator), foam stability (drainage, density, size, and shape) and surfactant characteristics (type of surfactant, viscosity, and surface tension) (Sahu and Gandhi, 2021; Selija and Gandhi, 2022). Although these properties are attainable with other cellular concretes, FC has the advantage of being suitable for both cast in-situ and pre-cast industries, with low capital requirement. However, in precast industry, assembling the formwork in desired shape is a labour intensive work and difficult to mould the formwork if the design is complex. Moreover, cost of formwork is around 30 to 50% of the total cost of construction. To overcome these limitations, an advanced construction technique like 3D printing can be adopted. An automated extrusion process like 3D printing could reduce material wastage, increase the productivity, eliminate the need for formwork, optimize the cost of elements like labor, material, design and planning costs in comparison to conventional construction methods (Panda and Tan, 2018; P. Wu et al., 2016). For instance, due to the heat-insulating properties of the FC, the complete work step needed for the assembly of the external or internal insulation for printed wall elements can be omitted. This simplification of the manufacturing process may considerably reduce construction costs. In particular, shortening the construction time results in reduced costs of, for example, facade scaffolding, construction management and the rent-time for the construction site equipment. Additionally, 3D concrete printing can be applied to other areas such as bullet traps, acoustic panels, and sacrificial facades for blast mitigation, due to their structural complexity and cost and time efficiencies.

1.4 3D concrete printing

Recent developments in the construction industry are paving the way for low-cost, and sustainable production (Chen et al., 2022). 3D printing is one such advancement in this industry that has been adapted from other fast-growing fields such as aerospace, medicine, and automobiles (Al Rashid et al., 2020; Y. W. Tay et al., 2016; Y. W. D. Tay et al., 2017). It's worth noting that 3D printing in construction mainly includes particle bed printing (Lowke et al., 2018), and extrusion-based concrete printing (Buswell et al., 2018; Dey et al., 2023; Menna et al., 2020). Similar to other extrusion-based process, in 3D concrete printing (3DCP), fresh material is extruded through nozzle in layer by layer manner until the part is completed (du Plessis et al., 2021; Gosselin et al., 2016; Panda and Tran, 2022). The main challenge involved in this technique is to develop the material that can be simultaneously extruded and built in layers without any failure (Kristombu Baduge et al., 2021; Panda et al., 2018; Wangler et al., 2019). In this regard, rheology of material plays a key role, which can be commonly analyzed though assessment of characteristics such as pumpability, extrudability and buildability (Hou et al., 2021; Khan, 2020; Mohan et al., 2021). Figure 1.2 is a typical schematic sketch illustrating 3DCP process flow. Stage 1 depicts a large-scale conveying pump pumping fresh material to an extruder through a long hose. The material is extruded by a screw extruder in Stage 2, which is subsequently built in layers.

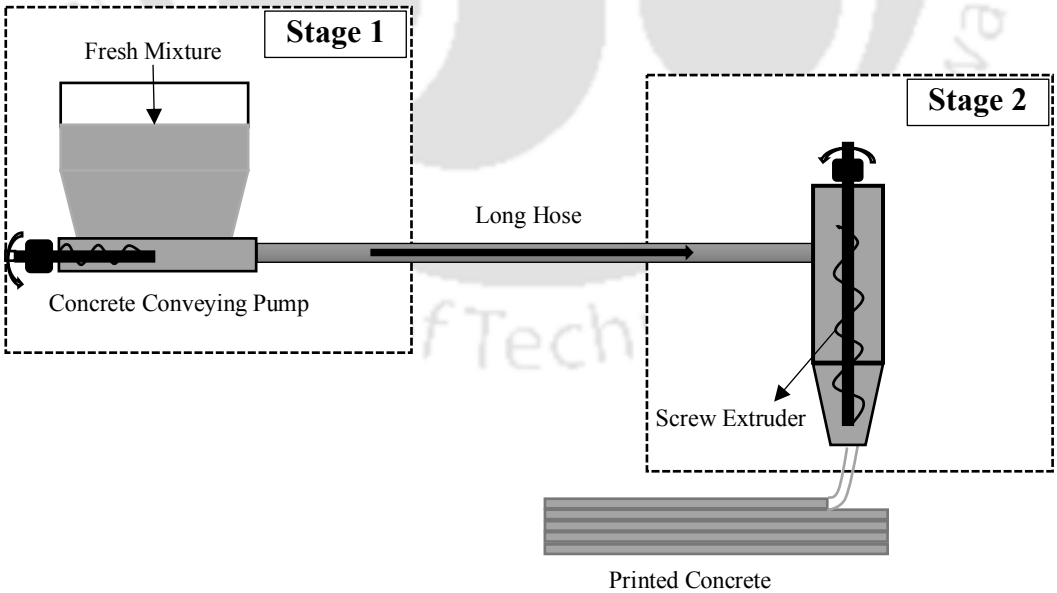

Figure 1.2: Schematic diagram of 3D concrete printing system (Chen, et al., 2020a).

According to Mechtcherine et al., (2020), there are two asymptotic regimes of material deposition by extrusion. One is infinite brick regime (i.e. extrusion of stiff materials) and other is extrusion of flowable material with or without the addition of admixtures. The realistic behaviour of the printable material lies between these regimes. The mix design helps to achieve the desired rheological parameters of printable material depending on the type of cementitious material. As shown in Figure 1.3, a successful printing process needs several iterative materials mix design steps.

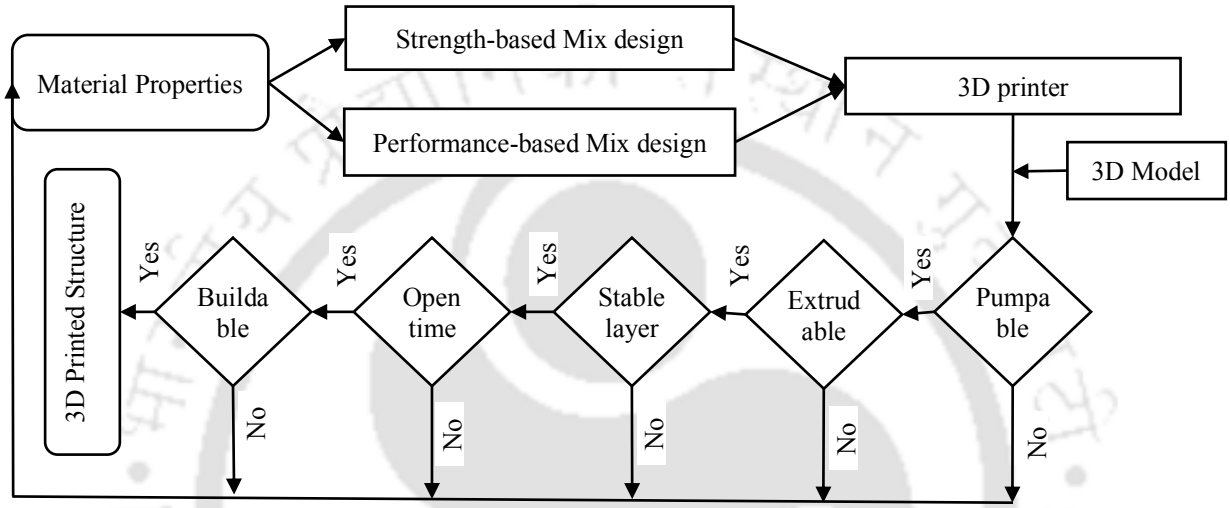

Figure 1.3: Various steps involved in material mix design for successful mortar printing.

1.5 3D printing of foam concrete

Adopting these new-era construction methods for FC structures, accelerates the construction simultaneously improving mechanical and functional characteristics (Falliano et al., 2020). While designing the 3D printable foam concrete (3DP-FC) dimensional stability plays an important role (Boddepalli et al., 2023). When classical FC mixes (i.e. mixture of cement, sand, water and foam) are adopted for 3D concrete printing, due to low yield stress dimensional stability is not achieved (Falliano et al., 2019b; Falliano et al., 2020). However, with modified mixes, Falliano et al., (2020), also observed that the 3DP-FC shows a more homogeneous distribution of air bubbles with smaller dimensions when compared to the classical FC due to the increased consistency as shown in Figure 1.4. Recently many researchers are adopting this 3DP-FC as an environmentally sustainable solution for both structural and non-structural applications (Cho et al., 2021; Falliano et al., 2020; Markin et al., 2019). Markin et.al., (2021), using laboratory tests concluded that 3DP-FC is economical in terms of both construction times and costs. Even though, due to usage of high amount of cement content in FC, it is not

considered as a good sign from ecological point of view but the additive manufacturing proved to be sustainable by reducing the carbon emissions and resource demands, lowering energy usage, lesser waste generation, and good recyclability (Ford and Despeisse, 2016; Markin et al., 2021; De Schutter et al., 2018). Environmental impact of 3D printed structures has to be seen in complex structures where, structural optimization and hybrid functional design strategies are used (i.e. production of structures with higher complexity with minimal environmental costs) (De Schutter et al., 2018).

(a)

(b)

Figure 1.4: Pore distribution of (a) classical FC and (b) printable FC (both having a density of 1000 kg/m^3)

1.6 Organization of report

This thesis is further organized in six chapters followed by bibliographical references. For the clarity of report, each chapter is subdivided into sections and sub sections as per the requirement. A brief overview of chapters are as follows:

- ***Chapter 2*** provides the literature review conducted through various research journals, conference papers, books and standards. This section is further divided into three sections –

  First section reviews literature on materials required for FC, preparation methods, and properties of FC (fresh, mechanical and thermal).

  Second section reviews literature on 3DCP – rheology, printability, and influence of mix design and chemical admixtures on rheology of 3DCP.

  Third section discusses a detailed study on stability, rheology, mechanical properties of 3DP-FC.

  Fourth section summarizes and highlights the research gaps identified through the literature review. Further it also sheds a light on the motivation and need for the current study.
- ***Chapter 3*** illustrates the research objectives and scope of the work to be carried out. Later, methodology to perform the proposed study is discussed.
- ***Chapter 4*** depicts the studies conducted to analyze the influence of surfactant characteristics on stability and printability of 3DP-FC. Further, influence of surfactant properties on fresh state and air void characteristics of 3DP-FC is evaluated.
- ***Chapter 5*** gives a detailed study conducted on the synergistic influence of fly ash and polyvinyl alcohol fibers on stability, rheology, and mechanical properties of 3DP-FC. Further, the effect of these materials on thermal performance, sorption characteristics are evaluated. Nonetheless, microstructural studies are conducted to validate the mechanical performance of 3DP-FC.
- ***Chapter 6*** provides the conclusions drawn for the studies and brief insight into the future research.

Chapter 2

Literature Review

2.1 General

Chapter 1 briefs the introduction to cellular concrete, highlighting the FC. There are different classifications of cellular concrete based on the type of agents used for making the porous concrete. However, the advantage of using foaming agents over gassing agents is its flexibility of using both on site and precast production. Further, first chapter introduces 3DCP, its advantages and applications. It is a process of extruding the concrete through the nozzle in layers until the product is built of required size and shape. It also sheds a light on the importance of rheology in 3DCP. Additionally, the advantages, environmental impact and challenges associated with adoption of FC to 3DCP was discussed. This chapter attempts to review the literature available on FC and 3DCP predominantly focusing on the problems associated with 3DP-FC in terms of rheology and mechanical performance.

2.2 Review on foam concrete

2.2.1 Constituents of FC

2.2.1.1 Binder

Cement is the most significant binder used in FC. In order to reduce the consumption of energy and ecological impact, researchers have considered the use of various sustainable cements (including calcium sulphoaluminate cement, calcium aluminate cement, and alkali activated materials) and supplementary cementitious materials (SCMs) (silica fume, fly ash, ground granulated blast furnace slag, and etc.) as alternative binders (Kamisetty et al., 2023). However, certain cements and mineral admixtures help in rapid setting or hardening, while the other retard the hydration process. For example, fly ash replaced with cement delays the setting process, but use of calcium sulphoaluminate cement as a full or partial binder replacement causes rapid hardening (Cho et al., 2022). These SCMs also help in reducing the shrinkage of FC at early ages which is very high when compared to normal concrete (Ge et al., 2020; Nambiar and Ramamurthy, 2009).

2.2.1.2 Aggregate or filler

Fillers are used in FC to the increase the volume and consequently reduce the demand for binder content. Furthermore, when compared to FC manufactured with pure binders, these filler ingredients aid to reduce shrinkage (Nambiar and Ramamurthy, 2009). Most fillers adopted in FC are finer than 600 microns to ensure the stability of foam. Fillers of maximum size more than the specified has negative influence on fresh density, compressive, flexural and durability properties (Lim et al., 2015). Various industrial wastes like recycled glass, rice husk ash, fly ash, quarry finer, lytag fines, and etc. are used as alternative materials. Few of these materials are proved to work better than the river sand (Nambiar and Ramamurthy, 2006a). Further, the energy required to reduce the size of river sand is high. As a result, the use of industrial waste as a filler material in FC was demonstrated to be both economically and environmentally sustainable.

2.2.1.3 Surfactants

Surfactants (or foaming agents) has a vital role in foam generation and stabilization through reduction of surface tension of water. Commonly surfactants are classified into two types based on their origin: natural and synthetic. Further, synthetic surfactants can be subdivided into ionic (anionic and cationic) and non-ionic surfactants (Khwairakpam and Gandhi, 2020). The efficacy of the surfactants used in the foam formation varies substantially because they come from a range of sources. As a result, surfactant selection and foam properties are likely to have a considerable impact on FC microstructure (Khwairakpam et al., 2023; Sahu et al., 2021; Sahu and Gandhi, 2019).

Natural surfactants are plant based products or animal protein sources. These are surface active due to the presence of saponin (in plant based sources) and protein (in animal based sources). For instance, Balanites aegyptiaca, commonly known as hingot, is found worldwide, from tropical Africa to Myanmar. Hingot contains a variety of bioactive compounds, including saponins, alkaloids, flavonoids, and glycosides. Molecular formula is $C_{27}H_{42}O_3$ and molecular weight is 414.62 g/mol. This molecular weight varies depending on the specific lipid structure. Phytochemical studies of various parts of the plant reveal that the fruit, seeds, and bark contain 22-27% saponin. Saponins, which consist of a nonpolar sapogenin and a water-soluble side chain, produce foam similarly to synthetic surfactants with both lipophilic and hydrophilic molecular components. Additionally, the plant's adaptability, high yield, and abundant

availability make it a promising candidate for study, offering both economic and environmental benefits (Khwairakpam et al., 2023). However, there few limitations such as variability in raw material and limited storage life. To overcome these limitations of natural surfactants, synthetic foaming agents are used that can easily dissolve and produce air bubbles (Sahu et al., 2018).

Synthetic surfactant consists of a hydrophobic long chain hydrocarbon group and the hydrophilic head which can be ionic or non-ionic. Ionic surfactants are contribute to foam formation and stabilization because of the electrical double layer present at interface which interact with opposing interface to form disjoining pressure and thus results in more stable foam. Cationic surfactants (positively charged head group) are expensive and has lower solubility with higher surface active properties. Whereas, Anionic surfactants (such as sodium lauryl sulfate (SLS)) are negatively charged head group and are sparingly soluble with optimum surface active properties (depending on the chain length) (Sahu et al., 2018). SLS is composed of a 12-carbon (dodecyl) hydrocarbon chain attached to a sulfate group. The chemical formula is $C_{12}H_{25}OSO_3Na$. It has a polar sulfate head group and a nonpolar hydrocarbon tail, making it amphiphilic. The molecular weight of SLS is approximately 288.38 g/mol. As an anionic surfactant, SLS carries a negative charge, which contributes to its ability to emulsify oils and remove dirt by reducing surface and interfacial tension.

Foam is produced by forcing the compressed air into surfactant solution to expand. It is an assortment of air bubbles divided by a thin liquid film (lamellae) that is generated by the juxtaposition of bubbles, resulting in air dispersed in surfactant solution. The critical lamellae thickness required to sustain the pressure in air bubbles is 5-15 nm (Sahu et al., 2018). Foam properties like texture (size and shape), density, stability and expansion ratio have significant impact on the quality of foam. Uniform texture with small spherical bubbles produces the FC of closed cellular structure. The foam produced in a pre-foaming method could be a wet foam or dry foam. If the foaming agent is sprayed over a fine mesh, it produces wet foam of 2-5 mm size air bubbles and is very less stable compared to dry foam. Whereas dry foam is produced by entraining the pressurized air into the surfactant solution and making it to expand. It has a size of 1 mm and extremely stable.

Various researchers have incorporated different additives (stabilizers) like carboxymethyl cellulose (CMC) (Sahu et al., 2021), xanthan gum (Raj et al., 2023), sodium hydroxide, sodium carbonate, and sodium chloride (Siva et al., 2015) to enhance the viscosity of the foaming solution which resulted in improvement of foam density and subsequent in foam concrete

characteristics. Out of these, CMC and xanthan gum are widely used stabilizers. CMC and xanthan gum are versatile hydrocolloids widely used in various industries for their thickening, stabilizing, and emulsifying properties. CMC, derived from cellulose, is water-soluble and forms viscous solutions, whereas, Xanthan gum, produced by the fermentation of glucose or sucrose by the bacterium Xanthomonas campestris, also forms highly viscous solutions and is noted for its stability across a wide range of temperatures and pH levels. CMC solutions exhibit pseudoplastic (shear-thinning) behavior, where viscosity decreases with increasing shear rate. The carboxymethyl groups increase the hydrophilicity of CMC, enhancing its interaction with water molecules. Hydrogen bonding between carboxymethyl groups and hydroxyl groups within the polymer and with water molecules contributes to its solubility and gel-forming properties. The presence of salts can affect the viscosity and stability of CMC solutions. Divalent cations (e.g., $Ca^{2+,}$ $Mg^{2+)}$ can cause gelation or precipitation due to ionic cross-linking between carboxyl groups (Sahu et al., 2021). On the other hand, Xanthan gum is a high molecular weight polysaccharide widely used as rheology modifier due to its thickening and stabilizing properties. Xanthan gum is composed of a cellulose backbone (β-D-glucose units) with trisaccharide side chains attached to alternate glucose units. The side chain consists of mannose, glucuronic acid, and another mannose in the sequence of mannose-(1→4)-glucuronic acid-(1→2)-mannose. Xanthan gum is highly soluble in cold and hot water, forming viscous solutions even at low concentrations. Xanthan gum can form synergistic gels with other hydrocolloids like locust bean gum and guar gum, enhancing its thickening and gelling properties. It also stabilizes emulsions and suspensions by increasing the viscosity of the continuous phase and preventing the separation of dispersed particles (Wagh et al., 2024).

2.2.1.4 Chemical admixtures

Different admixtures are adopted in the FC production to reduce the water demand, shrinkage reduction, and viscosity enhancement. However, few compatibility issues were also reported due to the destabilization of air voids. For instance, when melamine and naphthalene-based superplasticizers (SPs) are considered along with air entraining agents, it was reported to result in the destabilization of air voids (Saucier et al., 1990). However, polycarboxylate ether-based SP showed better performance when compared with other SPs (Huang et al., 2019). Similarly, few accelerating admixtures and viscosity modifying admixtures used at higher dosages caused the increase in air content with coarser sizes, ultimately leading to destabilization of existing air void system. Although the use of viscosity modifying agents like hydroxy propyl methyl

cellulose at optimum dosages helps in stabilizing the air bubbles, but at higher dosages the destabilization occurred (Liu et al., 2021). Further, addition of viscosity modifying agents prevents segregation of air bubbles (Zhang et al., 2020). Hence it is essential to examine the compatibility of admixtures with air entraining agents.

2.2.1.5 Fibers

Fibers are used to improve the strength, ductility and impact resistance of FC. Few of the fibers used in FC are polypropylene, poly vinyl alcohol, glass, steel, polyolefin, and kenaf (Chica and Alzate, 2019). The addition of individual fibers was reported to improve the compressive and tensile strength of the FC due to the fiber bonding with paste matrix (Gandhi et al., 2023). Furthermore, hybrid fiber (combination of monotype fibers) addition was observed to perform better than the individual fiber addition (Raj et al., 2020). However, glass fiber addition has a negative effect on compressive strength due to the load transfer through the fibers resulting in fibre-cement debonding, instead of progressive and steady collapse. But the post peak behavior was observed to perform better unlike sustaining the peak load (Akthar and Evans, 2010).

2.2.2 Production methods of FC

FC is produced based on two different methods. One is pre-foaming method and other is mixed foaming method. Although the materials used in both the methods are same, the point of introduction has a significant impact on FC properties. Figure 2.1 shows the schematic representation of FC production methods. In case of pre-foaming method, the mortar is prepared initially and then freshly produced foam is added to the mortar to prepare FC mixture as shown in Figure 2.1(a). Conversely, in mixed foaming method, the surfactant is added along with the ingredients of mortar mixture (mixing using a tilting drum mixer for rapid mixing) to form FC as shown in Figure 2.1(b).

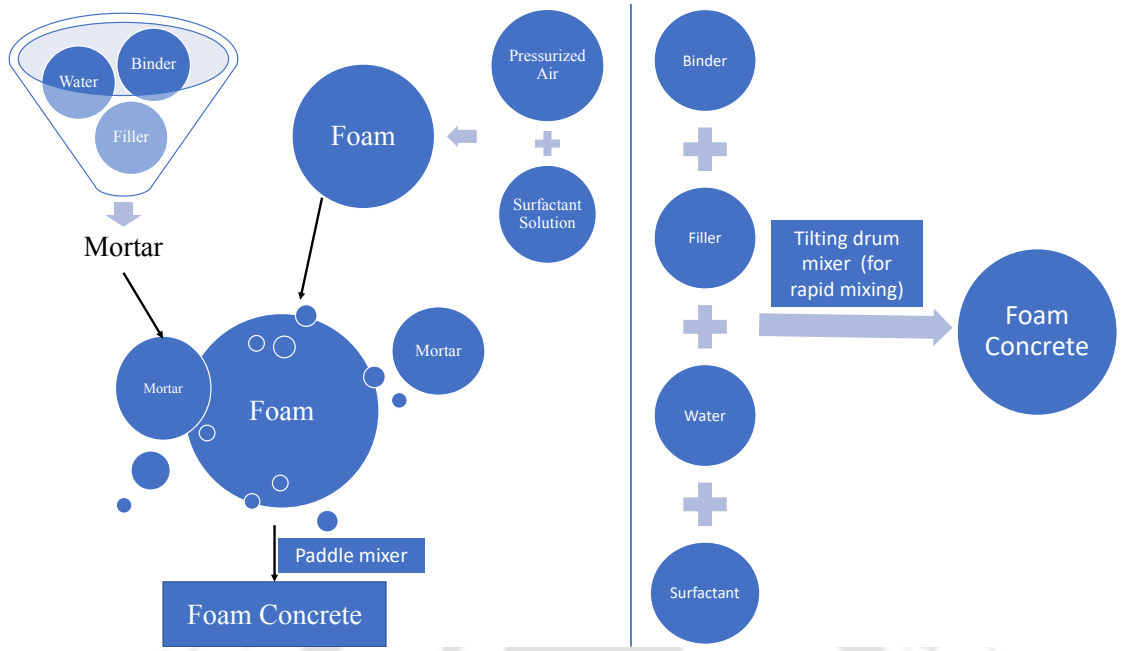

(a) (b)

Figure 2.1: Production methods of FC, (a) pre-foaming method, (b) mixed foaming method.

2.2.3 Properties of FC

2.2.3.1 Fresh state properties of FC

In the fresh state, FC exhibits a flowing and self-compacting behaviour, with consistency and stability being crucial parameters. These factors primarily rely on the water-to-cement ratio (w/c), supplementary materials, fine aggregate, and the volume and type of foam agents (Ranjani and Ramamurthy, 2010a; Ranjani and Ramamurthy, 2010b). Consistency is evaluated through standard flow cone and marsh cone tests, with an optimal spreadability range of 40% to 60% for acceptable performance (Amran et al., 2015; Nambiar and Ramamurthy, 2006a). Exceeding this range can lead to segregation during casting, affecting workability. Increased foam volume decreases consistency due to reduced self-weight and increased cohesion and stiffness. Stability, determined by the density ratio, hinges on the base mix's consistency and water-solids ratio, varying with filler type. Generally, with addition of foam to the mix, FC consistency decreases. Stability assessment involves comparing calculated and actual foam quantities and w/c ratios to achieve the desired density. Determining the water-solids ratio is crucial for ensuring both stability and consistency (Nambiar and Ramamurthy, 2008).

2.2.3.2 Mechanical and thermal properties of FC

The compressive strength of FC is influenced by various factors including the mix constituents like water-to-solids (w/s) ratio, type of ingredients (filler, binder, and surfactant), foam production parameters, foam volume, and curing method (Falliano et al., 2020). Air void quantity, which determines concrete density, is the primary factor affecting strength. Lower-density mixes are particularly affected by entrained air voids, impacting strength significantly (Falliano et al., 2022; Nambiar and Ramamurthy, 2007a). While the w/s ratio typically influences strength in conventional concrete, in FC, density plays a more significant role. Studies show that increasing the w/s ratio can notably enhance strength due to improved cement hydration (Ramamurthy et al., 2009). Additionally, factors such as foam stability, type of foaming agent, and incorporation of foam stabilizers and fillers like fine recycled glassy aggregates and fly ash influence strength (Nambiar and Ramamurthy, 2006a, 2006b; Ramamurthy et al., 2009). Research indicates a limited focus on the tensile properties of FC. FC typically exhibits lower splitting tensile strength compared to traditional concrete mixes. Mixes containing sand generally outperform those with fly ash due to improved shear strength between sand particles and the paste, as proposed by (Jones and Mccarthy, 2005; Kearsley and Wainwright, 2001). Incorporating fibers can enhance tensile and flexural strength, provided they do not disrupt the behaviour of freshly poured concrete or its self-compaction (Gencel et al., 2021).

Thermal properties of FC are primarily influenced by density and porosity. Earlier studies have shown that thermal resistance decreases with increasing density (Wagh et al., 2021). Porosity affects radiation heat transfer; high porosity enhances thermal resistance while decreasing porosity diminishes radiation influence (Wei et al., 2013). Moisture content amplifies conductivity, while temperature variations influence conductivity differently based on moisture evaporation and radiation in pores (Valore, 1954; Othuman and Wang, 2011). Curing conditions also affect conductivity; air-cured FC exhibits lower conductivity due to lower moisture content (Zhao et al., 2015; Ji et al., 2019). Aggregate/filler substitution alters thermal properties; incorporating lightweight aggregates or porous fillers enhances thermal resistivity (Kashani et al., 2017; Li et al., 2019; Salvini et al., 2012).

2.3 Review on 3DCP

3DCP is one of the digital construction techniques that demands the fulfilment of particular material properties. One of the most important requirements for 3DCP is the material's rheology. This section provides a comprehensive review of the rheology of Portland cement-based materials used in extrusion-based 3DCP.

2.3.1 Rheology of 3DCP

Printable cementitious materials are reported in various studies to behave as visco-plastic Bingham fluids. Below critical yield stress, these materials are found to exhibit elasto-plastic behaviour (Mechtcherine et al., 2020; Roussel, 2018; Weng et al., 2018). Being a Bingham material, printable mortar will start to flow if the induced shear stress is greater than the static yield stress or critical yield stress. Hence, the static yield stress is the force required to initiate the flow (Tay et al., 2019). The shear thinning behaviour brought on by the application of increased shear rate to initiate the flow may result in a reduction in the yield stress and viscosity of the mixture. To maintain flow with low pressure applied, the reduction in yield stress (dynamic yield stress) should be as small as possible (Kruger et al., 2019a). Typical picture illustrating the static and dynamic yield stresses for a thixotropic material under constant shear rate is shown in Figure 2.2(a). Shear stress versus strain rate of a cementitious material have a linear relationship while flowing and gradient of this curve is called as viscosity (η). The typical variation of shear stress with strain rate and thixotropic behavior of material under hysteresis loop is shown in Figure 2.2(b) (Zhang et al., 2019). Generally, changes in viscosity happen due to thixotropic behavior (time dependent shear thinning behaviour) of cementitious materials. During the dormant period (material remains in plastic state and little physical changes happen), apparent yield stress of cementitious materials increases continuously. However, this can be disturbed by a strong shearing or remixing and thereafter, the material can be brought back to the reference state (Roussel et al., 2012). Rheology of these materials is reported to depend not only on shear rate applied but also on age and the resting time (Paul et al., 2018; Roussel, 2018). In the following subsections, the requirements of these rheological parameters in achieving the pumpability, extrudability, and buildability of 3DCP are discussed.

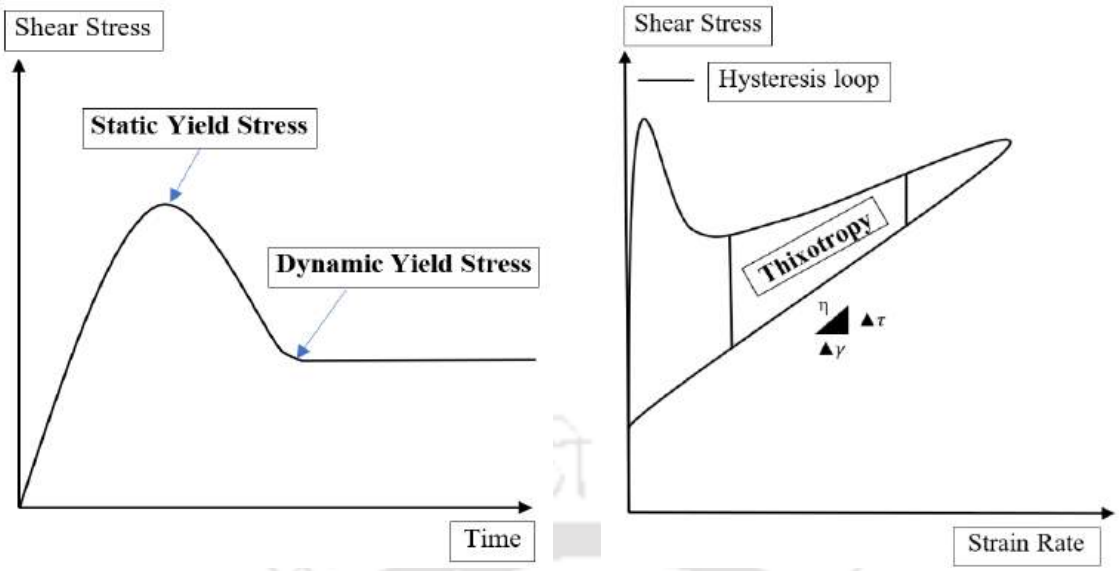

(a) (b)

Figure 2.2: (a) Static and dynamic yield stress of a thixotropic material under constant shear rate, (b) Typical variation of shear stress with strain rate and thixotropic behavior of material under hysteresis loop.

2.3.1.1 Pumpability

Pumpability refers to the printable mix's ability to transport under pressure to the print head (or extruder). It is usually performed with progressive cavity pumps or piston pumps, with the former being the most common for extrusion-based additive manufacturing. The application of pressure is the basic mechanism for pumping the material via a hose pipe. Due to this pressure, material is sheared in a decreasing order from the pipe's outer edge to the center (zero shear stress at the center in the case of plug flow), with the maximum shearing at the pipe's outside edge and the lowest shear stress at the center. The bulk material travels towards the center due to the shear stress gradient difference, leaving the paste at the outer edge (Nerella and Mechtcherine, 2018; Vallurupalli et al., 2021). Hence the stiff mixes (with less paste content) are harder to pump as it requires high pumping pressures. It could also lead to blockage in the pipe due to segregation of bulk material and paste. As a result, 3DCP requires mixes with moderate yield stress and low viscosity which can be pumped with optimum pumping pressures. There are different test methods using rheometers, viscometers, and etc defined in the literature to characterize pumpability required for 3DCP (Mohan et al., 2021; Nerella and Mechtcherine, 2018; Tay et al., 2019).

2.3.1.2 Extrudability

Extruding is the action of extrusion of fresh materials from the print head (Barbosa et al., 2022; Ducoulombier et al., 2020; Sanjayan et al., 2021). Extrusion of soft solids like cement-based materials is either done by ram extruder or screw type extruder (auger extruder) (Vallurupalli et al., 2021). There are different shapes of nozzles like circular, rectangular, square, and etc. in practice that are intended to produce different shapes as per the usage. The filament extruded through the nozzle should be smooth and continuous. Further, the extrudability of the 3DCP depends on the size and composition of mixture ingredients (Rahul et al., 2020; Rahul and Santhanam, 2020). Researchers have used ram extruder (Figueiredo et al., 2019; Chen et al., 2019), penetration resistance (Pott and Stephan, 2021), squeeze test method (Toutou et al., 2005), and desorptivity test (Rahul et al., 2020) to study the extrudability of 3DCP. However, the test method that mimics the exact 3DCP process could help in eliminating the geometry induced artifacts. For example, Nerella et al., (2019) characterized the extrudability by measuring both the energy (electric power) consumed and flow rate while extruding a particular mixture. Similarly, Ducoulombier et al., (2021) used the technique of measuring the yield stress of the material at the nozzle exit using the slug test. In this test, the mass of the slugs (formed due to yield stress) are measured using the simple balance. Then the average mass of the slugs collected are incorporated in the Eq. 2.1 derived from the dimensionless relation to calculate the yield stress. Where, τ_c is the yield stress, S is area of nozzle section, g is the acceleration due to gravity, m_s is the mass of the slug = $\rho S L_s$, and L_s is the length of the slug.

$$\tau_c = \frac{g}{\sqrt{3}S} m_s \tag{2.1}$$

2.3.1.3 Buildability

The ability of the printable mixture to be sequentially stacked up to a certain height without suffering major deformation or layer collapse is known as buildability (Jeong et al., 2019; Wu et al., 2021; Zhang et al., 2018). After the deposition of the material layer by layer on the print bed, the material should retain its shape either due to the physical changes (due to thixotropic recovery) or chemical changes (due to hydration) (Kruger et al., 2020). The height up to which the material is built in layers is called structural build-up. The early age behaviour of 3DCP plays a key role in the structural build-up of a printed structure (Nerella et al., 2019; Reiter, 2019; Suiker et al., 2020). However, the structural build-up should not affect the open time of the printable mixture. Open time refers to the amount of time available to print the material

without any breakages (Natanzi and McNally, 2020). Buildability of 3DCP is characterized by different tests in the literature. The most common test method for evaluating the buildability is printing the maximum number of layers before failure. Other test methods like penetration resistance (Pott and Stephan, 2021), green strength test (Chen et al., 2020a; Jayathilakage et al., 2020; Pham et al., 2022), plate stacking test (Perrot et al., 2016), calorimetry tests (Bhattacherjee and Santhanam, 2022; Rubin et al., 2021), and etc. are in practice.

Apart from these, wolfs et al. (Wolfs et al., 2018) proposed a model based on Mohr-Coulomb failure theory using finite elemental modelling. This model is proposed to study the early age behaviour of 3DCP (0 to 90 minutes). To obtain the material properties, they used direct shear test and unconfined uniaxial compression test. Although this model analyses the structural behaviour qualitatively, but quantitatively overestimates the stability and strength parameters due to the overestimated material properties (mainly due to compaction) and other induced imperfections in the material properties during the printing process. To avoid the overestimation of material properties, Jayathilakage et al., 2020 used printed samples of 100 mm length, 10 mm thickness and 30 mm width instead of cylindrical specimens. The specimen size is valid as per ASTM D2166/D2166M standards. In the same line, Wolfs et al., 2019 used triaxial compression test to eliminate the variations caused from his previous study.

2.3.2 Relation between rheology and printability

The discussions above make it clear that there are some requirements for fresh state characterization of 3DCP that frequently conflict with one another. Pumpability, extrudability, and buildability are the sequential order of the fresh state qualities that need to be substantially addressed right from the mixer through the deposition of material for printing. Further, it is to be noted that the rheological parameters such as dynamic yield stress, static yield stress, and thixotropy are related intently to pumpability and extrudability. Firstly, to initiate the flow, the material must initially overcome the static yield stress. Further during the flow, dynamic yield stress should be maintained as low as possible to prevent flow disruptions. Later, the material filament should smoothly extrude without breaking at any point of time during the process, while maintaining its shape (due to thixotropy). On a similar note, thixotropic behaviour and static yield stress are related to buildability. Following layer deposition, the material should be able to support its own weight and the weight of succeeding layers owing to chemical hydration and the growth of static yield stress (Ivanova and Mechtcherine, 2020; Jiao et al., 2021; Pham et al., 2020). There are also studies that were reported in the literature that link printability and

rheological properties (Alghamdi et al., 2019; Alghamdi and Neithalath, 2019; Zhang et al., 2018). For instance, Alghamdi and Neithalath, (2019) and Alghamdi et al., (2019) correlated the printability of alkali activated fly ash-based binders (AAF) and OPC based binders to the yield stress and slump value (which can be linked to yield stress) as shown in Figure 2.3(a). Similarly, Kruger et al., (2019b) characterized buildability (growth of static yield stress with time) of the cementitious material based on two parameters such as re-flocculation rate (R_{thix}) and structuration rate (A_{thix}) as shown in Figure 2.3(b). Generally, when the flocculated material (formed due to van der Waals attraction forces) is extruded through the nozzle, the de-flocculation occurs due to breakage in the micro structure. After the extrusion, the deflocculated material tends to re-flocculate due to Brownian motion to rebuild the micro structure. The rate at which the re-flocculation occurs is defined as R_{thix} (caused due to the physical interactions). Later the static yield stress improvement is mainly due to the chemical interaction and the rate of increase is defined as A_{thix} (N. Roussel, 2018). The Eq. 2.2 and 2.3 represents the static yield stress at time 't' due to re-flocculation and structuration (Kruger et al., 2019b, 2019a; Pj et al., 2018) respectively. Thus, it is evident that these rheological properties pose greater influence on the concrete printing process.

$$\tau_S(t) = \tau_{D,i}(0) + R_{thix}t, \textit{ for } t < t_{rf} \quad (2.2)$$

$$\tau_S(t) = \tau_{S,i}(0) + A_{thix}(t - t_{rf}), \textit{ for } t > t_{rf} \quad (2.3)$$

Where,

$\tau_S(t)$ – static yield stress of material at time t (after the agitation),

$\tau_{D,i}$ – Initial dynamic yield stress of the material (from first rheological test),

$\tau_{S,i}$ – Initial static yield stress of the material (from first rheological test),

t – Time since the end of agitation,

t_{rf} – Re-flocculation rate time period over which the growth of static yield stress is dominated,

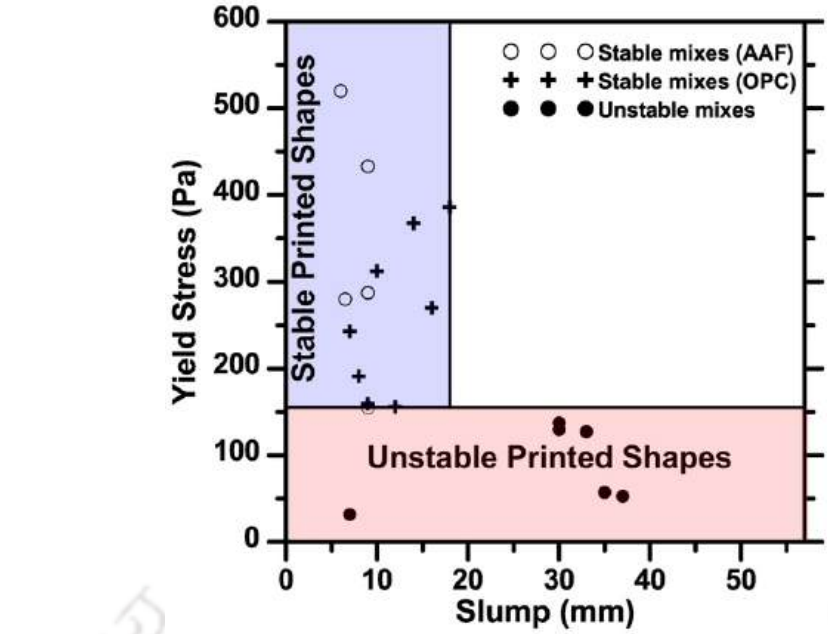

(a)

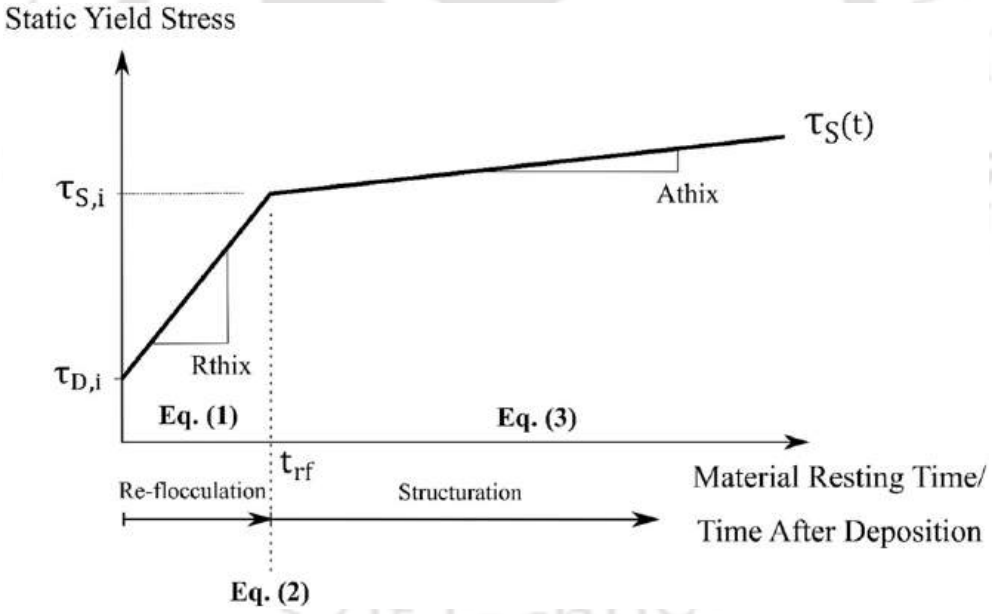

(b)

Figure 2.3: (a) The relationship between the yield stress and the printability of different mixtures (Alghamdi and Neithalath, 2019), (b) Bi-linear thixotropic model that characterizes the re-flocculation rate and structuration rate of printable cementitious materials (Kruger et al., 2019b).

2.3.3 Influence of mix design on the rheological properties of 3D printed mortar

From the discussions of previous sections, it can be inferred that material mix design has a greater influence on the rheological properties of 3DCP. According to Mechtcherine et al., (2020), there are two asymptotic regimes of material deposition by extrusion. One is infinite brick regime (i.e. extrusion of stiff materials) and other is extrusion of flowable material with or without the addition of admixtures. The realistic behaviour of the printable material lies between these regimes. The mix design helps to achieve the desired rheological parameters of printable material depending on the type of cementitious material. As shown in Figure 1.3, a successful printing process needs several iterative materials mix design steps. Unfortunately, no standard mix designs for printable cementitious mixtures are currently available. In order to achieve the rheological properties required for 3D printing, the mix composition of conventional mortar is usually adjusted by adding other raw ingredients such as fillers (Zhang et al., 2022; Ding et al., 2021; Zou et al., 2021), chemical (Hamidi and Aslani, 2019; Shahzad et al., 2020) and mineral admixtures (Chen et al., 2020b; Yoris-Nobile et al., 2022). The next sections go through the impact of mix design on the rheological properties of 3D printing OPC based mortars in depth.

2.3.3.1 OPC based mortars without fiber reinforcement

The ingredients in printable normal mortar play an important role in rheology modification. To achieve the precision required for printable mortars, both hydration and colloidal interactions must be regulated (Marchon et al., 2018). The sand gradation used in 3DCP is crucial in achieving buildability. Weng, et al., (2018) conducted rheological tests using six distinct sand gradations and discovered that the Fuller Thompson approach and Marson-Percy model could be used to tailor 3DCP mixes to meet the differing requirements when fitted using Bingham model (i.e. mixture-A with continuous gradation has high static yield stress with low viscosity) (Figure 2.4). On a similar note, buildability test also proved the impact of sand gradation on printability. The test outcomes showed that for mixes with optimized sand gradation, up to 40 layers could be printed easily without any notable deformation, while the other mixes tend to deform by 30th layer. Furthermore, changes in mix composition, such as increasing the sand to binder ratio, shown to enhance initial viscosity and initial yield stress while decreasing initial thixotropy (Zhang et al., 2019). It was also reported that increasing the aggregate content increased the lubricating layer's yield stress and viscosity values (Mohan et al., 2021).

However, due to the sand's higher specific surface area, sand fineness is vital in maintaining the yield stress (Zhang et al., 2019).

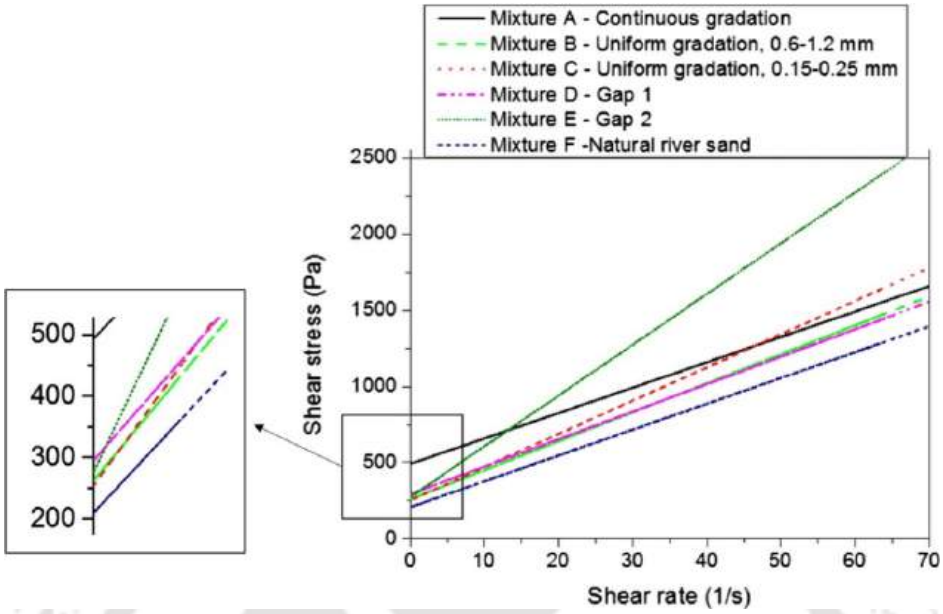

Figure 2.4: Mixtures with various sand gradations fitted using the Bingham model (Weng et al., 2018).

Ma et al., 2018 investigated the printability of cementitious materials infused with copper tailings up to 50% replaced by sand. With a rise in copper tailings replacement level, penetration resistance (buildability) of the cementitious material reduced, as did observations of a drop in slump height and an increase in slump flow. The finer particles in copper tailings are thought to be the cause of the above-mentioned behaviour. In a similar study by Li et al., (2020), it was demonstrated that substituting iron tailings for copper tailings at a 4:1 ratio resulted in improved flow and buildability. According to Rahul and Santhanam, (2020), adding a light weight coarse aggregate with a maximum size of 8 mm reduced the de-sorptivity results, indicating a limited water retention capacity. Further, it was reported that extrudability failed due to phase separation at a 30 percent replacement level. Below this replacement level, it was suggested that dewatering during extrusion would be helpful in improving the buildability. As a result, optimising the basic elements is critical for meeting the 3DCP's conflicting requirements.

Liu et al., (2019) used mixture design approach to evaluate the influence of sand, FA, and cement on both static and dynamic yield stresses and analysed the data using a ternary diagram as shown in Figure 2.5 to optimise the ingredients. The optimum sand, FA, and cement content

proportions are 0.215-0.230, 0.260-0.270, and 0.150-0.155 percent of total volume of the mixture, respectively. The aforementioned optimization was carried out with the goal of achieving a static yield stress of more than 4880 Pa and a dynamic yield stress of less than 220 Pa. The above-mentioned rheological tests were conducted using a rotational rheometer. The goal of the above optimization method is to improve buildability by increasing static yield stress while lowering the pressure required for pumping by setting the dynamic yield stress to low values. Although static yield stress is essential for achieving buildability, it should be noted that static yield stress beyond a threshold value may result difficulties in extruding the mixtures. However, Panda and Tan, (2019) developed a ternary blended high volume fly ash (HVFA) 3D printing ink comprising micro silica and OPC. As the amount of OPC is increased, the viscosity recovery in HVFA of OPC-replaced mixtures decreased but with the addition of micro silica significant recovery was reported.

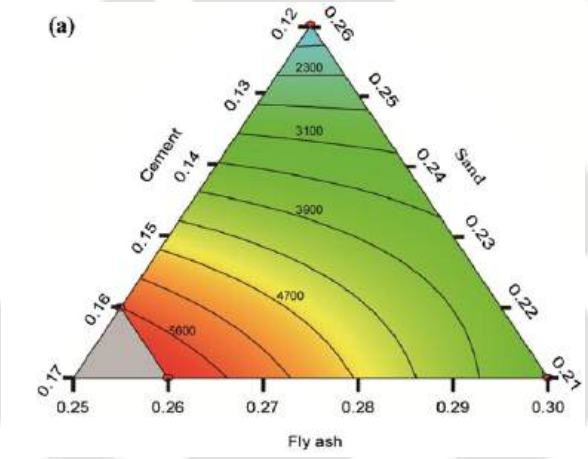

(a)

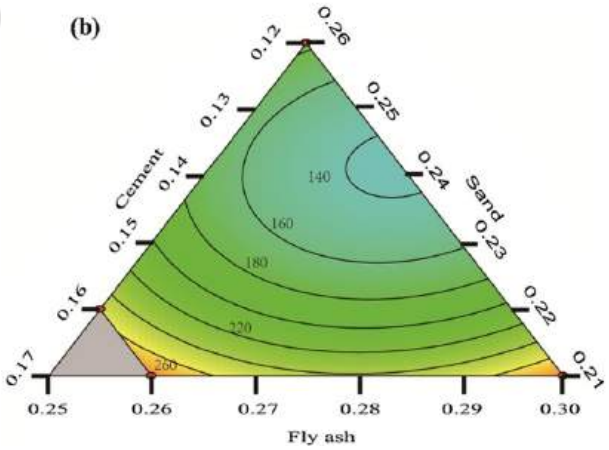

(b)

Figure 2.5: Influence of sand, cement and fly ash on (a) static yield stress (b) dynamic yield stress, represented in the form of ternary diagram (Liu et al., 2019).

Rahul et al., (2019) used yield stress-based mix design to understand the static yield stress requirements of 3DCP. According to the results of the experiments conducted using a vane shear apparatus, printed mixes should have a yield stress of 1.5 to 2.5 kPa, although the open time achieved in the study was 15 minutes (maximum). Zhang et al., (2018) prepared a novel material by doping SF and NC at 2% each and studied the thixotropy and buildability of the material prepared with the goal of generating a robust mixture. The addition of NC and SF increased the number of nucleation sites required for aggregation in the suspension, resulting in a reduction in open time and an improvement in buildability. In a similar manner, rice husk ash as a supplementary cementitious material (SCM) has shown to reduce yield stress while simultaneously causing workability loss and open time. The uneven shape and porous morphology of Rice husk ash were attributed for the decrease in flowability (Muthukrishnan et al., 2020). Open time was reported to reduce with the replacement of cement by calcium sulfoaluminate (rapid hardening cement) due to the presence of ye'elimite phase (Chen et al., 2020c; Khalil et al., 2017).

The use of Nano silica and silicate carbide increased the rheological parameters of the high-performance mortar mixture, such as static yield stress, dynamic yield stress, and thixotropy. When compared to Nano silica, which required less SP to disperse the material, the addition of 1 percent silicate carbide improved the thixotropy greatly due to 16 times reduced specific surface area. It should also be noticed that the addition of 1% Nano silica improved the static yield stress significantly (Kruger et al., 2019). Other SCMs and fillers like metakaolin (Chen et al., 2020a), limestone powder and others (Dey et al., 2022; Navarrete et al., 2020) are adopted in practice for improving the yield stress. Chen et al., (2020b) employed various grades of calcined clay (changing levels of low grade calcined clay (LGCC) and high grade calcined clay (HGCC)) as a supplementary cementitious material and discovered that the extrusion pressure rose as the grade of calcined clay increased. As shown in Figure 2.6, even though the mix named HCC (includes 20% LGCC and 20% HGCC) offers better buildability, the shorter open time, faster setting time, and higher extrusion pressure are challenges compared to mixes named LCC (includes 40% LGCC and 0% HGCC) and MCC (includes 30% LGCC and 10% HGCC) (Chen et al., 2020b). Silica fume has been observed to alter the printability of limestone calcined clay cement (LC3) mortar, which is a ternary blended cement consisting of calcined

clay, limestone powder, gypsum, and clinker (Dhandapani and Santhanam, 2020; Liu et al., 2021; Scrivener et al., 2018). Because of the rise in viscosity and yield stress, it enhanced buildability but decreased flowability (Long et al., 2021).

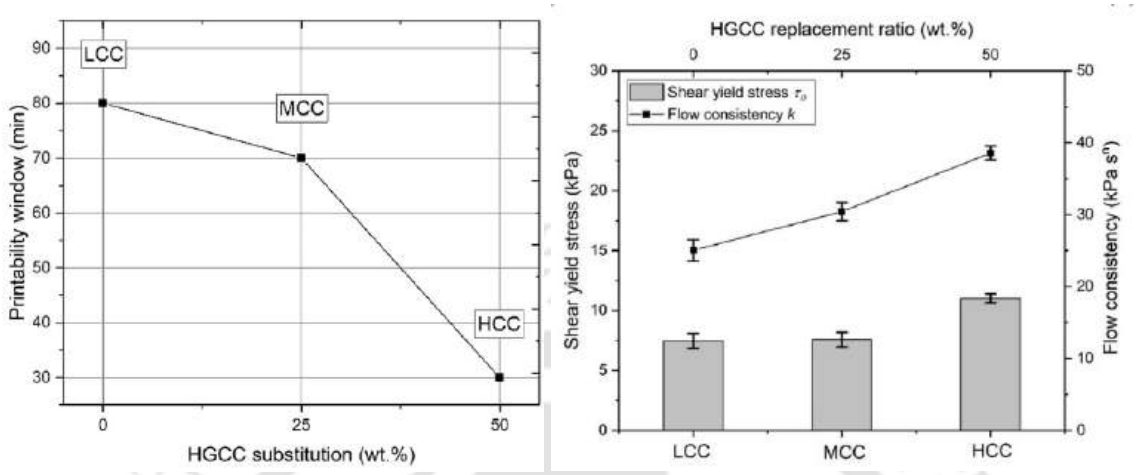

(a) (b)

Figure 2.6: Influence of grade of calcined clay on (a) open time (b) static yield stress and flow consistency (Chen et al., 2020b).

According to the literature, factors such as sand to binder ratio, sand gradation, and other factors significantly affect rheological properties. Apart from FA, replacing sand and cement with fillers and SCMs, respectively, has a positive impact on rheological characteristics. However, FA improves the viscosity and thixotropy of the mixture. Table 2.1 summarises the effects of several mix design parameters, SCMs, and thixotropic agents on the rheological properties of 3DCP.

Table 2.1: Influence of various parameters on rheologic properties of 3DCP

Parameter	SY	DY	V	T	Remarks	Ref.
S/B	↑	↑	↑	↓	Fineness of the sand is also a crucial parameter in yield stress growth.	(Mohan et al., 2021; Zhang et al., 2019a; Zhang et al., 2019b)
W/B	↓	↓	↓	↓	Higher water content leads to the phase separation and bleeding.	(Tay et al., 2019; Weng et al., 2018; Zhu et al., 2021)
Fillers (as a sand replacement) finer than sand	↑	↑	↑		However, these properties show an inverted 'V' trend,	(Li et al., 2020; Ma et al., 2018)

						indicating the need for optimization.	
SCMs and Other thixotropic agents	FA	↓	↓	↑	↑	Dynamic yield stress values after reaching certain dosage tend to increase as shown in the Figure 7 (b)	(Liu et al., 2019; Panda and Tan, 2019; Rahman et al., 2014)
	SF	↑	↑	↑	↑	However, there are also contrasting results reported in (Ahari et al., 2015; Zhang and Han, 2000)	(Kazemian et al., 2017; Yuan et al., 2019; Zhang et al., 2018)
	Calcined clay	↑	↑	↑	↑	Use of high-grade calcined clay shows greater improvement when compared with lower grade.	(Chen et al., 2020b; Chen et al., 2019; Chen et al., 2020d)
	Nano-silica, Nano-clay, Silicate carbide	↑	↑		↑	Depending on specific surface area, the improvement in thixotropy and yield stress values vary significantly.	(Nguyen-Van et al., 2022; Panda et al., 2019a; Panda et al., 2019b)

S/B – Sand to Binder Ratio, W/B – Water to Binder Ratio, SY – Static Yield Stress, DY – Dynamic Yield Stress, V – Viscosity, T - Thixotropy

2.3.3.2 OPC based mortars with fiber reinforcement

Fiber reinforcement is often used to increase the ductility of 3DCP. This is intended to cut down on the complexity and time required by embedded reinforcement methods (Le et al., 2012; Siddika et al., 2020). Although Nguyen et al., (2022) performed numerical simulations to conclude that slabs can be produced without rebar reinforcement using 3D printed fibre reinforced concrete, operational concerns are not addressed. Similarly, numerous researchers have employed fibers like polyethylene (PE) (Ding et al., 2020, 2021), polypropylene (PP) (Le et al., 2012; Tran et al., 2021), polyvinyl alcohol (PVA) (Pham et al., 2022; Sun et al., 2021; Sun et al., 2022), short glass (Panda et al., 2017), steel (Yang and Zhang, 2022; Yang et al., 2022), and other types of fibers in 3DCP.

To decrease deformation in the plastic state, Le et al., (2012) employed PP fibres at an optimized dosage of 1.2 kg/m^3. As workability and extrudability were considered, a shear strength (measured using soil vane shear apparatus) of 0.3-0.9 kPa was reported to be printable.

However, due to extrudability issues at larger dosages, the inclusion of fibres is limited to certain dosages. Sun et al., (2022) studied the effect of adding PVA fibres on flowability and found that as the fraction of fibres increased, flowability decreased. The incorporation of fibres, on the other hand, aids in the shape stability of printable mixtures. Furthermore, significant increase in the viscosity and dynamic yield stress was reported in the literature due to the addition of PP fibers (Tran et al., 2021; Zhu et al., 2019).

Ogura et al., (2018) studied the extrudability of strain hardening cementitious composites (SHCC) using a horizontal ram extruder at a rate of 15 mm per second and mixes up to 1.5% of 6mm PE fibrous SHCC could be extruded without any blockage. Soltan and Li, (2018) investigated the extrudability and buildability of SHCC (i.e. 12 mm PVA fibres added at 2% by volume), as well as the effects of other ingredients including calcium aluminate cement, silica fume, ground silica, and attapulgite Nano clay, using the drop table flowability test. Because of its initial high flowability and inability to withstand the shape of extruded elements, they concluded that the mix without any rapid hardening ingredients and viscosity increasing agent is not suitable for 3DCP. Similarly, Zhu et al., (2019) assessed the buildability of two similar mixes containing 2% of 12 mm PE fibres doped with and without Nano clay and hydroxy propyl methyl cellulose (HPMC), concluding that the mixture without thixotropic and viscosity-increasing additives has poor buildability. Using a ram extruder and the Benbow-Bridgwater equation, Figueiredo et al., (2019) studied the impact of rheological modifiers, water to solid ratio, and fibre volume (8 mm PVA fibers at 1, 1.5, and 2 percent by volume) on extrudability of SHCC (Figure 2.7(a)). They employed two sets of mixes, one containing cement, slag, limestone powder and PVA fibers and other containing cement, FA, sand, limestone and PVA fibers. VMA and SP dosages maintained at 0.3% and 2% by weight of the total binder. Due to the friction between fibres and particles during extrusion, they observed that initial bulk yield stress (intrinsic material property) and shear yield stress (physical property defining the friction of the material moving through the die) calculated using Benbow-Bridgwater model increase with increased fibre reinforcement (Figure 2.7(b)). When compared to the influence of particle size distribution and liquid to total surface area of all solids, they also observed that the contribution of rheological modifiers is minor in generating printable SHCC mixes. The liquid to solid ratio of all solids is said to have a greater impact on shape stability than the SP dosage.

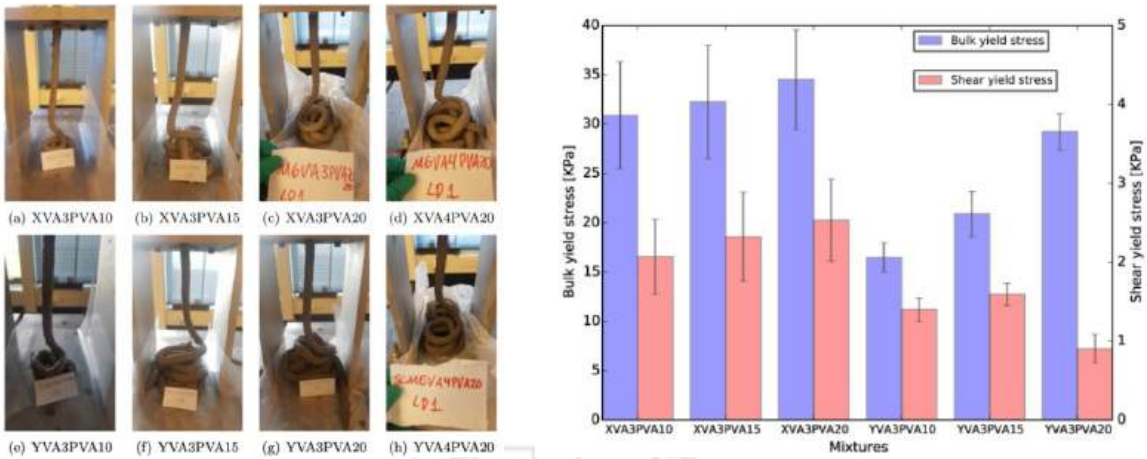

(a) (b)

Figure 2.7: (a) Extrusion of SHCC mixes (b) Influence of fibers on bulk and shear stresses (Figueiredo et al., 2019).

Steel fibres, on the other hand, improve the strain hardening behaviour as well as other mechanical properties. Steel fibres were added in the high-performance concrete by Arunothayan et al., (2020), which altered the fresh state behaviour of the mixture (i.e. workability reduced). Shape retention improved significantly when compared to a mixture without steel fibres as shown in the Figure 2.8, but workability reduced due to poor paste-fiber adhesion. Though there was no effect observed on the extrudability and buildability when tested by direct printing. Nonetheless, partial replacement of OPC with other SCMs, especially FA, reduces the structural build-up of the mixture (Arunothayan et al., 2022). However, fiber orientation in the direction of printing (causes anisotropy) would be higher with increased volume of fibers due to the inter-fiber interaction (Arunothayan et al., 2021).

The impact of various fibre dosages on the rheological characteristics of fibre reinforced mortars is shown in Table 2.2. Viscosity, bulk yield stress, dynamic yield stress, and static yield stress were all reported to increase with increasing fibre dosage. On the other hand, a decline in flowability was reported. Printability parameters like shape stability and buildability that is associated to yield stress largely is improved significantly. A maximum of 2% (of total volume) fiber dosage is used in the literature.

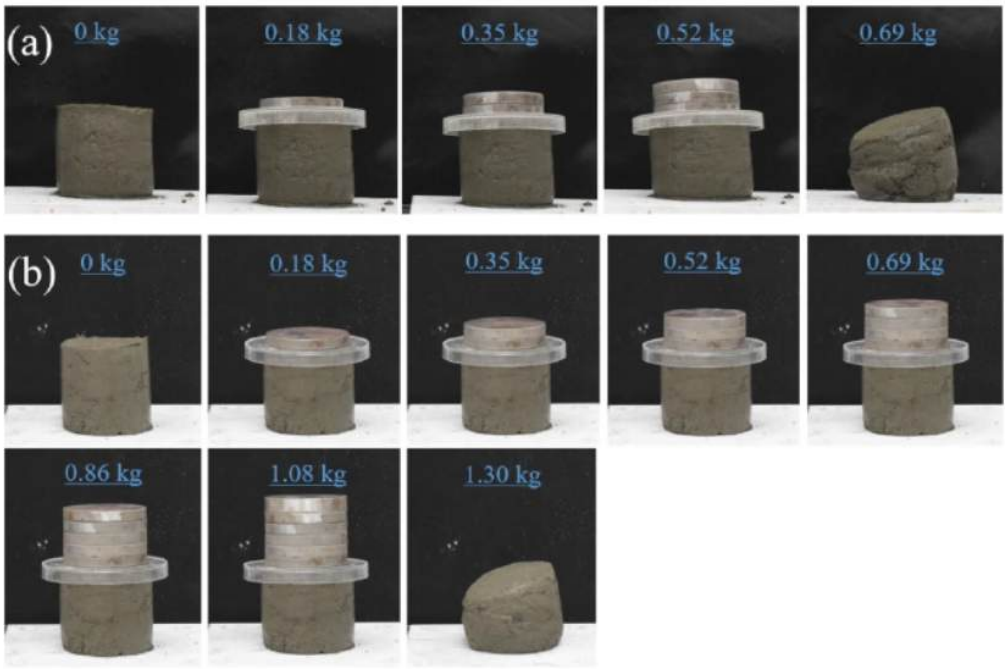

Figure 2.8: Shape stability of mixture (a) without steel fibers, (b) with steel fibers (Arunothayan et al., 2020).

Table 2.2: Summary of influence of fibers on fresh state properties

Ref.	Materials used	Details of reinforcement	Conclusions
(Le et al., 2012)	OPC, FA, SF, sand (2 mm max. size), SP, Retarder, Accelerator.	PP fibers of 12 mm length and 0.18 mm diameter. (at a dosage of 1.2 kg/m^3).	A shear strength of 0.3-0.9 kPa was reported to be printable.
(Sun et al., 2022)	CSA cement, mineral powder, and SF are used as binder. Sand (size of 0.1-0.5 mm), retarder, and SP.	PVA fibres (density of 1.3 g/cm^3) of length 9 mm and a diameter of 31 µm. (at a dosage of 0-1.6% by total volume)	Improved shape stability, and decreases the flowability of the mixture
(Tran et al., 2021)	OPC, class F FA, SF, fine limestone powder, river sand (2 mm max. size), SP.	PP fibres (density of 0.91 g/cm^3) of length of 6 mm and a diameter of 30 µm. (at a dosage of 1.35, 2.7, 5.4 kg/m^3)	Plastic viscosity and dynamic yield stress are increased due to the increase of PP fibers dosage.
(Ogura et al., 2018)	OPC, FA, SF, S/B ratio varied from 0.2 to 1.2, W/B ratio of 0.22 and 0.24.	PE fibres (density of 0.97 g/cm^3) of length 6 mm and diameter of 12 µm. (at a	Addition fibers reduced the spread percentage (after 15 blows)

Ref.	Materials used	Details of reinforcement	Conclusions
		dosage of 0.3-1.5% by total volume)	
(Soltan and Li, 2018)	OPC (type 1), class F FA, calcium aluminate cement, micro silica, ground silica, HPMC, SP, Nano-clay, fine sand.	PVA fibres of length 12 mm. (at a dosage of 2% by total volume)	Studied the influence of rapid hardening agents and thixotropic agents on flowability and printability of SHCC.
(Figueiredo et al., 2019)	Mix 1: OPC, slag, and limestone powder. Mix 2: OPC, FA, and sand. Both mixes contain VMA (0.3%) and SP (2%).	PVA fibres with a length of 8 mm. (at a dosage of 13, 19.5, and 26 kg/m^3)	Bulk and shear yield stress values increased with increase in the fiber dosage.
(Arunothayan et al., 2020)	OPC, SF, FA, slag, coarse and fine sand of max. size 0.498 and 0.176 mm respectively, limestone powder, SP, NC, and VMA	Brass coated micro steel fibers with a length of 6 mm and diameter of 0.2 mm. (at a dosage of 157 kg/m^3)	Shape retention improved due to addition of fibers, however, workability is reduced.

2.3.3.3 Discussion on mix design requirements

As seen in the preceding discussion, obtaining the required competing rheological properties of 3DCP poses several issues. Designing robust mixes is essential to overcome these challenges. The rheological requirements for lab scale printing might not be appropriate for large-scale printing. Despite the fact that trials for large-scale printing are conducted, the necessity of time-dependent rheology is to be properly established using laboratory rheological studies. Therefore, a standard rheological test protocol that is applicable for large scale printing should be established. Open time and structural build-up are the two key parameters that play a key role in large scale printing. The feasibility of the large scale 3DCP is demonstrated by structural build-up, which has been described in several studies (Jayathilakage et al., 2020; Leal da Silva et al., 2020; Wolfs et al., 2019). The fact that both physical interactions and chemical hydration play an important role in structural built-up. The idea of utilising high doses of chemical admixtures, on the other hand, may result in porous microstructures and reduced open time. Nevertheless, extruding high thixotropic material needs high pumping pressure to deposit the layers. After deposition, the layers will sustain the load of subsequent layers up to a point, but after that, structure may fail due to suppression of the bottom layers (lack of static

yield stress). Furthermore, because of its high cohesiveness nature and high thixotropy, the mix may generate poor surface roughness. As a solution, mix designs should be given high importance, incorporating both sustainable materials and proper chemical admixtures that aid in making the mixture thixotropic and robust. It also highlights the need for the development of novel mix designs in order to achieve the necessary 3DCP properties. However, in the section 4, the role of chemical admixtures in designing of such robust mixes is highlighted. Furthermore, a potentially novel method in 3DCP that allows for a higher structural build-up is active rheology control (ARC). For instance, Jiao et al., (2022) conducted the rheological tests using parallel plate rheometer equipped with magneto-rheological device on the mixture designed with Nano-Fe_3O_4. Structural build-up of the material is characterised by oscillatory time sweep test. Results show that mixture with nanoparticles showed better structuration due to the distribution of magnetic nanoparticles. However, more research in case of material design and machine design is to be conducted for practical applications of ARC technique.

2.3.4 Influence of chemical admixture on rheological properties of 3D printed mortar

In general, workable mortar is required for the labour to work with ease at the construction site. Thus, the consistency of mix should be satisfactory, so that the mortar can be easily transported, placed and compacted. But in case of 3DCP, admixtures are commonly employed to tailor the rheological and hydration properties necessary for printable mortar. Chemical admixtures are reported to interact with the constituents of the mortar and influence their performance in fresh and hardened states. In the 3DCP mixes, primarily admixtures contribute either to improvement or impairment of the rheology and later their effect is also seen in hardened properties. It is to be noted that the type of material, dosage, time of mixing and mixing duration can alter the rheology either way.

Chemical admixtures like accelerators (ACC) (Bhattacherjee and Santhanam, 2020, 2022; Rubin et al., 2021), retarders (RET) (Mohan et al., 2021), high range water reducers like superplasticizers (Markin et al., 2019; Qian, 2021; Rahul et al., 2020), viscosity modifying admixtures (Chen et al., 2019; Liu et al., 2021; Ma et al., 2018), and air entraining admixtures (AEA) (Markin et al., 2021; Tarhan and Şahin, 2021) are commonly used as rheology modifiers in various studies reported on 3DCP. The effect of these materials on the rheological behaviour is analysed in detail in the following sub-sections.

2.3.4.1 Superplasticizers

Superplasticizers, the commonly used high range water reducers, are added in 3DCP to maintain workability of the mix, till the end of dormant period. The synthetic water-soluble SPs like modified lignosulfonates (removing sugars which are responsible for high retardation) (Breilly et al., 2021), sulfonated naphthalene formaldehyde (SNF) (Hekal and Kishar, 1999) and sulfonated melamine formaldehyde (SMF) (Yilmaz and Glasser, 1989) causes loss in workability retention due to the presence of negatively charged groups (SO_3^-) that race with gypsum present in the cement to form ettringite in the concrete (Plank and Hirsch, 2007). However, the new age polycarboxylate-ether-based SPs are reported to be successful in maintaining workability retention due to the non-dependency on electrostatic repulsion. Rather, the phenomenon of steric hinderance or polymer adsorption is responsible for maintaining the fluidity in PCE based SP mixes (Collepardi, 2005). Hence, the effect of fluidity improvement of PCE based SP is found to be maximum, followed by modified lignosulfonates, SNF and SMF (Ma and Wang, 2018). Due to the above-mentioned reasons, most researchers prefer PCE based SPs in 3DCP to utilize the advantage of availability of open time (due to workability retention). However, when high dosages are adopted, the side effects of retardation is observed even in PCE based mixes (Qian, 2021).

On a similar note, when higher dosages of SP are added, the static and dynamic yield stress values are found to decrease significantly, with little effect on viscosity due to cement agglomerate dispersion (Marchon et al., 2018). In addition, at higher dosages of SP, the rate of structuration is also reported to decrease considerably (Souza et al., 2022). However, there is an ideal dosage level above which the efficacy of SP is diminished. The optimum dosage is dependent on the type of SP employed (Flatt and Schober, 2012). The efficiency of altering the rheological properties is also reliant on the molecular structures of the SP used. For instance, Winnefeld et al., (2007), carried out comparative analysis on influence of two different PCEs (methylpolyethyleneglycole-methacrylate copolymers and methacrylic acid copolymers) with variable side chain lengths and densities, and also different polymer molecular weights on the rheological properties of mortars. Based on their experimental outcomes, it was reported that side chain length and polymer molecular weight had only a minimal impact on mortar workability and rheology, however, decrease in side chain density (decrease in density of polyethylene-oxide) enhanced workability by lowering yield stress and viscosity. Furthermore, it was concluded that the adsorption of polymeric SP on the cement surface has a significant

impact in improving workability. When a high charge density polymer is utilised instead of a low charge density polymer, the adsorption is found to be higher. Hence, PCEs with a higher molecular weight, lower side chain densities, and shorter side chains were reported to have better adsorption.

Nevertheless, dispersion of SP in the cementitious mixture also effects the rheological parameters. For instance, Pan et al., (2022) used two different SPs to investigate structural characterisation and time-varying rheological parameters. They employed fluid retention polycarboxylate (FR-PC) and higher dispersion polycarboxylate (HD-PC) and found that although FR-PC has a larger re-flocculation rate than HD-PC, it has a lower structuration rate. Figure 2.9 depicts the influence of both SPs on thixotropic area and variation of shear yield stress with time. It illustrates that although the thixotropic area of the mixture with HD-PC is less but the growth of yield stress is dominating the mixture with FR-PC and vice-versa. Therefore adoption of optimized dosages of SP is needed as it could lead to colloidal flocculation and thereby maintain the static yield stress values required for 3DCP (Qian, 2021; Rahul et al., 2019).

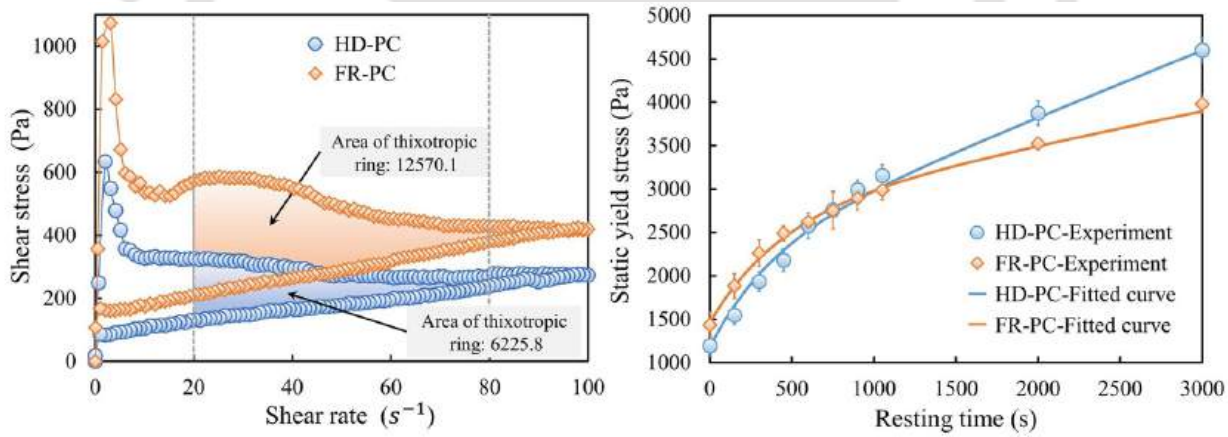

(a) (b)

Figure 2.9: Influence of two different SPs (HD-PC and FR-PC) on (a) Thixotropic area and (b) development of static yield stress with time (Qian, 2021).

2.3.4.2 Viscosity modifying agents

To maintain the cohesion, stability and viscosity of mortar, role of VMAs are considered to be pivotal. Organic based VMAs are basically classified into three types viz., natural, semi synthetic and synthetic based upon their source. Both inorganic and organic VMAs are reported

to influence the rheological properties (Bessaies-Bey et al., 2022). On the other hand, polymeric VMAs which are hydrophilic in nature are found to have the high capacity to bind water molecules and thereby enhances the viscosity (Khayat, 1998). VMAs in both aqueous and cementitious systems are reported to cause shear thinning behaviour. At lower shear rates, polymer entanglements are not disrupted and polymeric interactions occur without effecting the viscosity. But at higher shear rates, polymeric chains disentangle and align in the flow direction (Khayat, 1998). Apart from this, there are few more possible mechanisms with the addition of VMAs such as bridging flocculation, polymer association and depletion flocculation (Figure 2.10) (Palacios and Flatt, 2016).

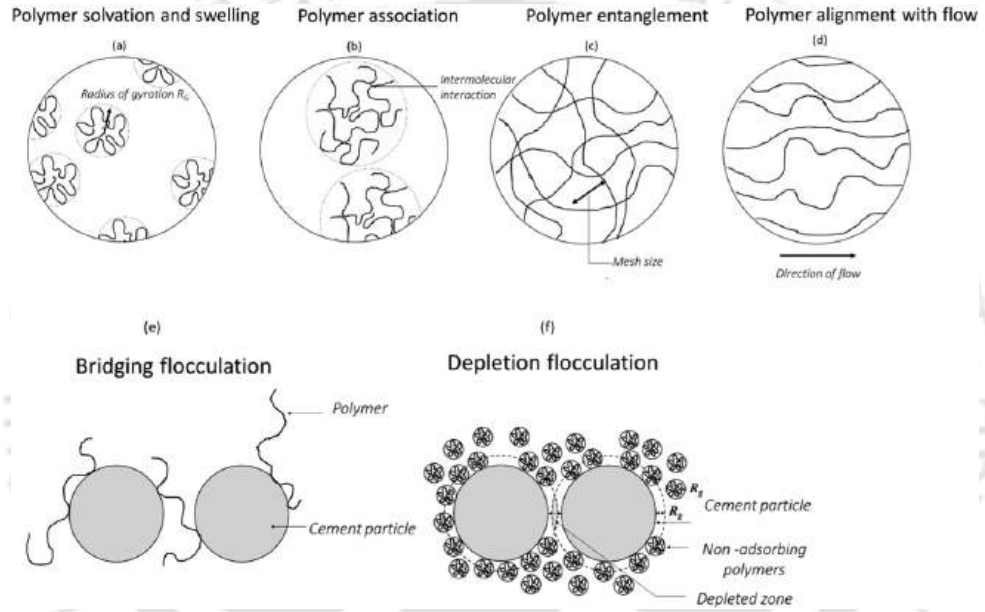

Figure 2.10: The various types of VMA's key mechanisms of action (Palacios and Flatt, 2016).

Studies (Bessaies-Bey et al., 2022; Chen et al., 2019; Leemann and Winnefeld, 2007) have proved that increase of VMA dosage, resulted in increase in viscosity and yield stress of the cementitious system. But the rate of increase of viscosity is found to be higher than the yield stress rate. The molecular weight of the VMA used is also said to influence the rheological properties, with higher molecular weight VMA causing more viscosity and yield stress, and vice versa. For instance, Ma et al., (2018) studied the effect of two different HPMCs of varying molecular weights on rheological properties of cement paste plasticized by PCE and concluded that HPMC with higher molecular weight shows improved static yield stress and viscosity. This is attributed to the high molecular weight of HPMC's better viscosity-enhancing nature

and the unfavourable influence on PCE dispersion induced by the high molecular weight of VMA's enhanced combination ability in pore solution.

Few studies have reported that increase in dosage of VMA in 3DCP, resulted in increase in extrusion pressure due to decrease in flowability of mix. This is owing to the higher extrusion pressure being caused by enhanced static yield stress and flow consistency (Chen et al., 2020a; Patural et al., 2011). Furthermore, the molecular weight of VMA used has an impact on the mixture's flowability. Patural et al., (2011) for example, used a variety of cellulose ethers (hydroxyethyl methyl cellulose (HEMC), hydroxyethyl cellulose (HEC), and HPMC) as well as starch ethers (carboxymethyl-hydroxypropyl and hydroxypropyl starches) to investigate the effects of dosage, molecular weight, and molar substitution on mortar flow consistency and water retention. Consistency and water retention were reported to improve as molecular weight and dosage increased. Molar substitution, on the other hand, has no impact on these properties. Nevertheless, it is to be noted that although flowability decreased, the retardation effect due to addition of VMA resulted in increase of open time. The retardation was ascribed to the adsorption of VMA on hydration phases (calcium silicate hydrate and portlandite) (Chen et al., 2020b). Moreover, VMA has a considerable effect on structuration. Sukontasukkul et al., (2022) studied the deformation of layers produced with mixtures (containing cement, sand, silica fume, polyethylene glycol and SP) of three different VMA dosages (0%, 0.1%, and 0.5% by weight of binder). They observed that after extrusion, the height of the layer decreased from 12 to 10 mm for control mix M0, but that the height of the first layer could be maintained at 12 mm for mix M2 (0.5 percent VMA). Figure 2.11 depicts the effect of the subsequent layers being added.

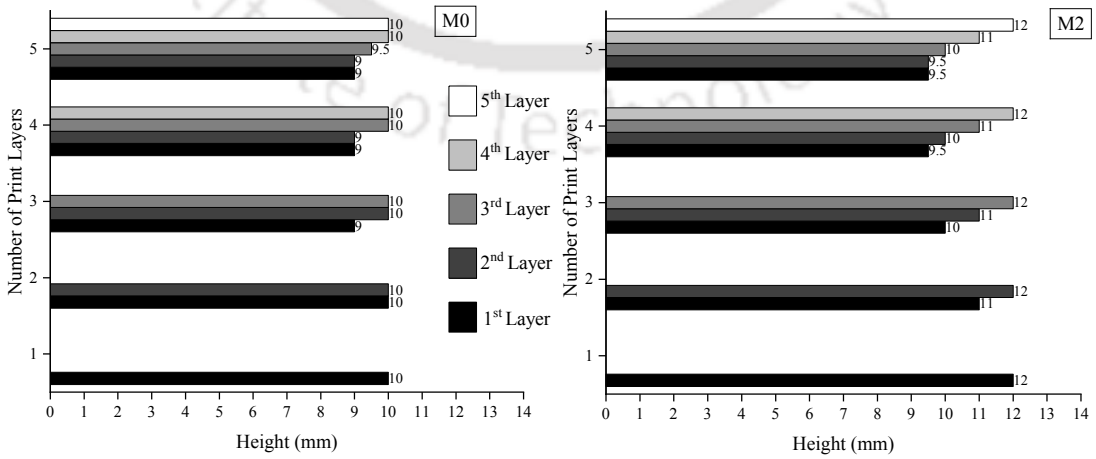

(a) (b)

Figure 2.11: Influence of VMA on layer deformation for the mixes (a) M0 and (b) M2 (Sukontasukkul et al., 2022).

2.3.4.3 Accelerators and retarders

Basically, accelerating admixtures causes increase in hydration rate and decreases the time required for setting. There are different types of setting accelerators as per ACI 212-3R-16, which are categorized as soluble inorganic salts (includes chlorides, bromides, fluorides and etc.), soluble organic salts (triethanol amine, calcium formate and etc.), quick setting admixtures and other miscellaneous accelerating materials. As few chemical admixtures like calcium chloride, potassium and sodium carbonate, triethanolamine hydrochloride etc. can act, both as accelerator as well as retarder depending upon the dosage adopted, it is critical to carefully optimise the dosage. Reason for the performance of accelerator as retarder beyond a particular dosage can be attributed to the retardation of tricalcium silicate phase, even when the hydration of tricalcium aluminate is accelerated (Yang et al., 2019). However, from an economic standpoint, it is also crucial to optimise the dosage of other accelerators and retarders.

To attain a good buildability, both physical and chemical interactions of admixtures are required. In 3DCP, attaining high structuration rate of printed filaments to accommodate the successive layers is the key factor for large scale printing. Setting accelerator plays a significant role in achieving the structuration rate by improving the static yield stress through chemical interactions. When compared to the reference mix, Nerella et al., (2019) discovered that adding 2.5 percent alkali-free accelerator increased yield stress by six times. However, yield stress improvement was not significant at lower dosages of 0.25 and 1.25 percentages. But when accelerators are used at high dosages, dispersion of other admixtures were not found to be homogenous. To cite an example, Rubin et al., (2021) used alkali-free aluminium based accelerating admixture in their study at dosage varying from 0 to 4% by mass of cement and reported that at low dosage, the dispersion of SP was found to be good. On the other hand, at higher dosages of accelerator, due to the rapid formation of ettringite needles, extrusion pressure was found to be very high, as well as the dispersion of material was not homogenous even when high dosage of SP was adopted. As a result, spraying an accelerator after extrusion and adding accelerator at the nozzle were found to be beneficial in improving the buildability. However, the dosage required to add at the nozzle is 2 percent, whereas at the mixer is 1 percent (Bhattacherjee and Santhanam, 2020, 2022). In light of the aforementioned difficulties of retarding effects and dispersion, it is clear that optimising the dosage of accelerators in the

mixture and selecting the correct method of admixture addition are critical for achieving the required performance in 3DCP as shown in Figure 2.12.

Retarders which commonly help to delay the setting time of mixture are essential for printable mixes to control the growth of yield stress with time and structuration rate with negligible effect on the viscosity (Muthukrishnan et al., 2021; Souza et al., 2022). The reduction in yield stress facilitates improvement of open time which is required particularly for rapid hardening cements. Mohan et al., (2021) studied the feasibility of the calcium sulfoaluminate cement based mixtures in 3DPC by controlling the rapid hardening through the use of retarders like borax and sodium gluconate. Use of borax was reported to improve the open time with good early age strength and its performance was better than sodium gluconate. As a result, choosing the proper admixture for retardation is crucial for achieving the requisite open time.

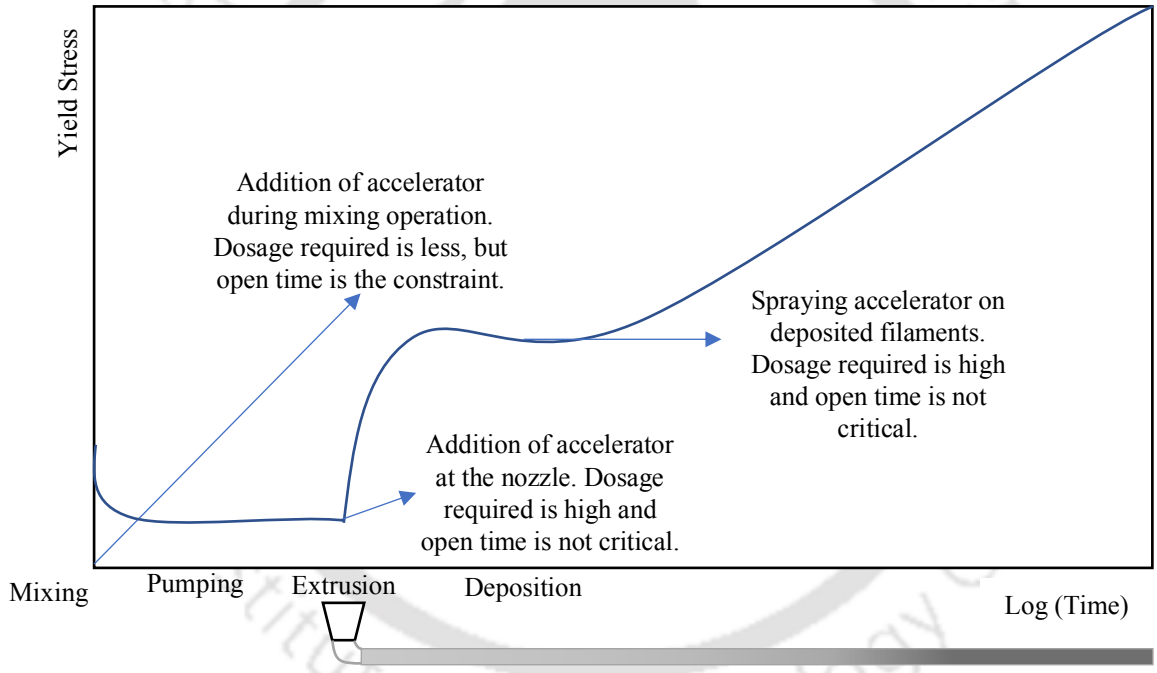

Figure 2.12: Variation of yield stress with time as a function of accelerator dosage and time of introduction (adopted from (Bhattacherjee and Santhanam, 2022; Marchon et al., 2018; Roussel, 2018)).

2.3.4.4 Air entraining admixtures

Air entrainment is the technique of inducing air bubbles in cementitious mortar by adding AEAs which can be natural or synthetic in nature. There are two types of AEAs, depending on the reaction. The first type combines with the cement paste's calcium hydroxide solution to

form an insoluble calcium salt. The surface tension of the water is not reduced in this type, but hydrophobic calcium salts precipitated at the water-air-cement grain contact regions are the primary cause of air entrainment and bubble stability (Chatterji, 2003). Surfactants, on the other hand, are AEAs that reduce surface tension at the water-air interface, allowing stable air bubbles to form (Siva et al., 2017). The later AEA is the most commonly used admixture among these AEAs. The addition of air bubbles to concrete improves pumpability and resistance to frost attack (Chatterji, 2003; Huang et al., 2018). The mixed and pre-foaming techniques are the most widely used for air entrainment (Chica and Alzate, 2019).

The effect of adding AEAs on the rheological properties of 3DCP has been examined in a very few studies. According to Tarhan and Şahin, (2021), as the amount of air bubbles added increases, yield stress values decreases. Higher dosages, on the other hand, were found to improve the viscosity and thixotropy of the mixture (Bagheri et al., 2019). Lu et al., (2019) investigated the effects of replacement of silica sand with FA cenosphere (up to 100% replacement) and addition of AEA (0-0.2 g/L) in spray-based 3D printed cementitious materials. At 100 percent cenosphere replacement, addition of 0.1 g/L of AEA lowered the flowability, viscosity, pumping pressure, and dynamic yield stress while maintaining the static yield stress, making it suitable for 3D printing. However, adoption of high dosage of air bubbles resulted in significant reduction of the density of the concrete.

2.3.4.5 Surfactants (used in foam concrete and controlled low strength material (CLSM)):

Surfactants or foaming agents are used commonly for the production of cellular structure in foam concrete and other CLSM. The cellular structure can be generated either based on pre-foaming method or mix foaming method. These foaming agents are basically powerful air entraining admixtures which aids in reduction of surface tension of water and facilitates air incorporation and stabilization. The characteristics of these surfactants (viscosity, adsorption, solubility and critical micelle concentration), are reported to affect the quality of foam generated to a greater extent (Sahu et al., 2018; Sahu and Gandhi, 2021; Wagh et al., 2021). The stability of the foam could also be improved by employing the foam stabilizers such as xanthan gum, carboxymethyl cellulose etc. (Hajimohammadi et al., 2018; Raj et al., 2022; Zhu et al., 2020). Limited studies available on 3D printable foam concrete in this regard have proved that increase of surfactant dosage and the foam volume in foamed concrete leads to decrease in the yield stress and viscosity (Alghamdi and Neithalath, 2019). Despite above mentioned

reduction, the thixotropy of foamed concrete was reported to increase with increase of foam volume (Tarhan and Şahin, 2021).

Hence it is recommendable to use chemical or mineral admixtures in the foam concrete to attain the rheological requirements for printability. However, use of various admixtures are reported to create compatibility issues with both synthetic and protein based natural surfactants (Amran et al., 2015; Khwairakpam and Gandhi, 2020; Sahu et al., 2018). The stability of the 3D printable foam concrete (3DP-FC) is influenced by both rheology of the mixture surrounding the material and the type of surfactant used. Cho et al., (2022) studied the influence of rheology on the stability of 3DP-FC and reported that the addition of more foam resulted in cushioning effect and reduced the stability issues. Although there are studies available on surfactant dosage and optimization of normal foam concrete, but they might not be applicable to 3DP-FC. The influence of surfactant characteristics is yet to be studied in 3DCP perspective. Nevertheless, there are also studies reported by few researchers on use of chemical admixtures in printable foam concrete without any compatibility issue. For instance, Markin et al., (2019), used protein-based surfactant and developed a printable foam concrete using SP. Another similar kind of study conducted by Liu et al., (2021) proved that addition of VMA and silica fume helped in improvement of the rheological properties without any effect on the stability of the mixture due to the bubble stabilization mechanism caused due to HPMC as illustrated in Figure 2.13. Similarly, Cho et al., (2021) developed a printable foam concrete using CSA cement (rapid hardening cement) instead of chemical admixture to achieve the desired rheological properties without causing instability due to higher bubble buoyant force.

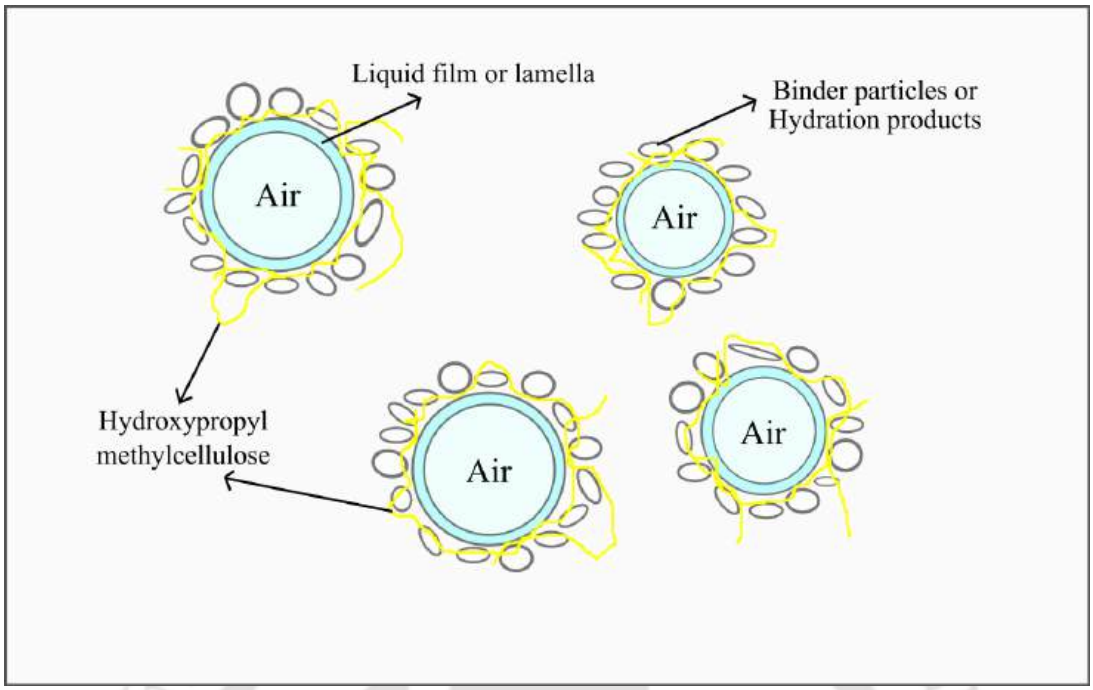

Figure 2.13: Mechanism of bubble stability caused by HPMC (Liu et al., 2021).

It is evident from previous discussion that the stability of 3DP-FC is impacted not only by the paste's rheology, but also by the surfactant properties. However, the impact of surfactant characteristics on 3DP-FC are yet to be established. Furthermore, the influence of various mineral admixtures like FA, rice husk ash etc. on the stability and rheology of the 3DP-FC is scarce. The incorporation of these industrial wastes in foam concrete and 3D printing applications could reduce the use of high cement content, lowering carbon emissions further more.

2.3.4.6 Discussion on optimization of the chemical admixture requirement for 3DCP

Table 2.3 summarizes the influence of chemical admixtures on 3DCP rheological requirements. It is critical to optimize the admixture dosage in order to reap the maximum benefits from the addition of admixture. Considering the significance of the bottom layer in attaining the required buildability, the addition of admixture should aid in the evolution of that layer's yield stress to the level needed to sustain the above layers as shown in Figure 2.14. Further, certain complications have been reported when admixtures are added in non-optimal dosages. For example, greater doses of SP and VMA resulted in a retardation effect, which influenced the rate of structuration. Similarly, the larger the accelerator dosage, the higher the extrusion pressure required to extrude the materials. Nonetheless, adding accelerators to increase structural buildup necessitates a thorough understanding of material chemistry, the selection of

the appropriate accelerator, its reaction mechanism, and dosage optimization. As a result, when creating the material for 3DCP, optimizing the chemical admixtures is critical. However, in order to progress from laboratory to large-scale printing, the method for selecting chemical admixtures must be enhanced. Thixotropy, static yield stress, and open time are three major factors to consider for large-scale printing; to achieve these properties, the material selection should be sustainable and cost-effective. Nonetheless, it is to be noted that the mechanism of above-mentioned chemical admixtures is expected to be similar even in castable mortars. However, in castable mortars, usually only few admixtures are used in mortars depending on the application, unlike 3D printed mortars wherein commonly different ranges of admixtures are used.

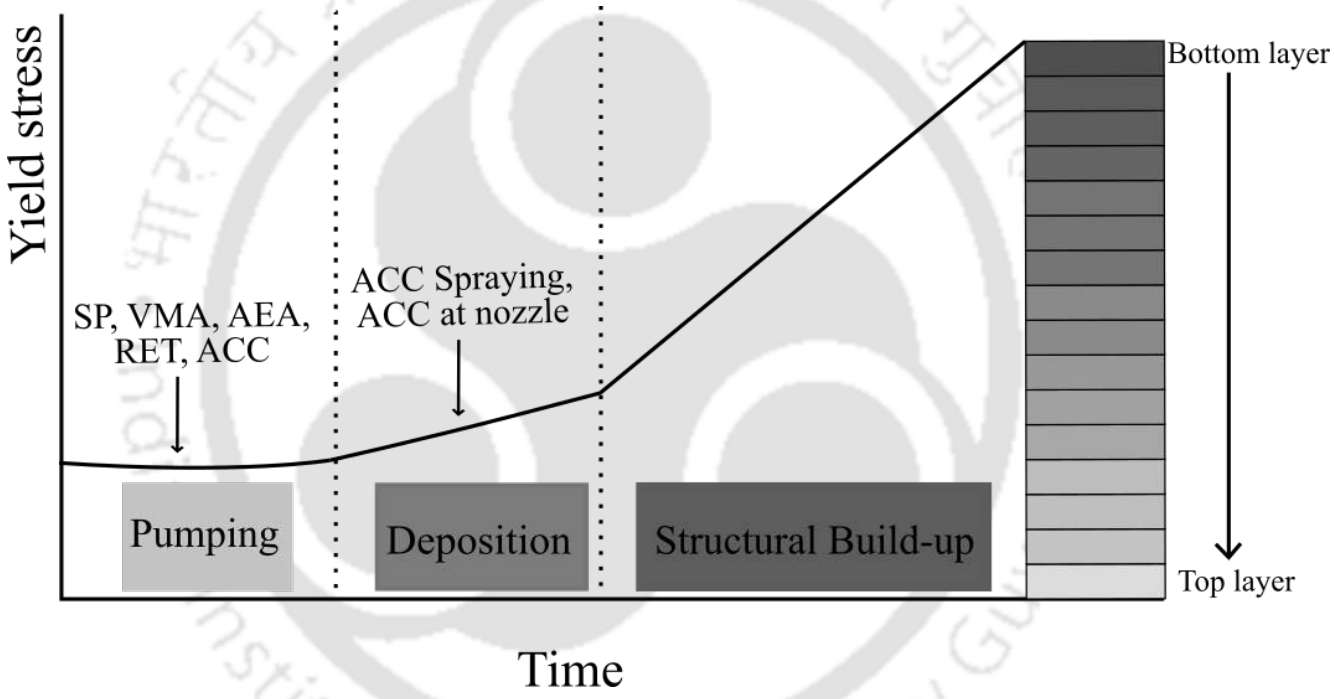

Figure 2.14: Schematic diagram of typical evolution of yield stress with time and introduction time of chemical admixtures for required buildability (adopted from (Panda et al., 2019)).

Table 2.3: Summary of influence of chemical admixtures on rheological behaviour of 3DCP

Admixture	SY	DY	V	T	Remarks	Ref.
SP	↓	↓		↓	Retards at higher dosages. The change in V is not significant.	(Papo and Piani, 2004; Qian, 2021; Souza et al., 2022)
VMA	↑	↑	↑	↑	Retards at higher dosages.	(Liu et al., 2021; Ma et al., 2018; Sun et al., 2020)

					The rate of increase in V is higher than SY and DY.	
ACC	↑	↑			Extrusion pressure is increased at higher dosages.	(Bhattacherjee and Santhanam, 2020; Rubin et al., 2021; Souza et al., 2022)
RET	↓	↓			Structuration rate is affected at higher dosages.	(Chen et al., 2020d; Mohan et al., 2021; Souza et al., 2022)
AEA	↓	↓	↑	↑	Instability is caused at higher dosages. Compatibility issues with other chemical admixtures	(Alghamdi and Neithalath, 2019; Markin et al., 2021; Tarhan and Şahin, 2021)

SY – Static yield stress, DY – Dynamic yield stress, V – Viscosity, T - Thixotropy

2.4 Review on 3DP-FC

Employing such multifunctional material (i.e. FC) to additive manufacturing helps in reducing the material wastage, time for construction and cost of production. 3DP-FC has attracted significant attention although the current status of studies conducted in this area is limited. Further, there are various challenges encountered in employing such material with conflicting attributes required for 3DCP. Therefore, this section provides a review on influence of various parameters on stability, rheology, mechanical characteristics of 3DP-FC.

2.4.1 Influence of admixtures on stability of 3DP-FC

Amongst the various foam properties, foam density is a key factor in determining the amount of foam requirement to obtain the desired concrete density. ASTM C796 has prescribed the desired foam density range as 30-65 kg/m^3 for preformed FC. The stability of the foam formed is critical in maintaining the desired concrete density. Hence the type of surfactant (which influences the bubble microstructure) and the rheology of the mortar enclosing the bubble are expected to play a vital role in achieving stable 3DP-FC mix with actual density within ±50 kg/m^3 of design density. The surfactant characteristics has significant impact on properties of foam as it affects the surface tension and gas liquid interfacial properties. In particular, the foam stability reflects the life of lamellae in the generated foam. It is the function of various parameters like thickness of lamellae, viscosity of liquid, elasticity of film and bubble size. Further, foam stability is an essential parameter for foam concrete production to ensure a uniform cellular structure of concrete as the bubble should remain stable till the concrete sets (sahu et al., 2018).

The rheology of the base mix influences foam stability by affecting the distribution and size of air bubbles. A stable rheological profile ensures that air bubbles remain uniformly distributed, preventing coalescence or segregation, which is essential for maintaining the lightweight and insulating properties of foam concrete. Proper rheology prevents foam from separating from the cement paste, which can otherwise lead to non-uniform density and compromised structural integrity, thereby reducing the overall stability of the printed object. Additionally, an optimal yield stress in the base mix supports the foam structure by providing a threshold stress above which the mix behaves as a solid, helping to maintain the stability of the air bubbles and preventing them from collapsing or merging. In this regard, study was conducted by Cho et al., (2022) on the influence of paste rheology on foam degradation during the pumping of 3DP-FC. Their experimental outcomes proved that mixes with higher foam content showed a better stability due to the cushioning effect of bubbles regardless of the stiffness of the base mix. However, on contrary to above, Markin et al., (2021) reported that when the density of the concrete mixture decreased, the stability of the foam in the mixture decreased significantly. They also concluded that although the increase in the surfactant concentration improved the stability, but the enhancement was not significant. Further, it was highlighted that as the rheology requirements of 3DP-FC are different, foams that are stable in conventional FC may not be suitable for 3DP-FC. In this line, Cho et al., (2021) used calcium sulfoaluminate cement (CSA) to reduce the setting time and subsequently enhance the thixotropy of 3DP-FC in the early age. Similar strategy has been reported by Jones et al., (2016) earlier in traditional FC mixes to counteract the foam instability issue. The authors pointed out that the buoyancy force of foam bubbles and bubbles with thin lamellae added to instability of foam particularly in mixes with lower density. Hence, the above problem was reported to be solved through use of CSA.

2.4.2 Influence of admixtures on rheology of 3DP-FC

Though researchers studied the rheology of FC in the past, a very few studied the rheology of printable FC. In designing the 3DP-FC, dimensional stability plays a key role as the formwork is not used. In case of FC (i.e. mixture of cement, sand, water and foam), due to low yield stress dimensional stability and buildability is not achieved (Falliano et al., 2018, 2020). However, researchers have attempted different mix design methods to print the FC by adopting various mineral and chemical admixtures.

Markin et al., (2019) used mixture design approach to obtain the printable FC. This approach can be applied to both pre-foaming and mixed foaming technique. In case of pre-foaming technique Foam and cement-based matrix were prepared separately and mixed later to obtain a stable mix of required density. Using mixed foaming method, they could produce and deliver the FC directly to print head using both cavitation disintegrator and turbulence mixers (Markin et al., 2019). Cho et al., (2021) attempted to print the FC without using any chemical admixture. Instead, they used calcium sulfoaluminate cement (rapid hardening) to attain the buildability. Static and dynamic yield stresses varied from 347 to 812 Pa and 158 to 623 Pa respectively for FC with densities ranging from 700 to 1400 kg/m^3. Falliano et al., (2020) studied the extrudability of FC by using a certain percentage of viscosity modifying admixture (not disclosed by the researcher). It was also concluded that air bubble size in 3DP-FC is more homogeneous when compared to classical FC. But the limitation of the study is that the results are obtained from a procedure similar to smart dynamic casting and not from 3D printing. The pumping and extruding actions might not produce the same results. Markin et al., (2021) reported that after printing, nearly 10 and 19% of deviation from the target density of 1200 and 800 kg/m^3 respectively. Furthermore, the influence of silica fume and hydroxypropyl methyl cellulose (HPMC) on 3DP-FC was studied by Liu et al., (2021) and they concluded that both materials reduced the foam bleeding rate. However, silica fume increased the wet density and static yield stress of FC whereas HPMC stabilized the foam along with increasing the dynamic yield stress and viscosity. The static yield stress, dynamic yield stress, and viscosity for a density of 1550 to 1850 kg/m^3 varied as 1113-1658 Pa, 66.4-230.1 Pa, and 2.08-3.71 Pa.s respectively. In the similar line, Cho et al., 2020 varied Nano-silica from 0 to 3% which helped in improving the static and dynamic yield stresses from 78 and 62 Pa to 386 and 292 Pa respectively. Pasupathy et al., (2022) used porous aggregate as a replacement of sand and concluded that the rheological properties are enhanced with this substitution.

2.4.3 Influence of admixtures on mechanical properties of 3DP-FC

There is very limited research available in describing the mechanical and functional characteristics of printable FC. The mechanical performance of 3DP-FC is highly dependent on the density and ingredients of the mixture. As observed from the literature, the influence of density on mechanical properties is clearly established (Ramamurthy et al., 2009; Sahu and Gandhi, 2021; Selija and Gandhi, 2022). Furthermore, the influence of admixtures on 3D printed specimens is summarized in Table 2.4. Falliano et al., (2020) compared the classical

FC with printable FC by curing the specimens in air, water and cellophane and concluded that the printable FCs perform better in compressive and flexural strengths irrespective of the density range. However, with the increase in water to cement ratio, the air curing resulted in good compressive strengths than the water and cellophane curing (Falliano et al., 2018). The increase in mixing intensity from 1200 to 3000 rpm increased compressive strength up to 70% and flexural strength up to 100%. Furthermore, homogeneity of bubble structure resulted in increased compressive strength when compared to classical FC (Falliano et al., 2020). Nevertheless, mechanical anisotropy was observed by Liu et al., (2022) in 3DP-FC when tested in different directions and it is worth noting that the anisotropy increased with increase in the admixture like sulphoaluminate cement that is replaced with cement at 0, 6, 10, 16, and 22%. On the other hand, fine aggregate replacement with porous aggregates also showed an improvement in the compressive strengths when compared to the control mixes (Pasupathy et al., 2022).

Table 2.4: Summary of mechanical properties of 3DP-FC reported in the literature.

Ref.	Materials	Target Density (kg/m^3)	Compressive strength (MPa)	Flexural strength (MPa)	Remarks
(Markin et al., 2019)	Cement (52.5), FA, SP, and foaming agents (SK-155 and Oxal PLB6).	800-1500	4.4-35 (7 days) 5.8-47.4 (28 days) 4.9-53 (120 days)	1.7-4.1 (7 days) 1.2-3.2 (28 days) 0.9-3.2 (120 days)	Flexural strength decreased due to drying shrinkage.
(Cho, 2019)	Cement, FA, fine sand, fibers (PP) (0.45%), NS (2%), foam.	1400	24.51-31.12 (7-28 days)	2.33-2.43 (7-28 days)	Addition of NS and PP improved the strengths.
(Falliano et al., 2020)	Cement (52.5 type 1, 42.5 type 2A, and type 4A), water, foam, W/C-0.3,0.5.	400-800	1.14-12.23	0.09-2.53	Specimens were cured separately in air, cellophane and water.
(Markin et al., 2019)	Cement (52.5), FA, SP, foaming agent (Oxal PBK6)	1000	8.20-10.40 (7-28 days)	1.94-2.12 (7-28 days)	
(Markin et al., 2021)	Cement, SF, FA, alumo-silicate,	1000	2.9-6.0 (6-9 days)	-	Addition of alumo-silicate improved

Ref.	Materials	Target Density (kg/m^3)	Compressive strength (MPa)	Flexural strength (MPa)	Remarks
	foam, SP, foaming agent (Oxal PBK6)		3.1-4.7 (12-14 days) 4.2-8.3 (35-38 days)		substantially followed by SF and control mixture.
(Pasupathy et al., 2022)	Cement, fine sand, EP, SP, foaming agent (sodium dodecyl sufate), W/C-0.32,0.52.	800-1350	0.5-9 (7 days) 1-17 (28 days)	-	Addition of EP improved the strengths.
(Liu et al., 2022)	Cement (42.5), SAC, fine sand, foaming agent.	1687-1778	6-20 (28 days)	-	Mechanical anisotropy increased with increase in SAC cement.
(Gao et al., 2023)	Cement (42.5), HPMC, PP fibers, W/B – 0.4, S/B – 1.1.	1159-2211	47-15 (28 days)	-	Thermal conductivity varied from 0.288 to 0.255 W/m.K (density ranged from 1600 to 1160 kg/m^3)

FA-Fly ash, SP-Superplasticizer, PP-Polypropylene, NS-Nan0-silica, W/C-Water to cement ratio, SF-Silica fume, EP-Expanded perlite, SAC-Sulphoaluminate cement.

2.5 Summary of literature review

3DCP is a digital construction technique that requires specific rheological properties. The rheology of these materials depends on shear rate applied, age, and resting time. Further, fresh state characterization of 3DCP involves addressing pumpability, extrudability, and buildability from the mixer to the deposition of material for printing. Rheological parameters like dynamic yield stress, static yield stress, and thixotropy are related to these qualities. These rheological properties significantly influence the concrete printing process. Moreover, mix designs should incorporate sustainable materials and proper chemical admixtures for thixotropic behaviour and robustness. Nevertheless, optimizing admixture dosage is crucial for achieving required buildability in 3DCP. Non-optimal dosages can cause complications, such as retardation effects and higher extrusion pressure. Understanding material chemistry, accelerator selection, reaction mechanisms, and dosage optimization is essential for 3DCP.

3D printing of FC poses many challenges during and after the printing. For instance, FC is generally designed to have self-flowing nature with high workability which may restrict the buildability of FC. On the other hand, if the mixes are designed to be stiffer, it may affect the stability of foam. Hence consistency of FC needs to be designed from 3D printing perspective which is a novel research area to be explored. The maintenance of desired density in 3DP-FC hinges on foam stability, influenced by factors such as surfactant choice, bubble microstructure, and mortar rheology. While it is reported by one of the research group that the higher foam content improved stability due to bubble cushioning during pumping, but the other research group observed a substantial decline in foam stability as 3DP-FC density decreased, resulting in significant deviations from target densities. Although increasing surfactant concentration enhanced stability, the improvement is not statistically significant. Additionally, conventional foam stability may not translate to 3DP-FC due to differing rheological requirements. To address this, CSA cement is utilized to enhance stability, a method previously employed by many researchers in conventional FC mixtures to mitigate foam instability caused by thin lamellae and buoyant force in lower density mixes. The use of CSA effectively resolved these issues, emphasizing its potential for stabilizing 3DP-FC mixes.

Several studies have delved into optimizing mix constituents for 3DP-FC to attain desired rheological and mechanical properties. Researchers explored printing of FC using CSA cement, observed the variations in static and dynamic yield stresses across different densities. Scholars have also investigated the effects of silica fume and HPMC on 3DP-FC, noting reductions in foam bleeding rates and improvements in various properties with their addition. Further, the observations made on enhancements in yield stresses with Nano-silica and HPMC additions, respectively. Mechanical performance in 3DP-FC is heavily influenced by density and mix ingredients, with superior performance in printable FC compared to classical FC across various densities and curing methods. Increased water-to-cement ratios favoured air curing for higher compressive strength, while intensified mixing improved both compressive and flexural strength. However, mechanical anisotropy was observed with higher cement replacement levels. Various admixtures and fine aggregate replacements have shown promise in enhancing compressive strength compared to conventional aggregates. Overall, optimizing mix constituents and printing parameters are crucial for achieving desired properties in 3DP-FC.

2.6 Research gaps

The literature review identified major research gaps, indicating potential future research directions. Following are the research gaps identified.

- Stability of 3DP-FC: The review shows that stability of 3DP-FC can be altered by the paste stiffness encircling the bubble and surfactant characteristics. Also, studies have proved that low density mixes and mixes with high stiffness (caused by the paste enclosing the bubble) are more susceptible to greater extent of air bubble breakage. Further, researchers have used different alternatives to increase the yield stress and rate of hydration to tackle the instability of 3DP-FC. However, research on influence of surfactant characteristics on stability of the 3D printable foam concrete are scarce.
- Buildability of 3DP-FC: From the review conducted, it is understood that the foam causes the reduction in buildability and this reduction is commonly addressed by enhancing the reactivity of the binding material. Further, attempts were made to enhance buildability by improving the segregation resistance with the aid of HPMC and by increasing the static yield stress through silica fume addition. However, silica fume replacement at higher levels is found to reduce the mechanical properties of foam concrete. Moreover, it is to be noted that addition of CSA cement reduces the open time. Hence, there is need to improve the rheology of paste surrounding the bubble and thereby improve the buildability without causing the stability problems in the mixture.
- Mechanical and functional performance of 3DP-FC: There is a very limited research available in describing the mechanical and functional characteristics of printable FC. The mechanical performance of 3DP-FC is highly dependent on the density and ingredients of the mixture. With implementing new strategies to enhance the stability and buildability of 3DP-FC, the mechanical and thermal performance tend to get altered.

2.7 Motivation for research

FC is a cementitious mixture entrained with air through the use of foam to reduce the density and improve the functional properties like thermal insulation, acoustic isolation, fire resistance, and energy absorption. Thanks to the researchers for employing such multifunctional material to sustainable technology of additive manufacturing. Adopting these new-era construction methods for FC accelerates the construction simultaneously reducing the cost and labour

requirement. Further, it is observed that the 3DP-FC shows a more homogeneous distribution of air bubbles with smaller dimensions when compared to the classical FC due to the increased consistency. Recently many researchers are adopting this 3DP-FC as an environmentally sustainable solution mostly for non-structural applications as it is proved to be economical in terms of both construction times and costs. Even though in the case of FC, utilization of cement on slightly higher side is not commonly regarded as a good sign from ecological point of view, nevertheless the additive manufacturing proved to be sustainable by reducing the carbon emissions and resource demands, lowering energy usage, lesser waste generation, and good recyclability. Generally, it is preferable to analyze the environmental impact of 3D printed structures in complex structures wherein, structural optimization and hybrid functional design strategies are used (i.e. production of structures with higher complexity with minimal environmental costs) (Markin et al., 2022). The maintenance of desired concrete density relies heavily on foam stability. Consequently, the choice of surfactant, impacting bubble microstructure, and the mortar's rheology encompassing the bubble, are anticipated to be pivotal factors in achieving a stable 3DP-FC mix, ensuring an actual density within ±50 kg/m^3 of the intended target density. Further, literature review reveals that there is a very limited research available in this regard. As a result, there is a pressing need for comprehensive studies to examine the influence of surfactant characteristics and the properties of the paste surrounding the bubbles. Additionally, the mechanical and functional properties of 3DP-FC need to be studied due to its influence on pore distribution and rheology of the paste enclosing the bubble.

Chapter 3

Objectives and Methodology

3.1 General

The previous chapter explored the necessity of in-depth investigation on influence of rheology and surfactant characteristics on stability, printability, and mechanical properties of 3DP-FC. Further it is recommended to use appropriate admixtures for maintaining the stability and improving the buildability of 3DP-FC mixes. Through the review of prior research in this field, objectives and extent of the current research is described in the following sections.

3.2 Objectives

The objectives of the current study are

- To study the influence of surfactant characteristics (viscosity and surface tension) on stability of 3DP-FC.
- To improve the buildability and stability of 3DP-FC by enhancing the rheological behaviour of mixture with different densities (for both design densities 1000 and 1300 kg/m^3) using fly ash (FA) as a filler replacement and adding poly vinyl alcohol (PVA) fibers as reinforcement.
- To study the mechanical properties (compressive strength, flexural strength, and bond strength) of 3DP-FC and compare it with control mixes (printed samples) and samples cast with similar densities (for both 1000 and 1300 kg/m^3). Further their dependence on micro structure of the printable foam concrete will also be studied.
- To study the thermal and sorption characteristics of 3DP-FC samples prepared with addition of PVA fibers and sand replaced with FA for both the design densities 1000 and 1300 kg/m^3.

3.3 Scope of the present study

The scope of the study is limited to the following with respect to raw materials and methods to be adopted.

- ✓ This study is restricted to studies on one natural surfactant (saponin based hingot stabilized with additive xanthan gum) and one synthetic surfactant (sodium lauryl sulphate stabilized with additive carboxymethyl cellulose sodium salt). Different surfactants and stabilizers are chosen to understand the effect of type of surfactant and its compatibility with the stabilizer. Further, these combinations are well studied and established with conventional FC at Indian Institute of Technology Guwahati laboratory.
- ✓ The study is also restricted to use of materials from one source for each of mineral admixtures (FA and silica fume), chemical Different surfactants and stabilizers are chosen to understand the effect of type of surfactant and its compatibility with the stabilizer. Further, these combinations are well studied and established with conventional FC at Indian Institute of Technology Guwahati laboratory.admixtures (superplasticizer and viscosity enhancing agent) and fibers (PVA).
- ✓ Design densities of FC adopted for this study are 1000 kg/m^3 and 1300 kg/m^3.
- ✓ The mixes were considered to be printable, if the slump value is less than 8 mm for all the adopted mixtures (based on Tay et al., 2019).

3.4 Methodology

The present study is conducted in two different stages. In stage 1, the influence of surfactant characteristics on stability of 3DP-FC is studied. Later, in stage 2, the synergistic influence of admixtures (FA and PVA fibers) on enhancement of stability, buildability, and mechanical properties of 3DP-FC is studied. Figure 3.1 shows the flowchart depicting both stages of experimentation program.

- ➢ A review is conducted on foam concrete constituents, stability, and performance. Further, a review on 3D printing of foam concrete and challenges associated with this technology is carried.
- ➢ In stage 1, the influence of surfactant characteristics on stability of 3DP-FC is studied. Initially, studies are conducted in fresh state through measurement of slump, slump flow, yield stress and fresh density. Further, the visual observations studies are conducted to check the extrudability and buildability of 3DP-FC. Nonetheless, these mixes were printed and cured in water for 28 days. After the curing period these specimens are tested for air void parameters to study the effect of surfactants on the air void microstructure

- In stage 2, the influence of admixtures like fly ash (as a filler replacement) and PVA fiber addition as reinforcement on enhancement of stability, buildability and mechanical properties of 3DP-FC are studied. Initially, the printability (based on Tay et al., 2019) is achieved through adjusting the superplasticizer content for all the mixtures. Further, these mixtures are tested for the rheology and stability in the fresh state. Later these mixes are cast and printed to test the mechanical performance.
- Studies are conducted to measure the thermal and sorption characteristics of 3DP-FC specimens cured for 56 days. Later, microstructural studies are conducted to validate the mechanical and functional performance of 3DP-FC mixtures.

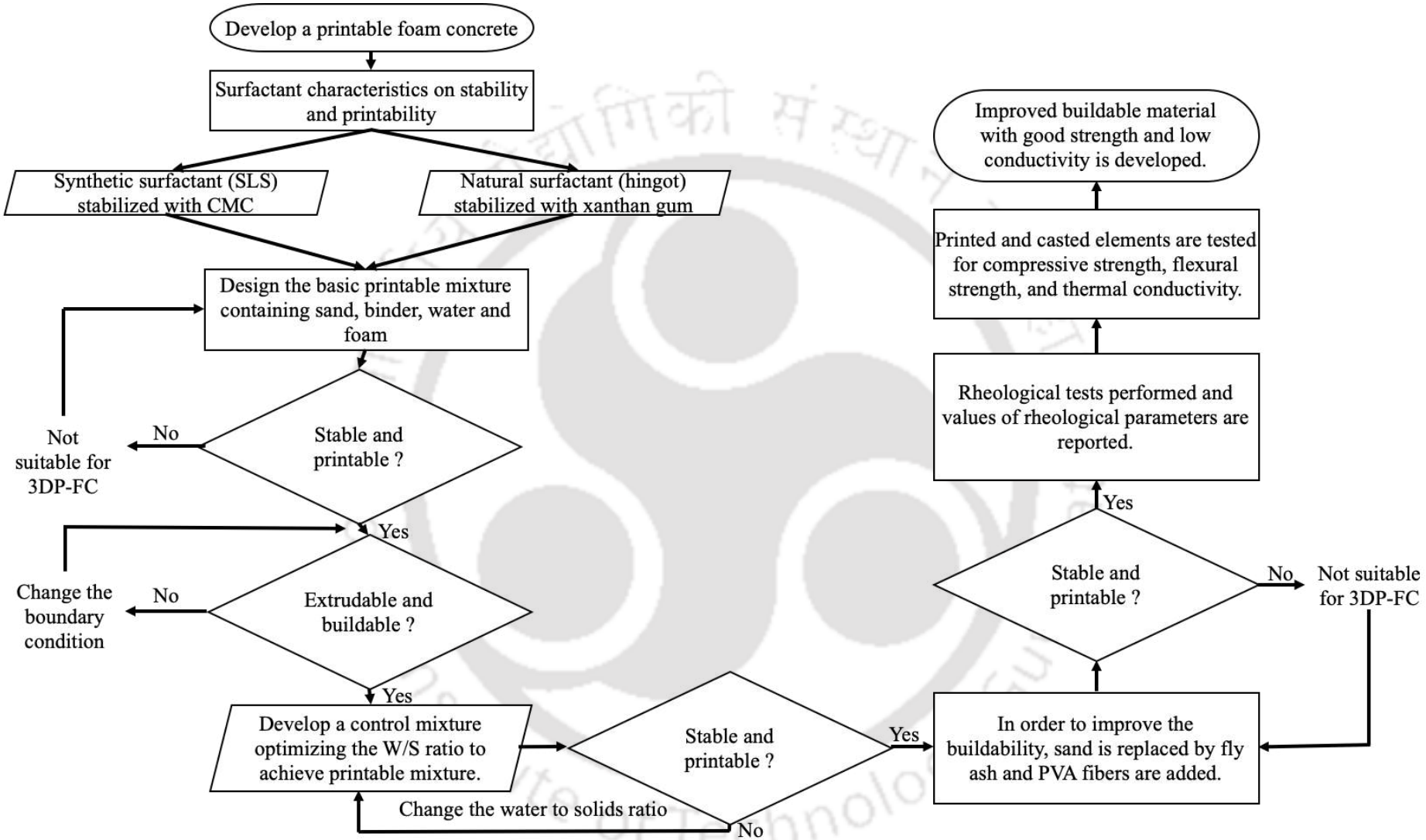

Figure 3.1: Flow chart describing the research methodology.

Chapter 4

Influence of Surfactant Characteristics on Stability and Buildability of 3D Printable Foam Concrete

4.1 General

Surfactants (or foaming agents) play a vital role in foam generation and stabilization by reducing the surface tension of the water. Stability of the formed foam is critical in maintaining the desired concrete density. Hence, surfactant characteristics (which influences the bubble microstructure) and rheology of the mortar enclosing the bubbles play a crucial role in achieving a stable 3DP-FC mixture with a fresh density within ±50 kg/m^3 of the design density. Therefore, this chapter aims to study the influence of surfactant characteristics on stability and buildability of 3DP-FC.

4.2 Materials, mixture design, and mixing method

This section provides an overview of the materials, mixing method, and mixture design adopted to study the influence of surfactant characteristics on stability and buildability of foam concrete.

4.2.1 Materials

The basic materials used in the current study are sand, binder, water and foaming agent. Binder is composed of cement and silica fume (SF) for all the mixes to increase the mixture's buildability. Two different surfactants are used in this study to investigate the effect of surfactant type on stability of 3DP-FC. The first is an anionic synthetic surfactant (i.e. sodium lauryl sulfate (SLS)) stabilized with carboxymethyl cellulose (CMC), while the second is a saponin-based natural surfactant (hingot stabilized with xanthan gum (XG)) (Sahu et al., 2021; Khwairakpam and Gandhi 2020; Selija and Gandhi 2022). Hydroxy propyl methyl cellulose (HPMC) is used as a viscosity enhancing agent at 0.1% of the binder content. Sieved sand finer than 300μm is used as fine aggregate. Table 4.1 shows the attributes of the materials used in present study.

Table 4.1: Characteristics of the materials used for the current study

Material	Characteristics	Source	Specific Gravity	Application
Cement	OPC - 43 grade confirming to IS 8112 – 2013 and having a bulk density of 1600 kg/m^3.	Dalmia cement plant, Morigaon, Baghjhap, Assam.	3.14	Binder
Sand	River sand sieved through 300µm conforming to IS 383 – 2016 and having a bulk density of 1628 kg/m^3.	Brahmaputra river, Dudhnoi, Goalpara, Assam.	2.65	Fine aggregate
SF	Conforming to IS 15388 – 2003 and having a bulk density of 500 kg/m^3.	Elkem micro silica, AKJ Engineers Pvt. Ltd., Behrabari, Guwahti.	2.17	Binder / Mineral admixture
Water	-	IITG Treatment Plant	1.00	-
H	Desert fruit containing extractable saponin	Madhya Pradesh	-	Surfactant
XG	Naturally occurring microbial expolysaccharide.	Loba Chemicals, Mumbai.	-	Stabilizer
SLS	Synthetic surfactant (Anionic)	Loba Chemicals, Mumbai.	-	Surfactant
CMC	Viscosity modifying agent	Loba Chemicals, Mumbai.	-	Stabilizer
HPMC	Model: HS 1218, Viscosity of 160000 mPa.s	Foroly Commercio Pvt. Ltd.	0.41	Viscosity Modifying agent

SF – Silica Fume, H – Hingot Fruit, XG – Xanthan Gum, SLS – Sodium Lauryl Sulfate, CMC – Carboxy Methyl Cellulose, HPMC – Hydroxypropyl Methyl Cellulose.

4.2.2 Mixture design

Experiments for the current study are conducted for sand (sieved through 300µm) to binder ratio of 2 and water to solids ratio (W/S) of 0.2. Binder is composed of 70 percent cement and 30 percent SF for all the mixes to increase the mixture's buildability. Density based mix-design depicted in ASTM C796 is followed for this study. The mix proportions adopted for various 3DP-FC mixes used in this study is shown in Table 4.2.

Table 4.2: Experimental mixture design to study the influence of surfactant characteristics

Type of Surfactant	**Surfactant + Stabilizer**	**Stabilizer (%)**	**Mix ID**	**For 1 m³ of 3DP-FC (in kg)**				
1300 kg/m³				C	SF	S	W	F
Synthetic	SLS + CMC	0 %	SLCM0	252.78	108.34	722.20	207.60	9.07
		0.1 %	SLCM1	252.78	108.34	722.20	207.06	9.61
		0.2 %	SLCM2	252.78	108.34	722.20	206.25	10.42
		0.3 %	SLCM3	252.78	108.34	722.20	205.98	10.69
		0.4 %	SLCM4	252.78	108.34	722.20	205.98	10.69
Natural	H + XG	0%	HXG0	252.78	108.34	722.20	205.43	11.23
		0.1 %	HXG1	252.78	108.34	722.20	203.51	13.16
1000 kg/m³				C	SF	S	W	F
Synthetic	SLS + CMC	0 %	SLCM0	194.45	83.34	555.56	151.32	15.34
		0.1 %	SLCM1	194.45	83.34	555.56	150.41	16.25
		0.2 %	SLCM2	194.45	83.34	555.56	149.04	17.63
		0.3 %	SLCM3	194.45	83.34	555.56	148.58	18.09
		0.4 %	SLCM4	194.45	83.34	555.56	148.58	18.09
Natural	H + XG	0%	HXG0	194.45	83.34	555.56	147.66	19.01
		0.1 %	HXG1	194.45	83.34	555.56	144.40	22.27

C - Cement, SF - Silica Fume, S - Sand, W - Water, F – Foam.

4.2.3 Preparation of foam concrete

In order to produce a homogeneous mixture, the mixing process and the amount of time required for mixing are crucial. The first step of the mixing process adopted in this study involves thorough mixing of the dry materials for 1 minute at 107 rpm using a Hobert planetary mixture. Then, approximately 70-80% of water blended with HPMC is added and mixed at 198 rpm for another 1 minute. Later, scrapped for 30 seconds and then the remaining water is added and mixed at 361 rpm for 30 seconds. The resulting mix is inspected for lumps that might affect the mixture's homogeneity. The pre-formed foam is then added and mixed at 107 rpm for 30 seconds and later scraping is continued for 30 seconds. Finally, another round of mixing is done for 30 seconds at 107 rpm to ensure homogeneity.

4.2.4 Foam production parameters

Two different surfactants are used in this study to investigate the effect of surfactant type on stability of 3DP-FC. Different surfactants and stabilizers are chosen to understand the effect of type of surfactant and its compatibility with the stabilizer. Further, these combinations are well studied and established with conventional FC at Indian Institute of Technology Guwahati laboratory. The first is an anionic synthetic surfactant (i.e. SLS) stabilized with CMC, while the second is a saponin-based natural surfactant (hingot stabilized with XG)) (Sahu et al., 2021; Khwairakpam and Gandhi 2020; Selija and Gandhi 2022). SLS is easily available synthetic surfactant and its performance is well established in literature (Sahu et al., 2021, Gandhi et al., 2010, Raj et al., 2023). Further, the stabilization of SLS with CMC is found to be highly compatible (Sahu et al., 2021). On the other hand, hingot is a natural surfactant and widely available in India. It contains 22-27% extractable saponin content (Selija et al., 2020). Further, the stabilization of hingot using xanthan gum is explored on conventional FC. All these combinations are well understood in the conventional FC, however, the conflicting rheological requirements in 3DP-FC could alter the stability and printability.

Figure 4.1: Surfactant solution preparation from hingot fruit.

Surfactant solutions are prepared by diluting the surfactant powder in water at a certain concentration. The dilution of surfactant solution depends on the stability of the foam. The concentration of surfactant solutions adopted in this research are adopted from the literature study. For synthetic surfactant (i.e. SLS) 5% concentration (i.e. 50g in 1000 ml) is adopted,

whereas for natural surfactant (i.e. hingot), it is 6% (Sahu and Gandhi, 2021; Selija and Gandhi, 2022). Although, SLS is commercially available in the market as powdered form, but saponin in hingot is extracted by following the procedure depicted in Figure 4.1. The stabilizers CMC and XG are added at varying dosages in combination with surfactants SLS and Hingot respectively. The upper limits of CMC and XG are fixed at 0.4% and 0.2% respectively of the volume of solution prepared based on preliminary studies.

The experimental set up of the foam generator used in the present study comprises of an air compressor with an outlet valve as shown in Figure 4.2. A pressure regulator valve included with the compressor, facilitates easy control of the needed pressure. In this study foam generation pressure is kept constant at 4 kgf/cm^2 (392.3 kPa) for synthetic surfactants and 5.9 kgf/cm^2 (578.6 kPa) for natural surfactants. The process of pumping pressured air into the solution causes the foam to expand, resulting in thick foam production.

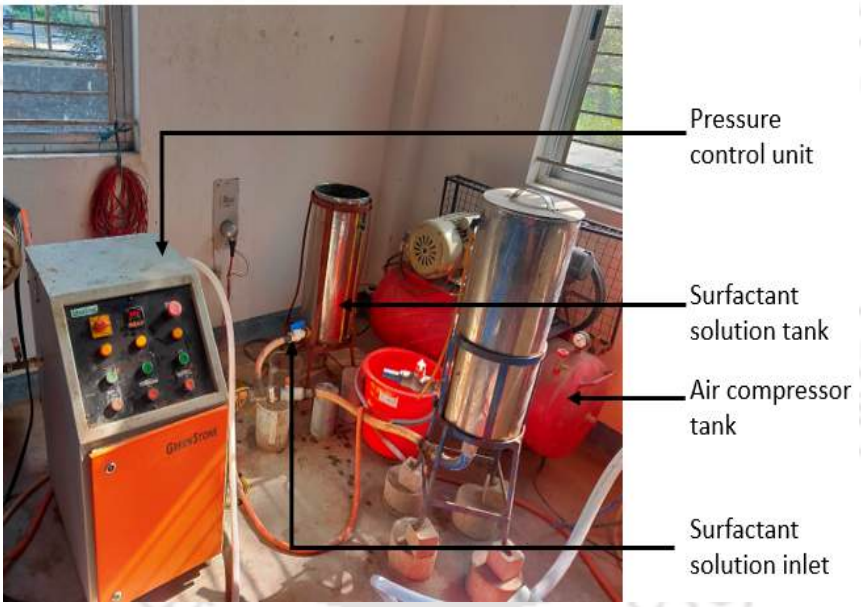

Figure 4.2: Foam generator set up

4.3 Tests conducted to study the influence of surfactant characteristics on stability and printability of 3DP-FC

This section describes the test methods that are adopted in the present study for assessing the effect of surfactant characteristics.

4.3.1 Printing parameters

The extrusion-based 3D concrete printer of print volume 1 m × 1 m × 1 m manufactured by Deltasys-Eforming is used in this study (Figure 4.3). The Gantry printer used has 3 degrees of freedom with a nozzle size of 20 mm and nozzle travel speed of 200 mm/sec (maximum). It is equipped with stepper motor of 0.1-0.5 mm accuracy and a Z-resolution of 1 mm.

Initially, digital CAD model is sliced using simplify 3D software and this information is given to the controller unit, which subsequently sends the commands to the printer to deposit the material. This printer contains a customized extruder unit, where the material can be fed continuously. Material fed into the extruder unit is extruded through the nozzle using an Archimedes screw to maintain the continuity in the material flow.

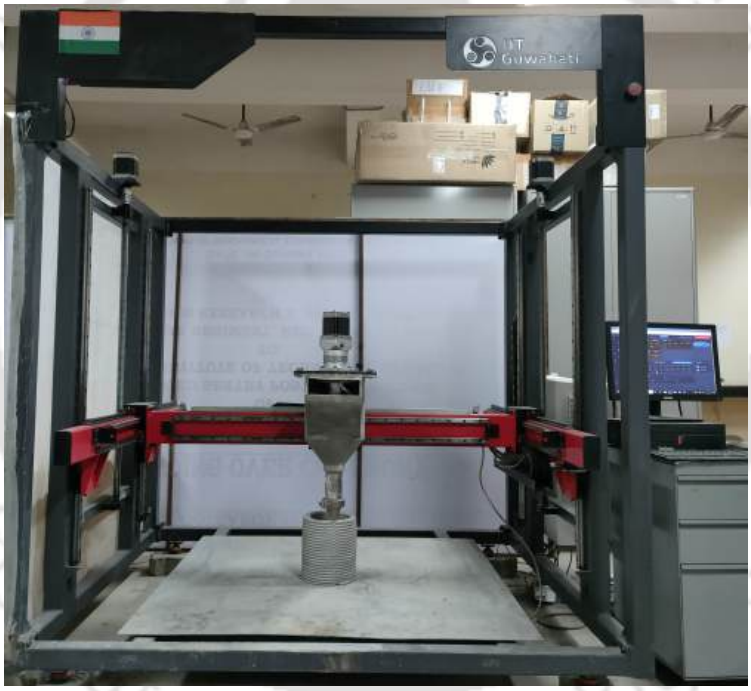

Figure 4.3: 3D concrete printer setup (Panda and Tran 2022; Dey et al., 2023).

Extruding is the action of extrusion of fresh materials from the print head. In this study, extrusion of soft solids like 3DP-FC is performed by screw type extruder (auger extruder). Beams of 700 mm length and 50 mm height are printed with 10 mm filament height to study the extrudability of 3DP-FC. The print speed of 80 mm/sec is kept constant for the whole study. Later these beams were cured for further studies. Following the extrudability test, buildability test is conducted by printing maximum number of layers without the discontinuity and structural collapse. A cylinder of 200 mm diameter is printed (10 mm filament height) for all

the mixes and a print speed of 80 mm/sec is kept constant. These printing tests are conducted at ambient room temperature (25^0C – 28^0C) and annual average relativity humidity of 76%.

4.3.2 Studies on surfactant characteristics

Earlier studies have proved that the essential characteristics of the surfactant such as viscosity and surface tension have significant effect on various foam properties (Raj et al., 2022). Hence the present study attempts to evaluate the above-mentioned surfactant characteristics. Surfactant viscosity is basically due to the collision of adjacent particles in a fluid flowing at differing speeds. As the number of particles increases, the viscosity also increases. In this study, the viscosity of the surfactant is measured using Anton paar rheometer MCR 101 (Figure 4.4) model employing a concentric cylinder geometry at a constant rotational speed of 150 rpm and a constant temperature of 25^0C.

Generally surface tension in liquids is caused by the discrepancy between the intermolecular cohesive forces of the fluid particles at its boundary. Tensiometer (Kyowa DY300) is used to study the surface tension of the surfactant solution using Wilhelmy plate method (Figure 4.5). In this method, platinum plate (chosen due its chemical inertness and easy to clean) is immersed in the liquid and the force required to hold the plate (i.e. to restrict the surface tension to pull the plate) is measured.

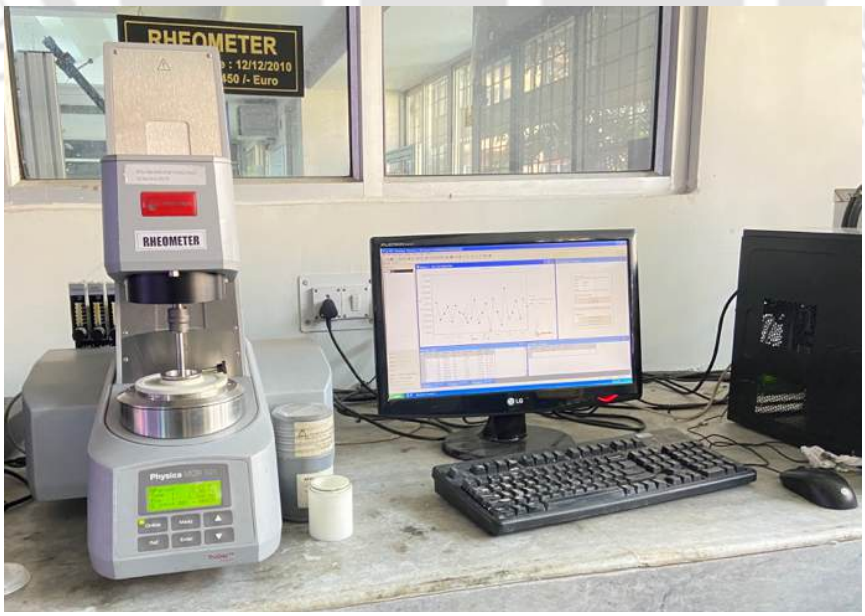

Figure 4.4: Rheometer with concentric cylinder geometry to measure viscosity of surfactant.

Figure 4.5: Tensiometer for measuring the surface tension of the surfactant.

4.3.3 Studies on foam characteristics

The term "foam density" describes the foam's unit weight. Initial foam density (IFD), of the foam is measured immediately after its generation as shown in Figure 4.6(a). To assess the foam stability, free foam drainage test is adopted. The foam drainage setup employed in this investigation consists of a drainage pan with a conical base and a nominal volume of 1.612 litres. The drainage pan's conical base is equipped with a polymethyl methacrylate tube with a 12.7 mm internal diameter, 25 mm length, and a 1.6 mm diameter hole at its bottom end (according with Def-stand 42-40/2) (Figure 4.6(b)). The drainage pan is filled with foam and the volume of the solution drained in 30 minutes is measured to measure the foam stability.

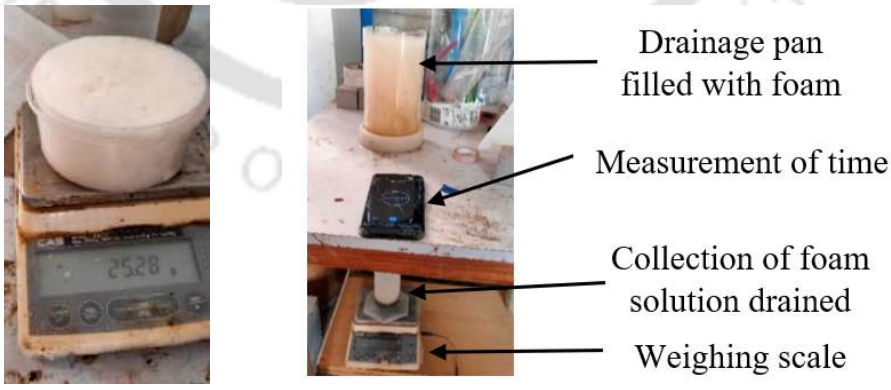

(a) (b)

Figure 4.6: (a) Measurement of IFD, (b) Experimental setup for foam drainage study (Def-stand 42-40 (2002)).

4.3.4 Studies on fresh state properties of 3DP-FC

Fresh density is an important physical characteristic which helps to assess the stability of the mix. In the present study, the stability of air bubbles in the 3DP-FC is assessed through measurement of the fresh density of the material before and after the extrusion process.

The consistency of foam concrete is measured using slump and slump flow tests. In order to determine the slump, the produced mix is fed to the slump cone in two layers, with each layer being tamped 20 times in line with ASTM C230 (Figure 4.7(a)). Using a trowel, extra material from the top surface is removed. Later, the cone is lifted gently and reduced height of the sample is measured and reported as slump (Figure 4.7(b)). Further, to assess the mixture's flowability, the flow table test is carried out in accordance with ASTM C1437. The mean diameter is determined by measuring the flow's diameter in two perpendicular directions after 25 blows.

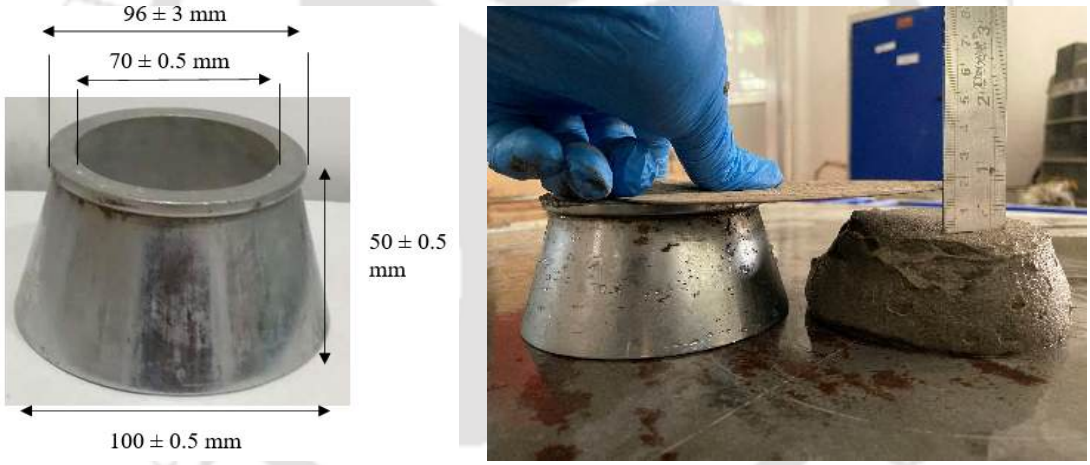

(a) (b)

Figure 4.7: (a) Flow cone as per ASTM C230, (b) Measurement of slump in flow table.

The static yield stress of the material is determined to study the force required to initiate the flow. The yield stress of the mixture of 3DP-FC is measured using a four-bladed (24 mm height (H) and 12 mm diameter (D)) vane shear equipment that is often used to assess the shear strength of soft clays (Figure 4.8). Vane is fully driven into the 3DP-FC filled mould until its top is 20 mm below the material's surface. The rotation is then maintained at 0.1°/sec until the sample failed. The maximum torque (T) at failure is calculated using the difference between

the beginning and final readings. The yield stress (τ_y) of the 3DP-FC sample is then calculated using the equation 1 suggested by Duzy and Boger (Dzuy and Boger, 2000).

$$T = \frac{\pi D^3}{2}\tau_y\left(\frac{H}{D} + \frac{1}{3}\right) \quad (4.1)$$

Figure 4.8: Laboratory vane shear test set up.

4.3.5 Air void characterization

Review shows that many researchers have studied the influence of different surfactants and stabilizers on micro structure of FC. However, in 3DP-FC, its unique rheological behaviour is expected to result in different micro structure with entrained macro pores unlike traditional FC. The current work attempts to investigate the air void parameters of concrete using optical microscope coupled with image analysis. It should be emphasized that for the successful use of image analysis, the specimen's surface treatment quality is crucial for the generation of reliable data. From the beam printed, four 50 mm cube examples for each density are cut, then moist-cured for 28 days (Figure 4.9(a) and (b)). All specimens are later split into 9 samples, with interlayer porosity taking into account as shown in the Figure 4.9(c) and (d). The surface treatment procedure is followed as per ASTM C457. Figure 4.9(e) shows the specimens after the surface treatment. A freely available image analysis software 'Image J' is used for the analysis of macro pores. Air voids of size more than 50 microns are considered for the analysis in order to study the macro pores entrained (Nambiar and Ramamurthy, 2007a). Four pictures from each sample is captured using an optical microscope at 0.7 X magnification. Calibration

studies showed that each pixel represented 0.183 microns. For each 3DP-FC mixture, a total of 36 images are taken at arbitrary positions on the six prepared surfaces. Later these images are digitized and converted to binary form for further analysis. The Feret diameter, which is the largest distance between two parallel tangential lines drawn to the air void, is used to estimate the air void size distribution in concrete. The air void parameters D50 and D90 derived from cumulative frequency curves indicate medium air void size and 10% oversize air void respectively. For each mix, the circularity factors were calculated as a function of the perimeter and surface area of each pore (Circularity index = 4π (Area/Perimeter^2)). For a perfect pore, circularity equals 1; for irregular shapes, it is smaller.

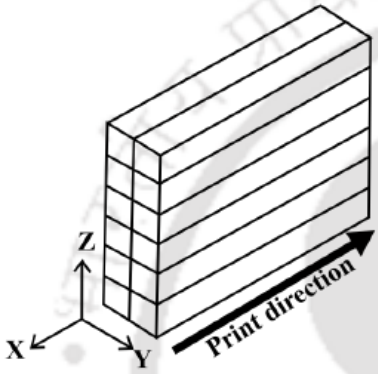

(a)

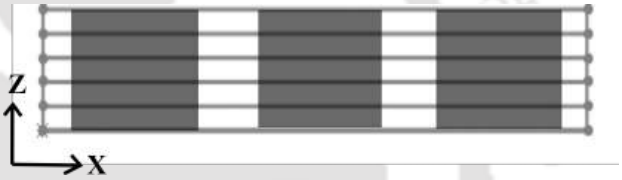

(b)

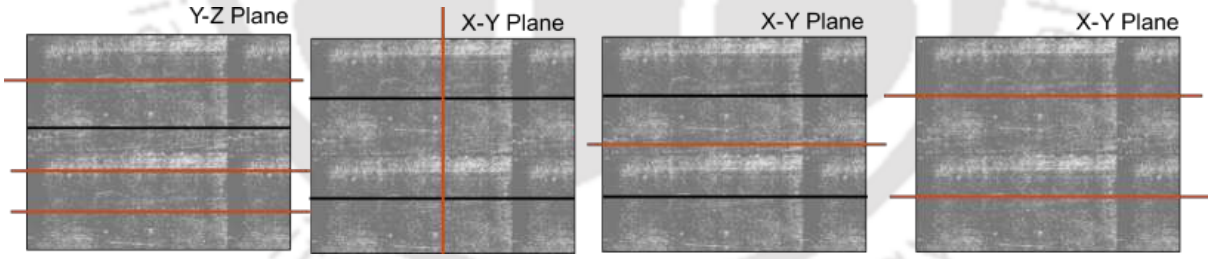

(c)

(d)

(e)

Figure 4.9: Schematic diagram of (a) printed beam, (b) extraction of specimens, (c) cutting the specimens into slices for the image analysis, (d) typical cut specimens for image analysis, and (e) typical specimens after the surface preparation.

4.4 Results and discussion

In this section, a detailed discussion of results obtained from the tests described in the previous section is presented. The influence of stabilizer concentration and surfactant characteristics on foam properties is analysed. Later, the effect of surfactant characteristics on fresh state properties and air void characteristics of 3DP-FC are discussed.

4.4.1 Influence of stabilizer on foam properties

Foam density and drainage are observed to be dependent on the stabilizer dosage for both natural and synthetic surfactants used in this study. Experimental outcomes indicated that addition of 0.1% and 0.2% dosages of XG improved foam density by 16% and 184% respectively (Figure 4.10(a)). Despite the significant reduction in foam drainage observed at 0.2% dosage of XG, as the foam density did not meet ASTM C796 prescribed density range, the upper limit of XG is fixed as 0.1% for the present study. Nevertheless, foam drainage at 0.1% dosage of XG shows a reduction in foam drainage of 24%. On a similar note, in case of synthetic surfactant, addition of CMC up to a dosage of 0.4% improved foam density by 17% and reduced the foam drainage from 99% to 63% (Figure 4.10(b)). Improvement in these foam properties can be attributed to the enhancement of surfactant viscosity and lamella thickness in bubble microstructure as established in previous literature (Sahu and Gandhi 2021; Hajimohammadi et al., 2018). The above fact will be experimentally verified in later sections.

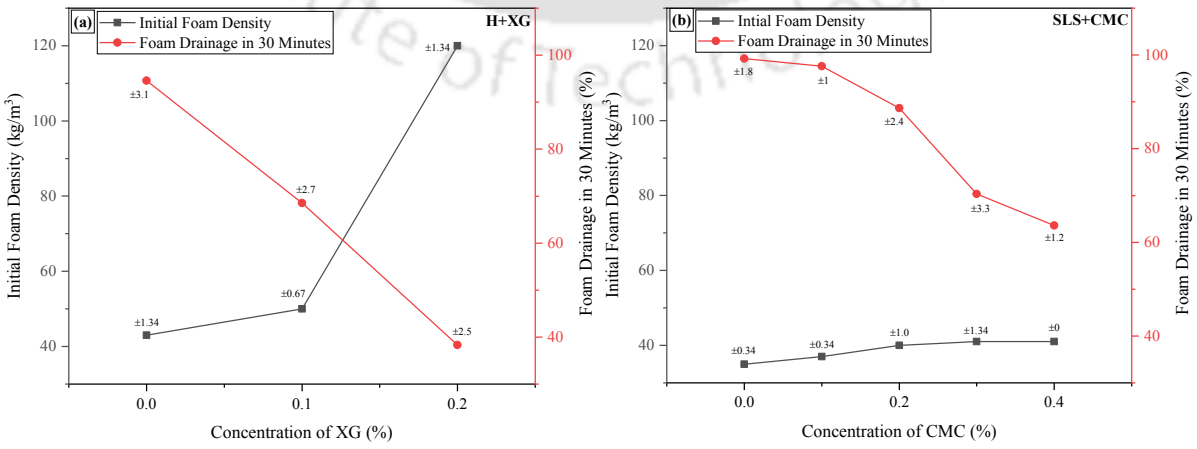

(a) (b)

Figure 4.10: Influence of stabilizer on IFD and foam drainage at 30 minutes of (a) hingot stabilized with XG (b) SLS stabilized with CMC.

4.4.2 Influence of stabilizer on surfactant characteristics

Viscosity and surface tension of the surfactant solution are seen to have contrasting trend with the increase in stabilizer concentration for both natural and synthetic surfactants. Increase in dosage of XG from 0 to 0.2% enhanced the viscosity of Hingot surfactant solution by 302% and decreased its surface tension by 6.3% (Figure 4.11(a)). This can be ascribed to the thickening nature of XG that helps in improving the viscosity of the solution and condensing the liquid film around the bubble (Hajimohammadi et al., 2018). In line with most of the studies of relevant literature, the impact of XG on viscosity of surfactant solution is more significant when compared to its role on surface tension (Zhu et al., 2020). On a similar note, increase in CMC concentration from 0 to 0.4% enhanced the viscosity of SLS surfactant solution by 472% and reduced the surface tension by 6.5% (Figure 4.11(b)). This can be attributed to an increase in the concentration of water-soluble polymer, which caused a change in the micellar structure of the molecules, increasing viscosity (Porter, 2013; Sahu and Gandhi, 2021). The above-mentioned increase in viscosity due to increase in stabilizer concentration can be correlated to the positive impact on foam properties in terms of density and drainage as discussed in earlier section.

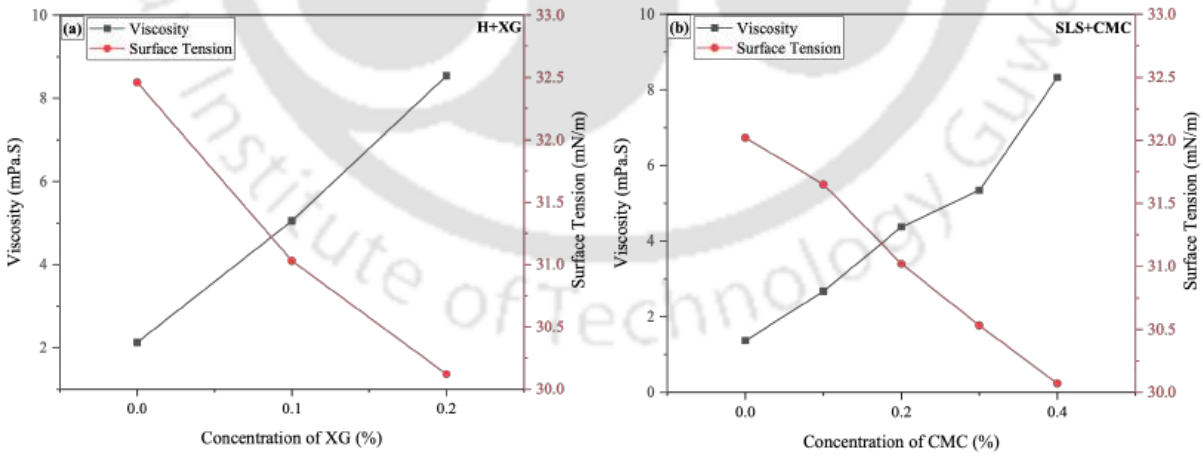

(a) (b)

Figure 4.11: Influence of stabilizer on viscosity and surface tension of (a) hingot stabilized with XG and (b) SLS stabilized with CMC.

4.4.3 Influence of surfactant characteristics on fresh properties of 3DP-FC

Fresh density of the mixture produced is examined immediately after the mixing (i.e. before extrusion) and after the extrusion process. ASTM C869 suggests that the variation between the target density and achieved density should be within the range of ±50 kg/m^3. As shown in Figure 4.12, the mixes SLCM3, SLCM4, and HXG1 could achieve the target density (within the tolerance limits) at both the stages of measurement for all the densities adopted in the present study. While SLCM2 could achieve the target density for 1300 kg/m^3 but failed to sustain the foam stability in 1000 kg/m^3. The above experimental outcomes indicate that mixes with higher viscous surfactant solution appears to be more stable. Adding to above, other research works in similar context have shown that increase in lamella thickness of foam bubble due to stabilizer addition contributes to enhancement in stability of foam concrete mix (Raj et al., 2022; Huang et al., 2021). From the obtained trends in Figure 4.11(a) and (b) and 4.12, it is possible to deduce the desirable values of viscosity and surface tension of surfactant to produce stable 3DP-FC mixes. It is evident from figures that the surfactant solution with viscosity above 5 mPa.S and surface tension less than 31 mN/m can result in stable foam concrete mixes with variation of actual fresh density from target densities within ASTM prescribed tolerance limits.

The mixes SLCM2, SLCM3, SLCM4, and HXG1 which proved to be stable are chosen for further investigation. Table 4.3 presents the results of the tests performed to investigate the various fresh state related properties such as slump, slump flow and yield stress. It is observed that the slump and slump flow values for 1000 and 1300 kg/m^3 are in the range of 2-6 mm and 150-165 mm respectively. The obtained results are in line with the desirable requirements of printability as stated by Tay et al., (2019) (slump 5-8 mm and slump flow 150-190 mm). Moreover, the difference in the slump values before and after extrusion are mostly unaffected, which also represents the stability of the foam during and after extrusion. Although, the slump value in SLCM2 (1300 kg/m^3) after extrusion is increased but it is within the range of printability. Unlike conventional foam concrete, the influence of variation of dosage of foam stabilizer on above fresh state related properties of 3DP-FC is insignificant. Moreover, the static yield stress values measured using vane shear apparatus for the densities 1000 and 1300 kg/m^3 ranges from 0.34-1.03 kPa which also satisfies the criteria for printability quantified by Le et al., (2012) (0.3-1.00 kPa). Nevertheless, visual observation tests are conducted to validate the printability of 3DP-FC for the densities 1000 and 1300 kg/m^3 in the later sections.

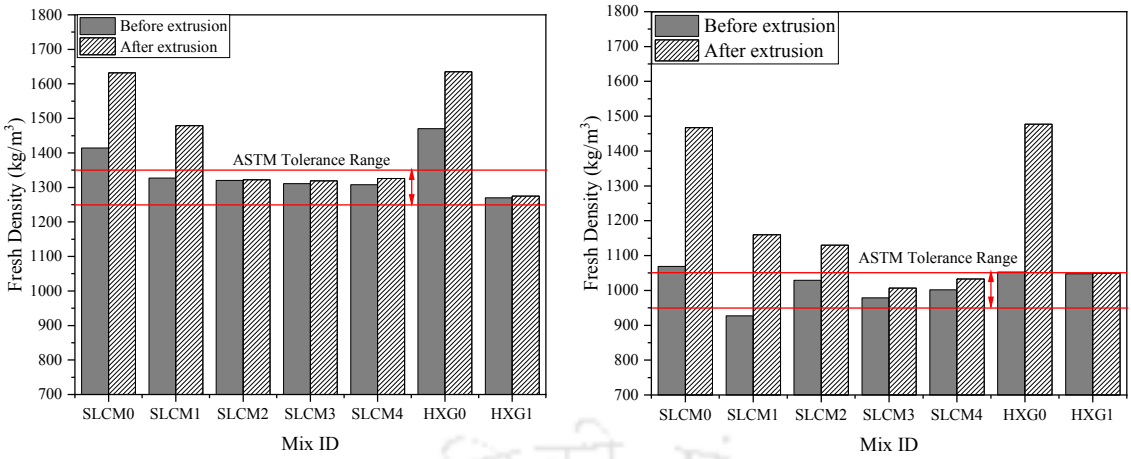

Figure 4.12: Fresh density of the 3DP-FC mixes produced before and after the extrusion process for (a) 1300 kg/m^3, (b) 1000 kg/m^3

Table 4.3: Fresh state properties of 3DP-FC

MIX ID	Target density (kg/m^3)	Slump (mm)		Slump Flow (mm)		Static Yield Stress (kPa)
		Before extrusion	After extrusion	Before extrusion	After extrusion	
HXG1	1000	4	4	158	157	0.34
	1300	6	6	156	157	0.86
SLCM2	1000	3	4	150	152	0.43
	1300	2	5	160	164	1.03
SLCM3	1000	4	5	152	163	0.34
	1300	5	6	149	164	0.92
SLCM4	1000	4	4	157	156	0.35
	1300	2	3	157	153	0.97

4.4.4 Printability of 3DP-FC

Visual observation tests for extrudability and buildability shows that mixes with design density of 1300 kg/m^3 failed at 13th layer while 1000 kg/m^3 failed at 10th layer (maximum) as shown in the Figure 4.13. Later, beams of 700 mm length and 50 mm height were printed without any discontinuity. It was also observed that height of the beam printed was in the tolerence limit of 1 mm (maximum). The above visual observations indicate that the volume of foam has more

significant effect on printability characteristics. Further, the variation of stablizer concentration for the stable mixes studied does not show much effect on printability, similar to trend observed on fresh state related characteristics discussed in the above section.

(a) HXG 1 (1300 kg/m^3)

(b) HXG 1 (1000 kg/m^3)

(c) SLCM 2 (1300 kg/m^3)

(d) SLCM 2 (1000 kg/m^3)

(e) SLCM 3 (1300 kg/m^3)

(f) SLCM 3 (1000 kg/m^3)

(g) SLCM 4 (1300 kg/m^3)

(h) SLCM 4 (1000 kg/m^3)

Figure 4.13: Visual observation results of buidability (Just before the failure and after the failure) and extrudbility (700 mm length beams) of mixes (a) HXG1 (1300 kg/m^3), (b) HXG1 (1000 kg/m^3), (c) SLCM2 (1300 kg/m^3), (d) SLCM2 (1000 kg/m^3), (e) SLCM3 (1300 kg/m^3), (f) SLCM3 (1300 kg/m^3), (g) SLCM4 (1300 kg/m^3), (h) SLCM4 (1000 kg/m^3).

4.4.5 Effect of surfactant characteristics on air void distribution of 3DP-FC

Air void microstructure of 3DP-FC is expected to show a different trend when compared to that of traditional FC. Air void size is characterized by feret diameter to study the both spherical and irregular shaped voids, while shape of the void is studied by circularity index. Table 4.4 and 4.5 shows the results of air void size and shape characteristics of 3DP-FC along with the

standard deviation (SD) and coefficient of variation (CoV). The median air void is represented by D50 while D90 represents the air void size below which 90 percent of voids are present. Similarly, median value of air void circularity is C50, and C90 represents the air voids with lower circularity (i.e irregular voids). Circularity of air voids is determined using equation presented by (Sahu and Gandhi, 2021).

4.4.5.1. Air void size distribution of 3DP-FC

For both the design densities of 1000 and 1300 kg/m^3, D50 and D90 value of all the samples are found to be of similar order with the exception of mixes SLCM2 (1000 kg/m^3) and HXG1(1000 kg/m^{3}and 1300 kg/m^3) which showed slightly lesser D50 values and higher D90 values respectively (Table 4.4). The above trend of results indicate that the stabilizers added are efficient and the rheology of all the stable mixes studied are appropriate with good bubble maintaining capacity (Nambiar and Ramamurthy, 2007a). However, in case of SLCM2 (1000 kg/m^3), the mixture didn't attain the design density due to instability of foam bubble caused by surfactant characteristics. Similarly, for mixes with Hingot surfactant, slightly higher D90 values are due to the difference in the type of surfactants. Hence it can be inferred that unlike the conventional foam concrete, the influence of surfactant characteristics and density has minimal impact on air void distribution of 3DP-FC. Therefore, the rheology of the paste sourrounding the air bubble has greater efect than the surfactant characteristics. Figure 4.14 shows the air void size distribution of the mixes SLCM2, SLCM3, SLCM4, and HXG1 with densities 1000 and 1300 kg/m^3.

Table 4.4: Air void size distribution of 3DP-FC.

MIX ID	1000 kg/m^3						1300 kg/m^3					
	D50 (μ)	SD	CoV	D90 (μ)	SD	CoV	D50 (μ)	SD	CoV	D90 (μ)	SD	CoV
SLCM2	236	16.5	0.07	694	121.7	0.17	238	12.6	0.05	730	81.3	0.11
SLCM3	262	33.6	0.13	716	137.3	0.19	237	27.4	0.11	674	115	0.17
SLCM4	258	36.6	0.14	740	133.2	0.18	250	25.3	0.10	697	115.8	0.17
HXG1	264	29.1	0.11	790	134.9	0.17	267	27.3	0.10	803	90.8	0.11

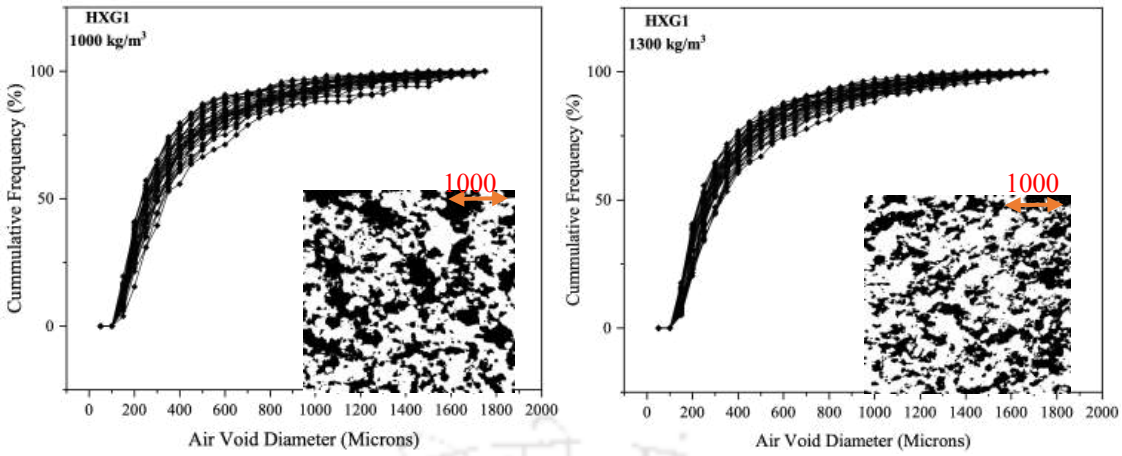
HXG1
1000 kg/m³
Cummulative Frequency (%)
Air Void Diameter (Microns)
1000

(a)

HXG1
1300 kg/m³
Cummulative Frequency (%)
Air Void Diameter (Microns)
1000

(b)

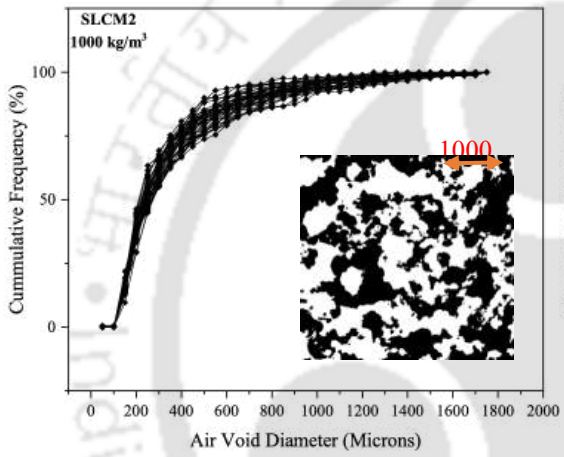
SLCM2
1000 kg/m³
Cummulative Frequency (%)
Air Void Diameter (Microns)
1000

(c)

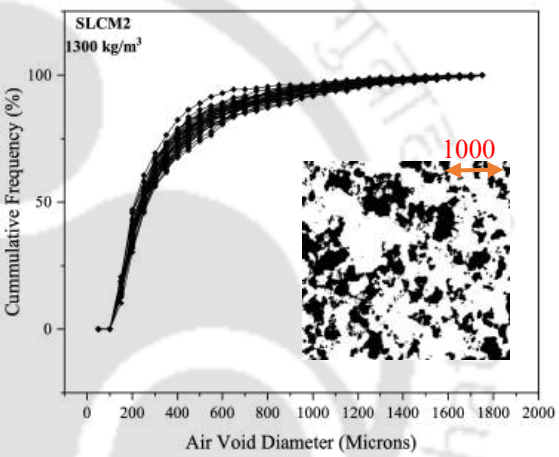
SLCM2
1300 kg/m³
Cummulative Frequency (%)
Air Void Diameter (Microns)
1000

(d)

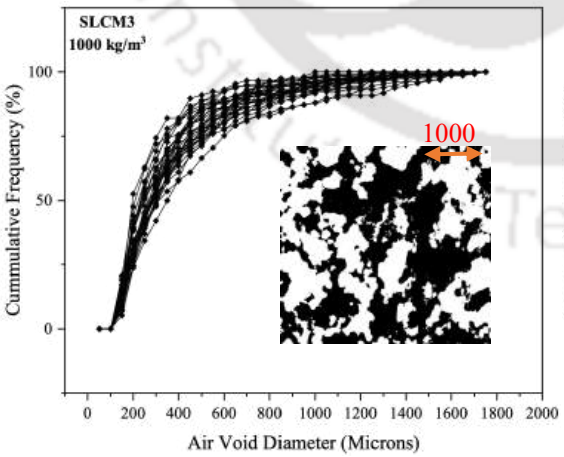
SLCM3
1000 kg/m³
Cummulative Frequency (%)
Air Void Diameter (Microns)
1000

(e)

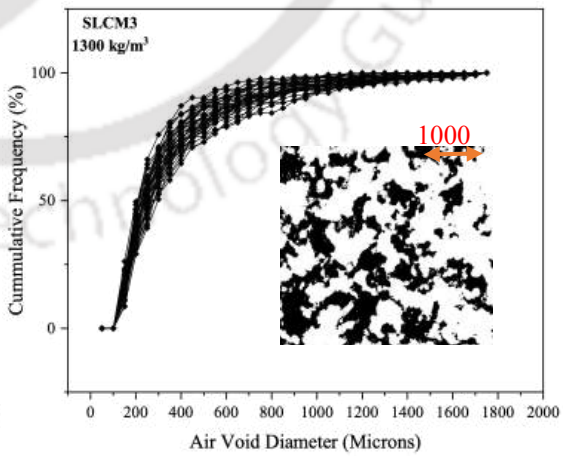
SLCM3
1300 kg/m³
Cummulative Frequency (%)
Air Void Diameter (Microns)
1000

(f)

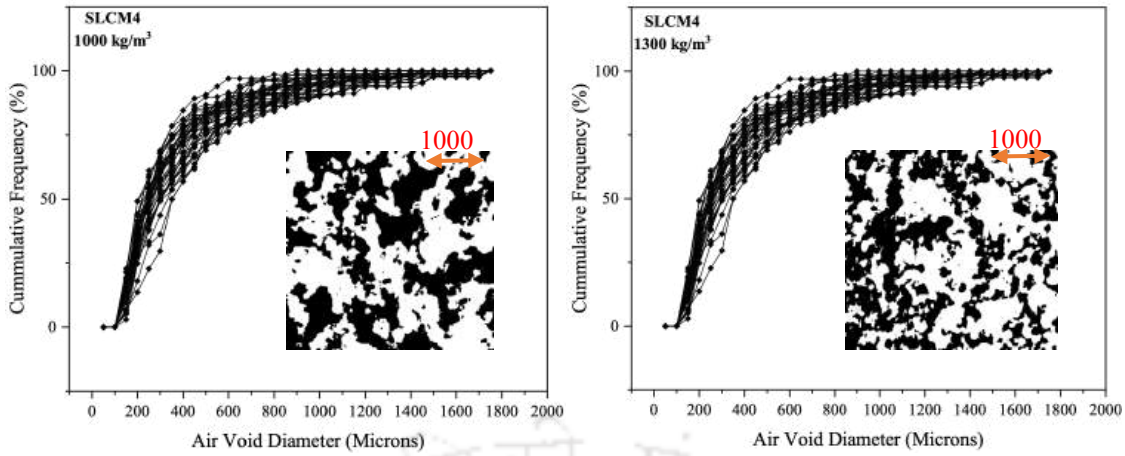

(g) (h)

Figure 4.14: Air void size distribution of the mixes (a) HXG1 (1000 kg/m^3), (b) HXG1 (1300 kg/m^3), (c) SLCM2 (1000 kg/m^3), (d) SLCM2 (1300 kg/m^3), (e) SLCM3 (1000 kg/m^3), (f) SLCM3 (1300 kg/m^3), (g) SLCM4 (1000 kg/m^3), (h) SLCM4 (1300 kg/m^3).

4.4.5.2 Circularity of 3DP-FC

In line with observations on air void size distribution, it is found that surfactant charateristics and density of concrete have no significant influence on circularity index also, as evident from results of image analysis (Table 4.5). However, the circularity of Hingot surfactant mixes are relatively less when compared to that of synthetic SLS surfactant. The difference in viscosity of both the surfactants can be used to justify the slightly irregular air voids in Hingot mixes. Figure 4.15 shows the circularity of the mixes SLCM2, SLCM3, SLCM4, and HXG1 with densities 1000 and 1300 kg/m^3.

Table 4.5: Circularity of air voids in 3DP-FC

MIX ID	1000 kg/m^3						1300 kg/m^3					
	C50	SD	CoV	C90	SD	CoV	C50	SD	CoV	C90	SD	CoV
SLCM2	0.70	0.04	0.05	0.91	0.02	0.02	0.69	0.04	0.05	0.91	0.02	0.02
SLCM3	0.69	0.05	0.07	0.88	0.02	0.03	0.68	0.02	0.04	0.89	0.02	0.02
SLCM4	0.69	0.05	0.07	0.88	0.03	0.03	0.68	0.04	0.06	0.88	0.03	0.04
HXG1	0.61	0.08	0.13	0.85	0.05	0.06	0.61	0.08	0.13	0.85	0.05	0.07

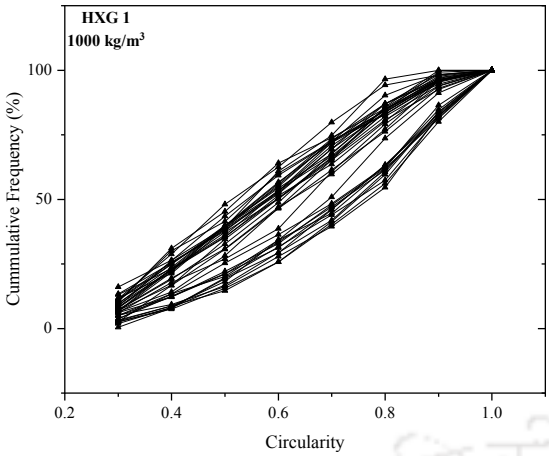
HXG 1
1000 kg/m3
Cummulative Frequency (%)
Circularity

(a)

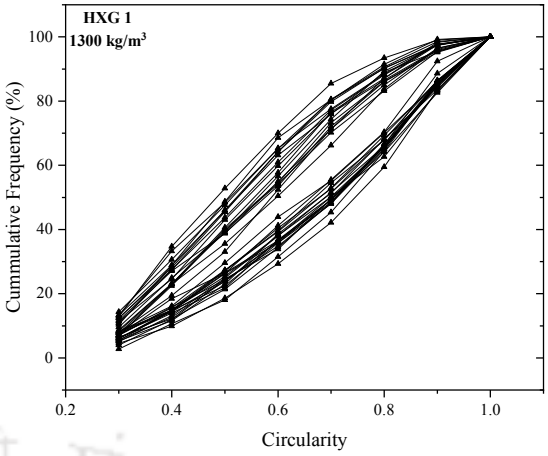
HXG 1
1300 kg/m3
Cummulative Frequency (%)
Circularity

(b)

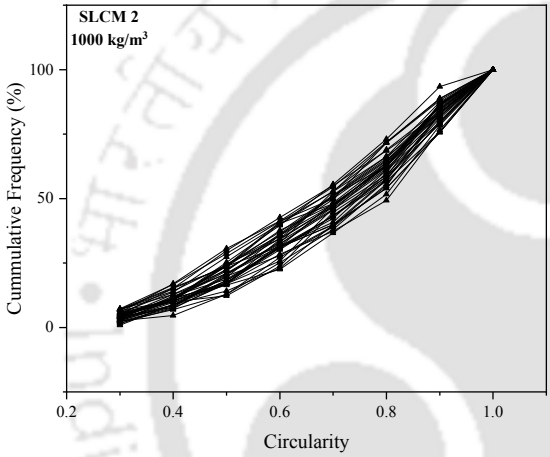
SLCM 2
1000 kg/m3
Cummulative Frequency (%)
Circularity

(c)

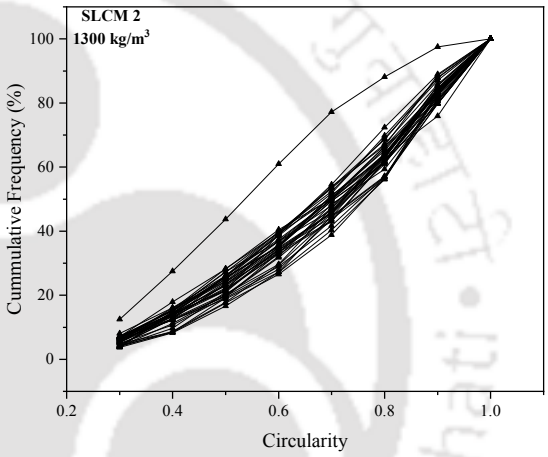
SLCM 2
1300 kg/m3
Cummulative Frequency (%)
Circularity

(d)

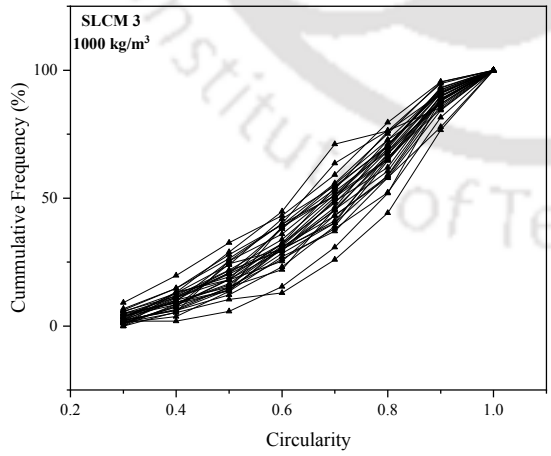
SLCM 3
1000 kg/m3
Cummulative Frequency (%)
Circularity

(e)

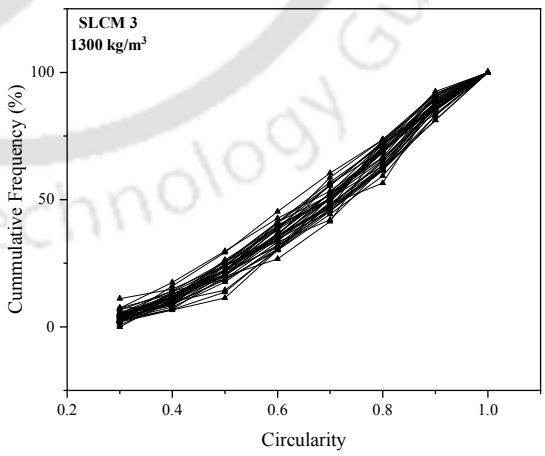
SLCM 3
1300 kg/m3
Cummulative Frequency (%)
Circularity

(f)

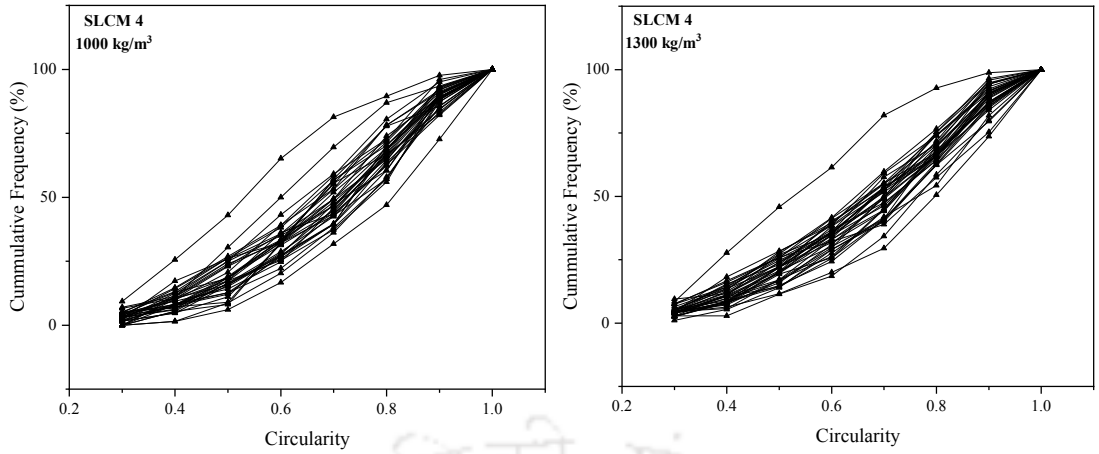

(g) (h)

Figure 4.15: Circularity of the mixes (a) HXG1 (1000 kg/m^3), (b) HXG1 (1300 kg/m^3), (c) SLCM2 (1000 kg/m^3), (d) SLCM2 (1300 kg/m^3), (e) SLCM3 (1000 kg/m^3), (f) SLCM3 (1300 kg/m^3), (g) SLCM4 (1000 kg/m^3), (h) SLCM4 (1300 kg/m^3).

4.5 Summary

This research intends to study the influence of surfactant characteristics on stability and printability of 3DP-FC. Different studies on fresh state related, printability and air void characterization of 3DP-FC have been carried out for two different surfactants (natural and synthetic based) along with different foam stabilizers. From the experimental results, it can be suggested that the surfactant solution with viscosity above 5 mPa.s and surface tension less than 31 mN/m can result in stable foam concrete mixes with variation of actual fresh density from target densities within ASTM prescribed tolerance limits. The variation in the stabilizer concentration of the stable mixes did not significantly influence the fresh- state-related characteristics, such as slump, slump flow, and static yield stress. Similarly, the impact on the air void characteristics on 3DP-FC was minimal, unlike traditional foam concrete. The above trends indicate that the adopted stabilizers and their dosages are efficient, resulting in stable 3DP-FC mixes with appropriate rheological characteristics that enhance the bubble maintaining capacity. Nevertheless, the volume of foam in the mix has significant impact on printability characteristics. Visual observation tests for extrudability and buildability shows that mixes with design density of 1300 kg/m^3 failed at 13th layer while 1000 kg/m^3 failed at 10th layer itself.

Chapter 5

Synergistic Effect of Fly Ash and Polyvinyl Alcohol Fibers in Improving Rheology, Stability and Mechanical Properties of 3D Printable Foam Concrete

5.1 General

The investigations pertaining to this study are carried out in two stages as discussed under methodology section; In first stage the influence of surfactant characteristics on stability of 3DP-FC is studied (discussed in Chapter 4) and the second stage includes the investigations on enhancing the buildability of 3DP-FC by incorporating various admixtures (current chapter). In the previous chapter, the influence of surfactant characteristics is studied and results showed that irrespective of the surfactant type and stabilizer used, the stability of the mixture is highly dependent on the surfactant properties. This chapter deals with the investigation of the synergistic effect of fly ash (as a filler replacement) and polyvinyl alcohol fibers (as reinforcement) in improving the stability and buildability of 3DP-FC.

5.2 Materials, mixture design, and mixing method

This section provides an overview of the materials, mixing method, and mixture design adopted to study the synergistic influence of fly ash and PVA fibers on stability and buildability of 3DP-FC.

5.2.1 Materials

Ordinary Portland cement (OPC) of 43 grade (Dalmia Bharat ltd., Thangskai, India), of relative density 3.14, conforming to IS 269:2020 and silica fume (SF) (relative density of 2.2) obtained from Elkem ltd., Hyderabad, India, conforming to IS 15388:2022 are used as binders. Class F fly ash (FA) (relative density of 2.09) obtained from Technocrete India pvt. ltd., Nashik, India, conforming to ASTM C618-22 and sand sieved on 300 micron mesh (from locally available fine river sand) are used as fine aggregates. Table 5.1 presents the characteristics of materials used in this study. Figure 5.1 and Table 5.2 shows the XRD spectra and composition (of OPC, FA, and SF) respectively. Where, Q, M, H, SiC, C, G,

C_3S, C_2S, C_3A, and C_4AF represent quartz, mullite, hematite, silicate carbide, cristobalite, gypsum, calcium trisilicate, calcium disilicate, calcium aluminate, and calcium alumina ferrite respectively. Chemical composition of the OPC, FA, and SF are determined using XRF (Table 5.2). FESEM images of basic constituents like OPC, FA and SF are shown in the Figure 5.2. Figure 5.3(a) shows the particle size distribution of materials (OPC, FA, sand, and SF) used for study that are measured using laser diffraction particle size analyser.

Poly vinyl alcohol (PVA) fibers are used as reinforcing material to improve the ductility of the wall panel. Table 5.3 shows the characteristics of the PVA fibers used for the current study. Hydroxy propyl methyl cellulose (HPMC) is used as a viscosity modifying agent at dosage of 0.1% by weight of binder content to improve the viscosity of mixture and stability of foam bubble. 3DP-FC is produced using pre-foaming method, in which the foam and mortar are generated separately and then mixed to deliver the mixture. Synthetic surfactant SLS + 0.4% CMC was chosen to conduct this study based on the experimental results presented in phase one.

Table 5.1: Summary of materials used in the production of 3DP-FC.

Material	Characteristics	Source	Specific Gravity	Application
Cement	OPC - 43 grade confirming to IS 8112 – 2013 and having a bulk density of 1600 kg/m^3.	Dalmia cement plant, Thangskai, Assam.	3.14	Binder
Sand	River sand sieved through 300µm confirming to IS 383 – 2016 and having a bulk density of 1628 kg/m^3.	Brahmaputra river, Dudhnoi, Goalpara, Assam.	2.65	Fine aggregate
SF	Confirming to IS 15388 – 2003 and having a bulk density of 500 kg/m^3.	Elkem micro silica, AKJ Engineers Pvt. Ltd., Behrabari, Guwahti.	2.20	Binder / Mineral admixture
FA	Class F type, Confirming to IS 3812 Part 1: 2013 and having a bulk density of 995 kg/m^3.	Technocrete India pvt. ltd., Nashik, India,	2.09	Fine aggregate
PVA fibers	Mono filaments of length 12 mm.	Lakhani Fabrics, RIICO industrial	1.29	Reinforcement

Material	Characteristics	Source	Specific Gravity	Application
		area, Napasar, Bikaner.		
Water	-	IITG Treatment Plant	1.00	-
Hingot	Desert fruit containing extractable saponin	Madhya Pradesh	-	Surfactant
XG	Naturally occurring microbial expolysaccharide.	Loba Chemicals, Mumbai.	-	Stabilizer
SLS	Synthetic surfactant (Anionic)	Loba Chemicals, Mumbai.	-	Surfactant
CMC	Viscosity modifying agent	Loba Chemicals, Mumbai.	-	Stabilizer
HPMC	Model: HS 1218, Viscosity of 160000 MPa.s	Foroly Commercio Pvt. Ltd.	0.41	Viscosity Modifying agent
PCE based SP	Model: Ecmas HP 904, pH > 6, liquid, pale brown in colour, and chloride content < 0.2%	Ecmas Group, Hyderbad.	1.11±0.02	High range water reducer

Table 5.2: Chemical composition of materials used for 3DP-FC.

Material	Chemical Composition						
	SiO_2	Al_2O_3	Fe_2O_3	CaO	MgO	SO_3	LOI
OPC	19.62	5.62	5.33	61.24	0.88	2.60	2.06
FA	56.50	26.16	7.24	7.50	1.60	0.55	2.08
SF	87	-	-	-	-	-	2

Table 5.3: Characteristics of PVA fibers used for 3DP-FC.

Property	Length, (mm)	Aspect ratio (L/d)	Tensile strength (MPa)	Young's modulus (GPa)	Density (g/cm^3)	Poisson's ratio
	12	300	1060	42.8	1.3	0.42-0.48

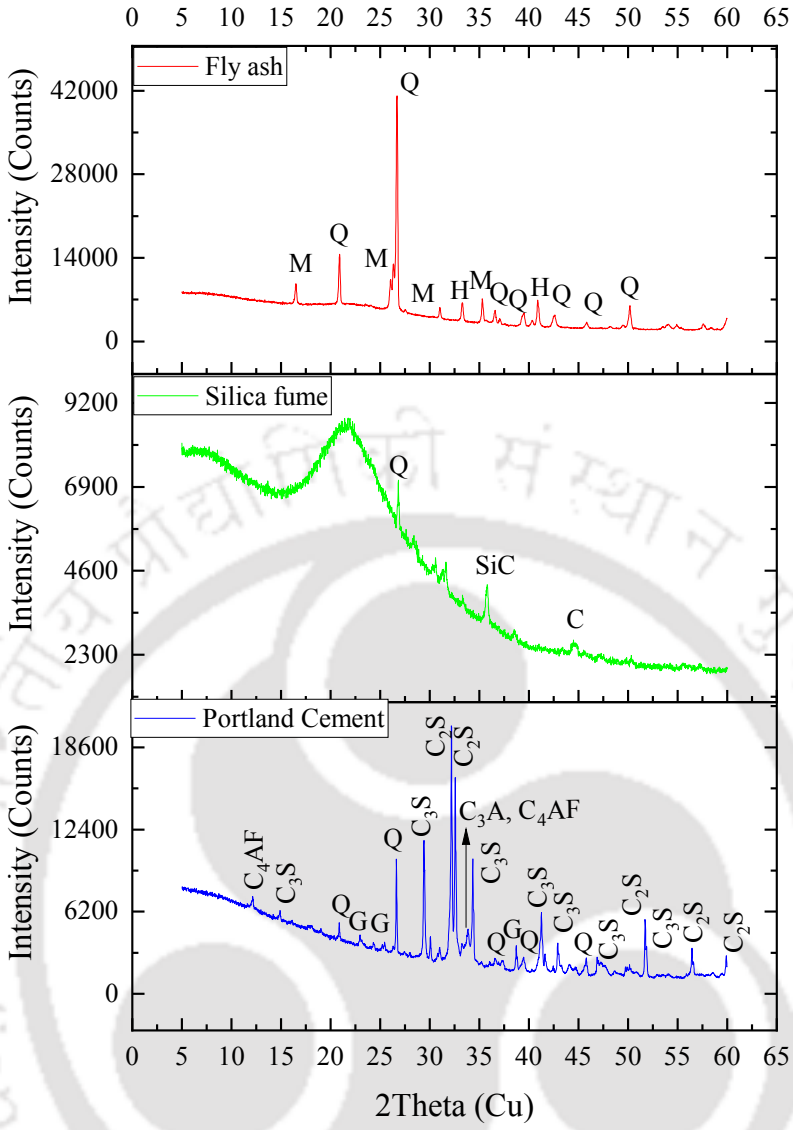

Figure 5.1: XRD spectrum of ingredients used for 3DP-FC.

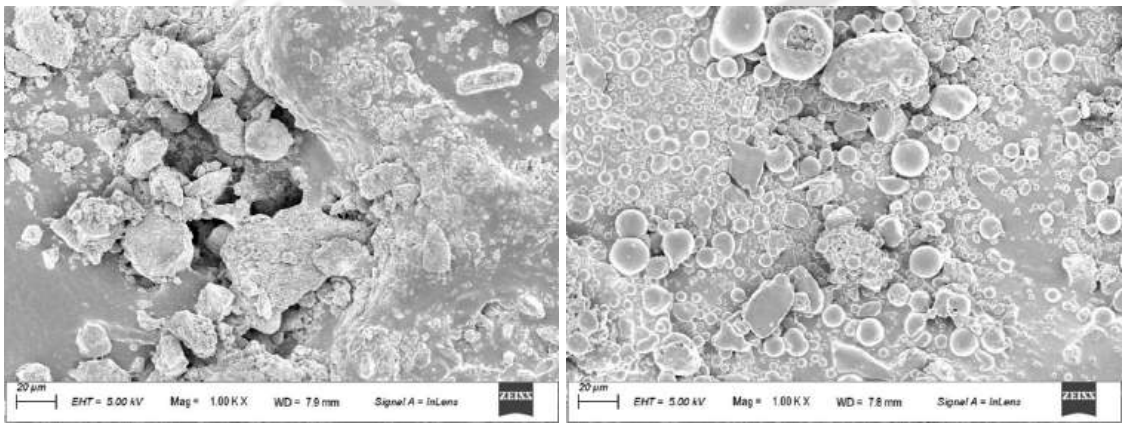

(a) (b)

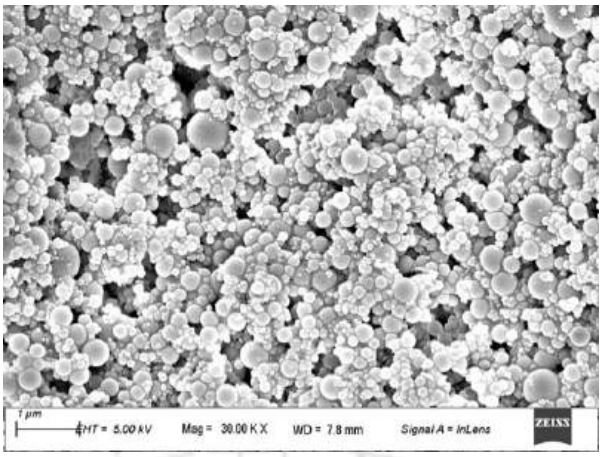

(c)

Figure 5.2: SEM images of (a) cement, (b) fly ash, (c) silica fume

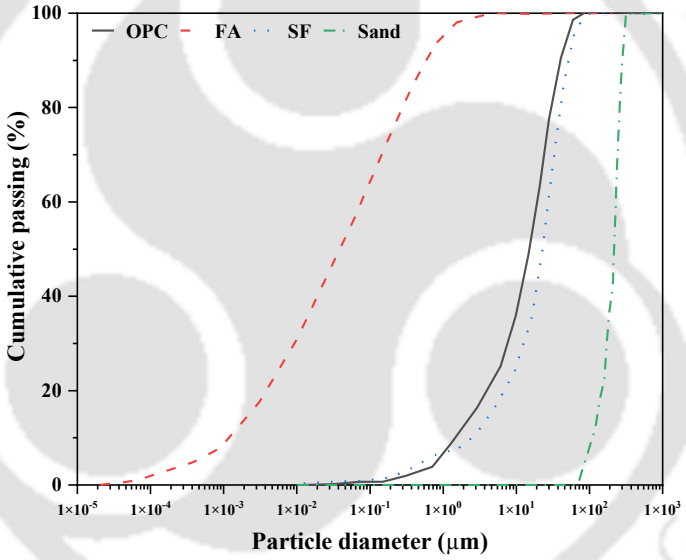

Figure 5.3: Particle size distributions of FA, OPC, SF, and sand

5.2.2 Mixture design

5.2.2.1 Mix design to study the influence of W/S ratio on stability and printability of 3DP-FC

This study is carried out in two phases. In the first phase, the water to solids (W/S) ratio is varied from 0.15 to 0.3 with 0.05 step to study the stability and printability of 3DP-FC. The procedure described in ASTM C796 was used to develop the mixture design. The ASTM mixture design has the advantage of effectively estimating the amount of foam necessary

for a given density and W/S ratio. Table 5.4 shows the mixture proportions adopted for the study of required W/S for 3DP-FC.

Table 5.4: Mixture proportions of 3DP-FC

Design fresh density kg/m^3	W/S	Cement kg/m^3	SF kg/m^3	Sand kg/m^3	Water kg/m^3	Foam kg/m^3
1000	0.15	391.30	43.48	434.78	117.22	13.21
	0.20	375.00	41.67	416.67	154.01	12.66
	0.25	360.00	40.00	400.00	187.84	12.15
	0.30	346.15	38.46	384.61	219.08	11.69
1300	0.15	508.70	56.52	565.22	159.45	10.11
	0.20	487.50	54.17	541.67	207.27	9.39
	0.25	468.00	52.00	520.00	251.26	8.74
	0.30	450.00	50.00	500.00	291.87	8.13

5.2.2.2 Mix design to study the influence of admixtures on enhancement of buildability and mechanical properties of 3DP-FC

The mix design for the enhancement of buildability, mechanical properties and microstructure using various admixtures is shown in Table 5.5 and Table 5.6 for the design densities 1300 kg/m^3 and 1000 kg/m^3 respectively. Where, CM represents control mixture with 13 and 10 representing 1300 and 1000 kg/m^3 respectively, F represents FA content with 0, 50, and 100% replacement levels, and P represents PVA fibers added at 0, 0.2, and 0.4 percentage.

Experimental study in the current study uses different water to solids ratios for different densities. The W/S is fixed based on the basis of density tolerance limits, slump and slump flow values that is discussed in detail in the section 5.2.2.1. W/S of 0.2 and 0.25 was selected for the densities 1300 and 1000 kg/m^3 respectively. A sand to binder ratio of 1 was adopted in order to improve rheology of the 3DP-FC. SF replaced by 10% of cement content as performance enhancer.

Table 5.5: Experimental mixture design (for design density of 1300 kg/m^3)

S. No	Mix Code	W/S	Mix Constituents (in kg/m^3)								
			C	SF	S	FA	PVA	VMA	SP	W	F
1	C13	0.2	487.50	54.17	541.67	-	-	0.54	-	203.47	13.20
2	C13P2		487.50	54.17	541.67	-	2.58	0.54	0.54	203.47	13.20
3	C13P4		487.50	54.17	541.67	-	5.16	0.54	1.08	203.47	13.20
4	C13F5		487.50	54.17	270.84	270.84	-	0.54	1.89	204.44	12.23
5	C13F5P2		487.50	54.17	270.84	270.84	2.58	0.54	2.16	204.44	12.23
6	C13F5P4		487.50	54.17	270.84	270.84	5.16	0.54	2.43	204.44	12.23
7	C13F10		487.50	54.17	-	541.67	-	0.54	4.05	205.41	11.26
8	C13F10P2		487.50	54.17	-	541.67	2.58	0.54	4.32	205.41	11.26
9	C13F10P4		487.50	54.17	-	541.67	5.16	0.54	4.59	205.41	11.26

Table 5.6: Experimental mixture design (for design density of 1000 kg/m^3)

S. No	Mix Code	W/S	Mix Constituents (in kg/m^3)								
			C	SF	S	FA	PVA	VMA	SP	W	F
1	C10	0.25	360.00	40.00	400.00	-	-	0.40	-	182.93	17.07
2	C10P2		360.00	40.00	400.00	-	2.58	0.40	-	182.93	17.07
3	C10P4		360.00	40.00	400.00	-	5.16	0.40	0.40	182.93	17.07
4	C10F5		360.00	40.00	200.00	200.00	-	0.40	0.40	183.65	16.35
5	C10F5P2		360.00	40.00	200.00	200.00	2.58	0.40	0.60	183.65	16.35
6	C10F5P4		360.00	40.00	200.00	200.00	5.16	0.40	0.80	183.65	16.35
7	C10F10		360.00	40.00	-	400.00	-	0.40	1.00	184.36	15.64

8	C10F10P2	360.00	40.00	-	400.00	2.58	0.40	1.20	184.36	15.64
9	C10F10P4	360.00	40.00	-	400.00	5.16	0.40	1.40	184.36	15.64

5.2.3 Preparation of 3DP-FC

3DP-FC is preparation method is similar to the method followed in the Section 4.2.3. Additionally, fibres are blended in water before being added to the mixer for fiber-based mixes to ensure equal distribution and prevent segregation. Mixing with water beforehand aids in the separation of individual fibres, resulting in a homogeneous base mix.

5.3 Tests conducted to study the influence of surfactant characteristics on stability and printability of 3DP-FC

This section describes the test methods that are adopted in the present study of assessing the effect of surfactant properties.

5.3.1 Rheology of 3DP-FC

The International Centre for Aggregate Research (ICAR) rotational rheometer is used for measurement of static yield stress, dynamic yield stress and viscosity of 3DP-FC. Two test protocols are considered (i.e. constant shear rate (CSR) and flow curve) for investigating these rheological properties as shown in the Figure 5.4. This rotational rheometer includes a container (of 15 L capacity) with a radius of 143 mm to place the mixture and a four bladed vane (of 63.5 mm radius and 127 mm height) to shear the material in the container as shown in the Figure 5.5. Initially, a 3DP-FC mixture is produced and fresh property tests such as flowability and density are carried out. It takes maximum of 10 minutes for the completion of entire process starting from addition of water to placement of mix in the container, including all the tests demonstrated previously (slump, slump flow, and fresh density). The mixture is thereafter investigated for the rheological properties. When the material is subjected to a shear rate (either constant or varying), the torque is measured by the instrument and the value is reported. In CSR test, mixture is subjected to a constant shear rate of 0.025 s^{-1} as suggested by the manufacturer and the recorded torque value is converted to yield stress as per the Equation 5.1. Where '*T*', '*H*', and '*D*' are torque recorded, height and diameter of the vane respectively. Further, the same mixture is subjected to a pre-shear of 0.5 s^{-1} for 20 secs to breakdown the material and then a stepwise

ramp down from 0.5 s^{-1} to 0.05 s^{-1} is applied in 7 steps with 5 secs at each step. The obtained results i.e. torque is plotted along with vane speed and linear fitted with Bingham curve to obtain the dynamic yield stress and viscosity of the 3DP-FC mixture using modified Reiner-Riwlin Equations (Figure 5.6(c)). Figure 5.6(a) and (b) shows the typical graphs showing results obtained from the tests conducted

$$\tau = \frac{2T}{\pi D^3 (\frac{H}{D} + \frac{1}{3})} \tag{5.1}$$

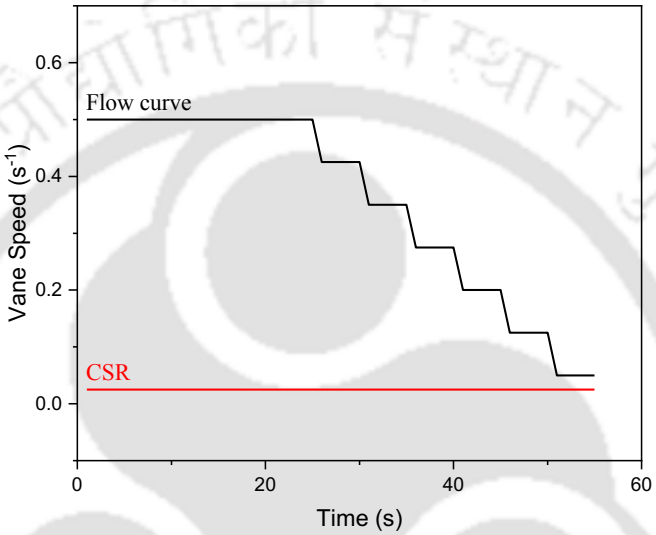

Figure 5.4: Protocols used in conducting the rheological testing of 3DP-FC.

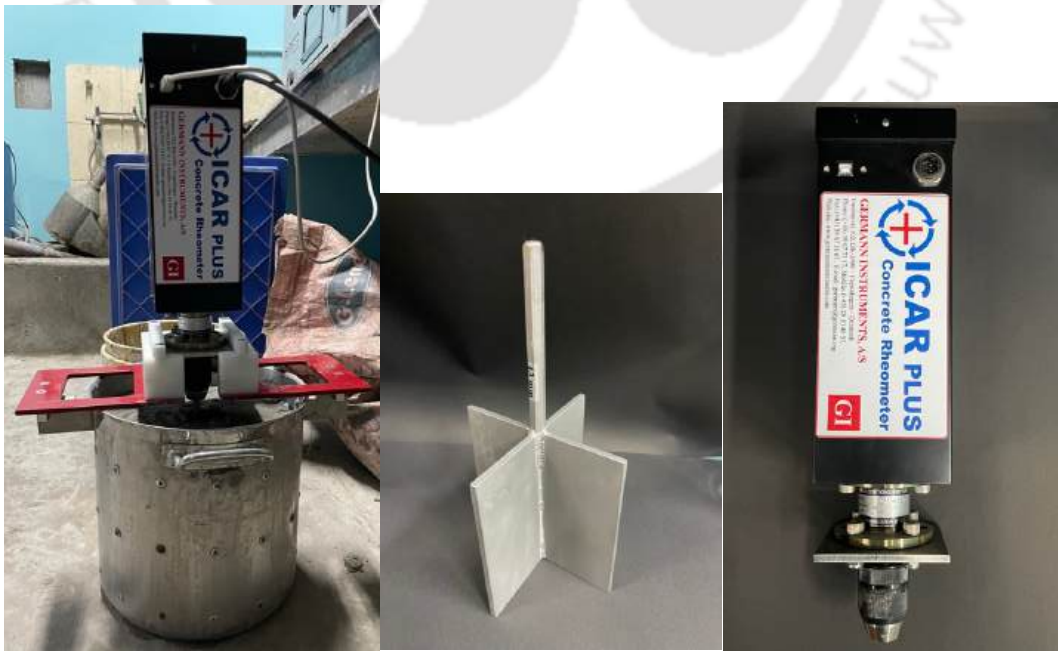

(a) (b) (c)

Figure 5.5: Picture depicting the parts of rheometers (a) rheological testing in action with 15L capacity container, (b) four blade vane, and (c) torque meter unit.

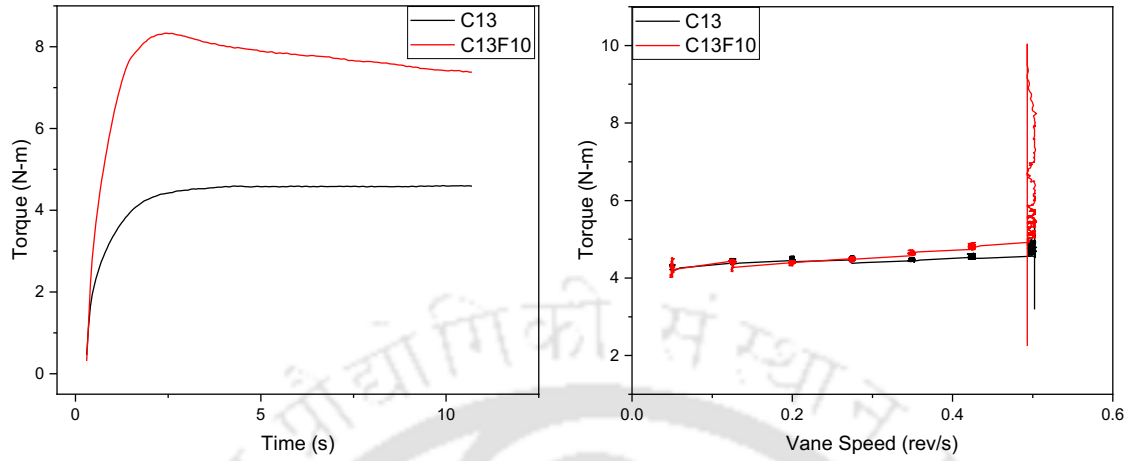

(a) (b)

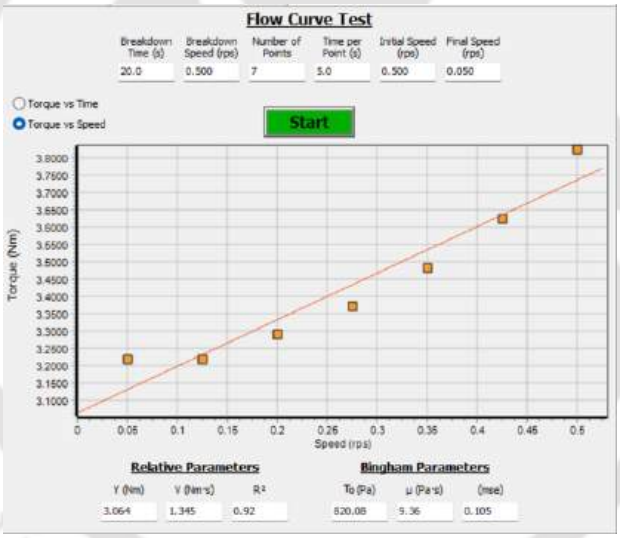

(c)

Figure 5.6: Typical graphs showing the results of C13, C13F10 (a) CSR and (b) flow curve, and (c) Bingham parameters through curve fitting.

5.3.2 Studies on mechanical properties of 3DP-FC

In order to study the mechanical properties like compressive strength, flexural strength and interlayer bond strength of 3DP-FC, specimens are cast and beams of 500 mm length and 60 mm height were printed with different widths (Figure 5.7(a) and (b)). Different widths have to be printed in order to test the specimens for flexure in the printing direction as

shown in Figure 5.7(b). These beams and cast specimens are cured and specimens are extracted from printed beams (compressive strength 50×50×50 mm, flexural strength 40×40×160 mm, and interlayer bond strength 40×40×40 mm) with procedures as suggested in the literature (Dey et al., 2022) (Figure 5.7(c), (d), (e), and (f)). For each set of tests, the average value of the tested strengths of the three specimens is used as the final strength. The specimens are water cured for 25 days and air cured for 3 days as per ASTM C796, prior to mechanical properties and directional anisotropy evaluation. Similarly, samples are water cured till 53 days and 3 days of air curing is provided to test the sample at 56 days. For measuring oven dry densities of the specimens, the samples are oven dried for 24 hours at 110^{0}C after 28 days and 56 days of curing.

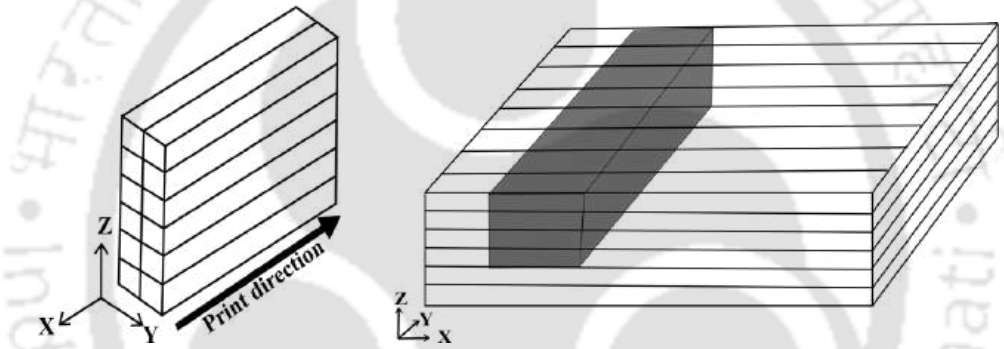

(a) (b)

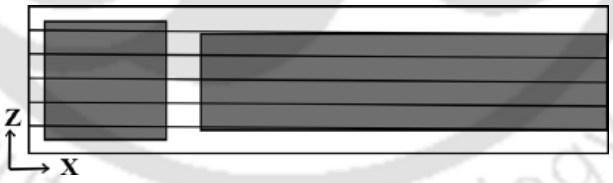

(c)

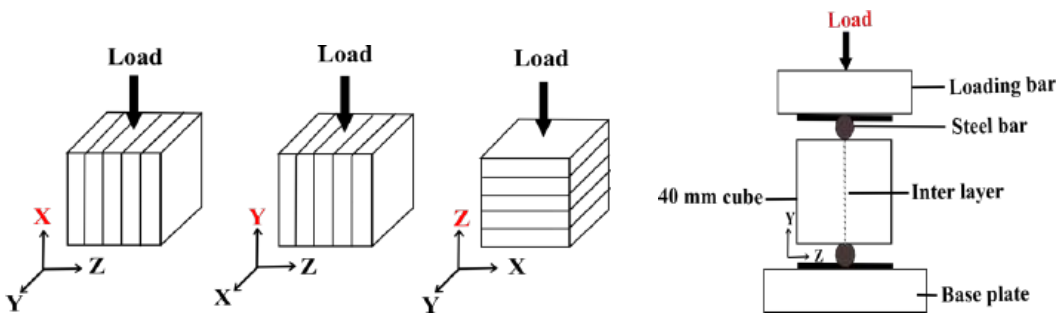

(d) (e)

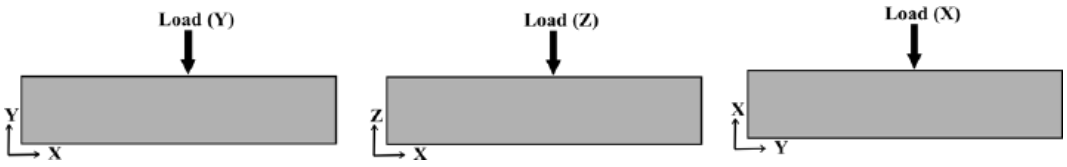

(f)

Figure 5.7: Schematic diagram of (a) printed beam, (b) beam printed to extract the specimens for flexural test in printing direction (X-direction), (c) extraction of cube and prism specimens, (d) extracted cube specimens (50×50×50 mm) and their loading directions for compression testing, (e) testing method for bond strength test, (f) extracted prism specimens (40×40×160) and their loading directions.

Further, the compressive anisotropicity (I_{3D}) of printed specimens is determined using the empirical parameter given in equation 5.2 (Srinivas et al., 2022). Anisotropicity in different directions is defined in the equation 5.3, 5.4, and 5.5. Where I_x, I_y, and I_z are anisotropy in X, Y, and Z-direction and f_x, f_y, and f_z are compressive strength obtained in the represented directions.

$$I_{3D} = \frac{(I_x + I_y + I_z)}{3} \tag{5.2}$$

$$I_x = \sqrt{(f_x - f_x)^2 + (f_y - f_x)^2 + (f_z - f_x)^2} \tag{5.3}$$

$$I_y = \sqrt{(f_x - f_y)^2 + (f_y - f_y)^2 + (f_z - f_y)^2} \tag{5.4}$$

$$I_z = \sqrt{(f_x - f_z)^2 + (f_y - f_z)^2 + (f_z - f_z)^2} \tag{5.5}$$

5.3.3 Studies on thermal conductivity of 3DP-FC

The C-Therm TC kit combined with the transient plane source (TPS) method is used to test the thermal conductivity of all specimens at ambient temperature and normal pressure. With a precision of above 2%, the TC kit has a measuring range of 0.03–60 W/mK. The temperature sensor used by TPS is an electrically conducting bifilar spiral that is positioned in between the specimens. The sensor is sandwiched between two 50 mm cube specimens. The spiral heating element positioned in between the standard calibrating material is

depicted in Figure 5.8. A voltage shift happens across the sensor element when it receives electrical power for its spiral heating element. The test duration of 40 seconds and the power level of 0.9 watts are determined based on the results of the first reconnaissance run. A temperature vs. time graph representing the test findings is presented in the software interface. Nonetheless, the samples before conducting the thermal conductivity test were subjected to 50^0C for 72 hours. This is to ensure that the moisture in the sample is completely dried (Chen et al., 2013).

Figure 5.8: Thermal conductivity measurement of 3D printed samples.

5.3.4 Studies on water absorption and sorption characteristics of 3DP-FC

Sorption and water absorption of 3DP-FC mixes are conducted on 50mm cube samples for both the design densities 1000 and 1300 kg/m^3. The weight gain of oven-dried specimens (to a constant mass) following a 24-hour immersion in water is used to quantify water absorption. While sorptivity describes the capacity of hostile liquids to enter the pore system due to capillary action in one direction, water absorption deals with water permeation, which is characterised as three-dimensional flow.

After 56 days of curing, samples are preconditioned in oven at 50^0C for 3 days until constant mass is attained. The samples are coated with epoxy on all the surfaces except the top and bottom surface. Later these samples are placed in the tray with the condition of water level maintained till 5 mm of the specimen from bottom. Figure 5.9 shows typical sorptivity measurement set up of the 3DP-FC samples. The weight of the samples are

measured at specified time intervals as per ASTM C1585-20. Further, the sorptivity is measured as the slope of the linear fitted graph plotted with cumulative water absorbed per unit area of inflow surface (i) against square root of time ($\sqrt{t}$).

Figure 5.9: Sorptivity measurement of 3DP-FC samples

5.3.5 Studies on chemical characterization of 3DP-FC

An X-ray diffractometer with Cu Kα radiation at a wavelength of 1.54 Å is used for the current study. It is scanned at a voltage of 40 kV, a current of 125 mA, and a speed of 20° per minute. Following 28 and 56 days of curing, specimens of 3DP-FC samples from each combination are ground into a powder and then run through a 75 micron sieve. The intensity of the reflected X-rays is measured while the sample and detector are rotated throughout two angular ranges, from 5° to 60°. The International Centre for Diffraction Data (ICDD) database is utilised for peak intensities at various angles, and the X-pert High Score Plus programme is used to assess the samples' mineral phases. Using the reference intensity ratio (RIR) matrix-flushing approach, semi-quantification analysis of the obtained X-ray diffractograms is used to calculate the weights of the minerals (Das and Pradhan 2022). Using equations 5.6 and 5.7, the weight (%) of the chemicals contained in the concrete mixes was calculated.

$$W_i = \frac{\frac{I_i}{RIR_i}}{\sum_{i=1}^{N} \frac{I_i}{RIR_i}} \quad (5.6)$$

$$W_1 + W_2 + \ldots\ldots + W_N = 1 \quad (5.7)$$

Where, N is the number of compounds taken into consideration in the sample, W_i is the relative mass of compound i, I_i is the integral intensity of the maximum peak of compound i (calculated using PANalytical X'Pert HighScore Plus software), and RIR_i is the reference intensity ratio of compound i (obtained from the PDF card of the International Centre for Diffraction Data (ICDD)).

Further, to examine the changes in concrete morphology, FESEM analysis is conducted on powdered and chunk samples collected from specimens, using Zeiss Gemini field emission scanning electron microscope and elemental content of FC mixtures is determined using the Zeiss Sigma 300, Energy Dispersive Spectroscopy technique (EDS). Later, thermo-gravimetry analysis is conducted on the powder 3DP-FC samples using the instrument NETZSCH STA 449F3. It measures the loss of volatile materials at different temperatures. The powdered sample is heated in a crucible from room temperature to 1000 °C at 10 °C/min.

5.4 Results and discussion

5.4.1 Determination of W/S ratio required for 3DP-FC

The fresh density ratio results showed that the stability of FC is attained after the W/S ratio reached 0.20 and 0.25 for design densities 1300 and 1000 kg/m^3 respectively (Figure 5.10(a)). The influence of W/S ratio on slump and slump flow further demonstrates that both properties tend to increase as the W/S ratio increases (Figure 5.10(b)). However, according to the ASTM tolerance limits on density variations and the printability window (slump 0-8 mm and slump flow 150-190 mm) developed by (Tay et al., 2019), it is observed that the minimum W/S ratio derived for stability requirement also met the printability requirements. However, when the W/S ratio is increased beyond 0.20 and 0.25 for 1300 and 1000 kg/m^3, it is observed that the slump and slump flow values are outside the printability window, making them unsuitable for printing. Hence it can be concluded that printability can be attained at W/S ratios of 0.25 and 0.20 for 1000 and 1300 kg/m^3 densities respectively.

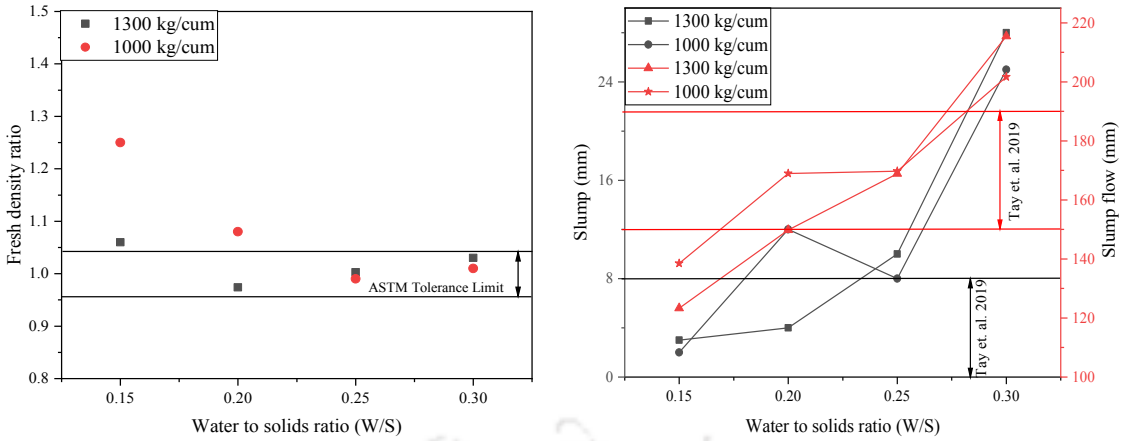

(a) (b)

Figure 5.10: (a) Fresh density ratio of 3DP-FC for varying W/S ratios, (b) Slump and slump flow values of 3DP-FC for varying W/S ratios.

5.4.2 Fresh state properties of 3DP-FC

Slump and slump flow values are adjusted using a suitable SP and reported as a satisfying criteria for printability. The slump values less than 8 mm and slump flow values between 150-190 mm are reported to be printable in earlier studies (Tay et al., 2019). In the present study, although, slump values are within the specified range for both the densities (Table 5.7 and 5.8), however the obtained flow values are less than 150 mm which is expected to affect the pumpability of material as reported for conventional concrete. Nonetheless, it is to be noted that pumping was not adopted in this research and the rheological behaviour of FC may vary from normal concrete due to air entrainment. Also, all the mixes considered are extrudable as observed visually (Figure 5.12, and 5.13). The above mentioned reduction in the slump flow values can be attributed to cohesiveness and congestion caused by the addition of FA and PVA fibers respectively. Rheological studies will be conducted to understand complete behaviour of these 3DP-FC mixes. Furthermore, fresh density measured are within the range of limitations as prescribed by ASTM C796. For both 1000 and 1300 kg/m^3 density, fresh density attained is in the range of ±50 kg/m^3 of the target density.

Table 5.7: Fresh state characteristics of 3DP-FC (1000 kg/m^3)

Target Density	Mix ID	Slump (mm)	Slump flow (mm)	Fresh Density (kg/m^3)
1000 kg/m^3	C10	8	157	1038
	C10P2	7	164	1040
	C10P4	4	147	1014
	C10F5	6	158	1010
	C10F5P2	7	157	991
	C10F5P4	6	147	1004
	C10F10	5	136	1011
	C10F10P2	3	139	955
	C10F10P4	2	133	1034

Table 5.8: Fresh state characteristics of 3DP-FC (1300 kg/m^3)

Target Density	Mix ID	Slump (mm)	Slump flow (mm)	Fresh Density (kg/m^3)
1300 kg/m^3	C13	4	150	1283
	C13P2	5	139	1298
	C13P4	5	142	1318
	C13F5	3	138	1270
	C13F5P2	2	134	1302
	C13F5P4	2	129	1282
	C13F10	6	134	1285
	C13F10P2	5	134	1302
	C13F10P4	6	134	1304

5.4.3 Rheology of 3DP-FC

Rheological tests on 3DP-FC mixtures show that the static yield stress (SYS) and dynamic yield stress (DYS) are highly dependent on the density of the mixtures due to foam addition. However, the percentage difference between SYS and DYS for the base mixes C13 and C10 are 7.3% and 11.52% respectively (Table 5.9 and 5.10, Figure 5.11(a) and (b)). Addition of PVA fibers to the base mixes has improved the SYS and reduced the DYS for all the mixes. Increase in the SYS can be attributed to the formation of network by fibers that resists movement and deformation and subsequently reduces foam coalescence. Further, this resistance to flow or increase in SYS depends on the fiber dosage and fiber matrix bond strength. However, reduction in DYS with the increase in fiber dosage might be due to the high strain rate applied as a pre-shear which in turn causes pull out of fibers affecting the results (Feys and Khayat, 2017). The above mentioned results are contradicting slump flow values obtained in this study as well as the literature available in this regard (Amran et al., 2020). The influence of shear rate on DYS need to be studied in detail in future for the better understanding of the contradicting results. Nonetheless, viscosity of the fiber reinforced mixes was found to increase due to the agglomeration of fibers (Table 5.9 and 5.10).

Moreover, substituting sand with fly ash has resulted in 156% and 81% improvement in SYS for 50% and 100% replacement levels for FC with density of 1300 kg/m³ (Figure 5.11(a)). Similarly, for density of 1000 kg/m³, the corresponding increase is 14% and 165% for 50% and 100% replacement, respectively (Figure 5.11(b)). The aforementioned enhancement in static yield stress can be ascribed to the adsorption of FA particles on foam lamellae resulting in loss of lamellae liquid and subsequent bubble collapse. However, in mixes with higher amount of foam particularly for partial FA replacement level, increase in fluid content due to collapse of foam can be attributed to reduction in SYS. Nevertheless, for high density mixtures, solids dominate SYS to greater extent. Similarly, the DYS is increased with the increase in sand replacement level with FA due to the both increased viscosity resisting the flow and bubble breakage. Similar to the results mentioned earlier, addition of fibers to mixes with sand replaced with FA has increased the SYS and viscosity due to the formation of networks and congestion of fibers resisting the flow.

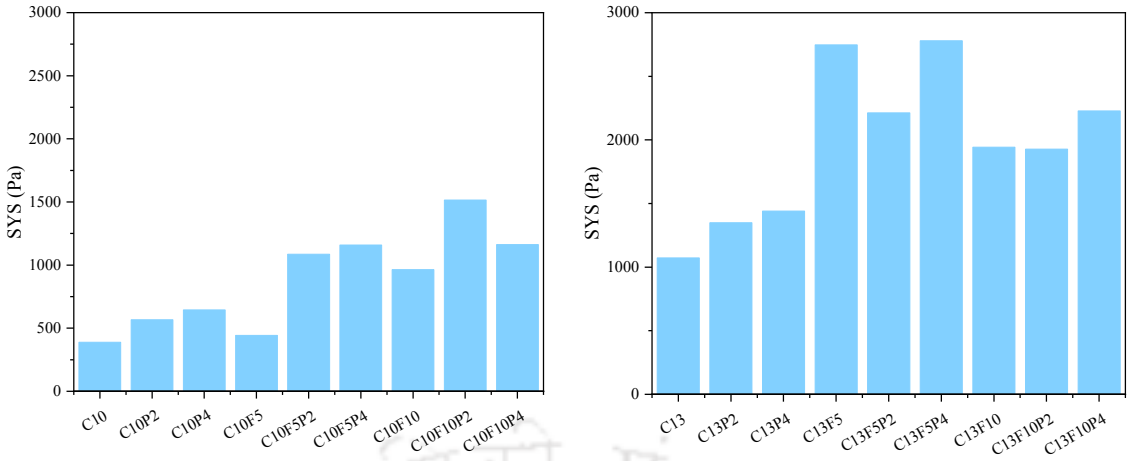

(a) (b)

Figure 5.11: Static yield stress values of 3DP-FC for the design densities (a) 1000 kg/m^3 and (b) 1300 kg/m^3.

Table 5.9: Rheological properties of 3DP-FC (of 1300 kg/m^3 density)

Target Density	Mix ID	DYS (Pa)	V (Pa.s)	R^2
1300 kg/m^3	C13	1000	7.13	0.87
	C13P2	820.08	9.36	0.92
	C13P4	700.91	8.67	0.99
	C13F5	-	-	-
	C13F5P2	988.45	4.8	0.8
	C13F5P4	718.67	22.57	0.97
	C13F10	1000	19.37	0.88
	C13F10P2	632.37	20.01	0.99
	C13F10P4	356.99	22.2	0.93

Table 5.10: Rheological properties of 3DP-FC (of 1000 kg/m^3 density)

Target Density	Mix ID	DYS (Pa)	V (Pa.s)	R^2
1000 kg/m^3	C10	348.44	1.25	0.8
	C10P2	227.89	5.51	0.96
	C10P4	152.9	6.9	0.99
	C10F5	369.63	1.77	0.98
	C10F5P2	240.86	20.75	0.99
	C10F5P4	110.83	16.59	0.98
	C10F10	870.47	6.38	0.97
	C10F10P2	493.54	18.6	1
	C10F10P4	130.66	28.37	0.97

5.4.4 Visual observation of buildability test for 3DP-FC

Figure 5.12 and 5.13 shows the results of visual observation of buildability test for both the densities. The base mixtures C13 and C10 failed at 20th and 8th layer respectively. Further, with addition of PVA fibers (0.2% and 0.4% by volume), 50%, 55%, 25%, and 175% improvement (in number of layers built) is observed for C13P2, C13P4, C10P2, and C10P4 mixes respectively when compared with the corresponding base mixes. However, print quality is not good when compared to the base mixes. Lower density mixes (i.e. 1000 kg/m^3) showed segregation of fibers from the mixture due to the presence of less solids and low static yield stress when compared to the higher density mixes (i.e. 1300 kg/m^3).

Replacement of sand with FA at 50% and 100%, improved the buildability in terms of number of layers by 100%, 100%, 62.5%, and 275% for the mixes C13F5, C13F10, C10F5, and C10F10 respectively when compared to base mixes. Reduction in improvement of buildability of the mix C10F5 is due to the bubble breakage caused by FA replacement which subsequently results in release of the water associated with foam and thereby increases flowability and affects buildability of the mix. This is not predominant in the mixture C13F5 due to relatively lesser amount of foam (33% lesser when compared to

C10F5) used in the mixture (Table 5.5 and 5.6). Similar findings are observed in rheological tests as well supporting the results of buildability test. Nevertheless, addition of 0.2% and 0.4% PVA fibers to mixes C13F5 and C13F10 reduced the number of layers built except for C13F5P4. But for 1000 kg/m^3 density, addition of fibers with C10F5 improved buildability by 38% and 46% for the mixes C10F5P2 and C10F5P4 respectively. This can be attributed to the positive effect of formation of network with fibers which helps to reduce the collapse of bubbles due to FA addition (Falliano et al., 2022). Furthermore, reduction in layers built is observed for the C10F10P2 and C10F10P4 when compared to C10F10. This reduction in buildability caused in C13F5P2, C13F5P4, C10F10P2, and C10F10P4 is due to the reduction in the densities of the mixes and print quality particularly for low density mixes.

(a) C13 (failed at 20th layer)

(b) C13P2 (failed at 30th layer)

(c) C13P4 (failed at 31st layer)

(d) C13F5 (failed at 40th layer) (e) C13F10 (failed at 40th layer)

(f) C13F5P2 (failed at 35th layer) (g) C13F5P4 (failed at 46th layer)

(h) C13F10P2 (failed at 33rd layer) (i) C13F10P4 (failed at 39th layer)

Figure 5.12: Visual measurement of layers built for different mixes of design density 1300 kg/m^3 (before failure (left), After failure (right)).

(a) C10 (failed at 8th layer)

(b) C10P2 (failed at 10th layer) (c) C10P4 (failed at 22nd layer)

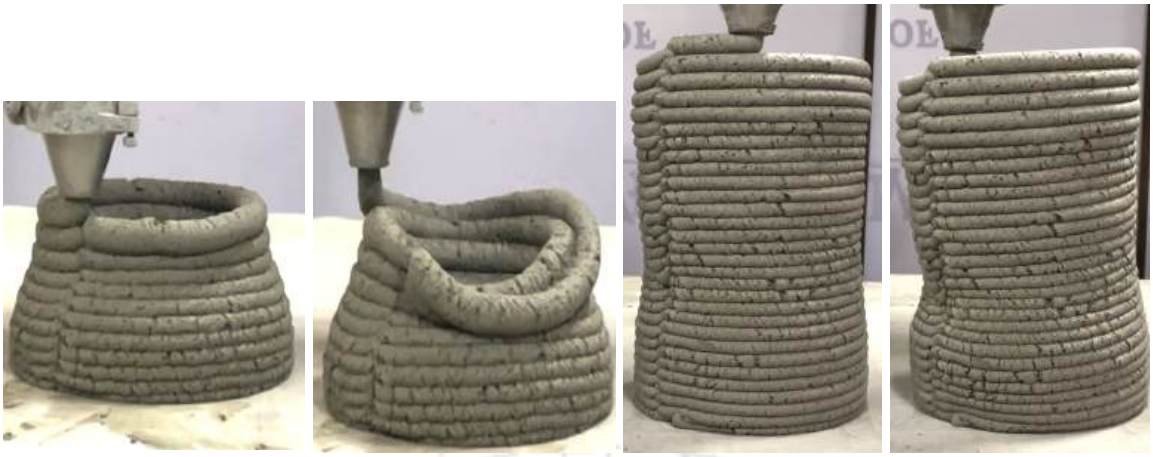

(d) C10F5 (failed at 13th layer) (e) C10F10 (failed at 30th layer)

(f) C10F5P2 (failed at 18th layer) (g) C10F5P4 (failed at 19th layer)

(h) C10F10P2 (failed at 24th layer) (i) C10F10P4 (failed at 29th layer)

Figure 5.13: Visual measurement of layers built for different mixes of design density 1000 kg/m^3 (before failure (left), After failure (right)).

5.4.5 Mechanical properties of 3DP-FC

Mechanical tests such as compressive, flexural, and bond strength are conducted as specified in section 5.3.2 and the results are presented below.

5.4.5.1 Compressive strength of 3DP-FC

Compressive strength results of 3DP-FC for both the densities are shown in Figure 5.14 and 5.15. Cast base mixes C10 and C13 achieved the strength of 1.39 and 6.04 MPa at 28 days and 1.45 and 7.03 MPa at 56 days respectively. Strength of cast samples exhibits 28% (at 28 days) and 32% (at 56 days) lesser strength than that of printed samples (when evaluated based on the average value of strength obtained in all the three directions) for C13. The corresponding decrements noted for C10 is 29% (at 28 days) and 4% (at 56 days). The above difference in strength can be attributed to the higher oven dry density of printed specimens due to the printing process (resulting in partial collapse of foam) as presented in Figure 5.12 and 5.13. Hence the observed trend is different from the studies reported in literature stating printed specimens exhibited lesser strength than cast ones (Srinivas et al., 2022). In line with above results, similar trend is observed for all the mixes considered for the study except for C10F5, C10F5P2, and C10F5P4. For the above mentioned exceptional mixes, the cast specimens exhibits higher strength than printed specimens as reported in literature for conventional 3D printed concrete (Panda et al., 2017). In the case of above mixes, foam collapse due to FA addition is more significant and hence resulted in higher oven dry densities. Another interesting observation is that there is not much difference in oven dry density of cast and printed samples of above mentioned exceptional mixes. This indicate that the influence of FA on bubble breakage of aforementioned mixes is more dominant than the effect of printing on foam stability. In this line, addition of PVA fibers also reduced the compressive strength of C10P2 and C10P4 printed specimens. This can be attributed to the lack of bonding between the matrix and fibers (Figure 5.16(a)). Cast and printed specimens of mixes C13P2 and C13P4 also exhibited similar trend of reduction in compressive strength.

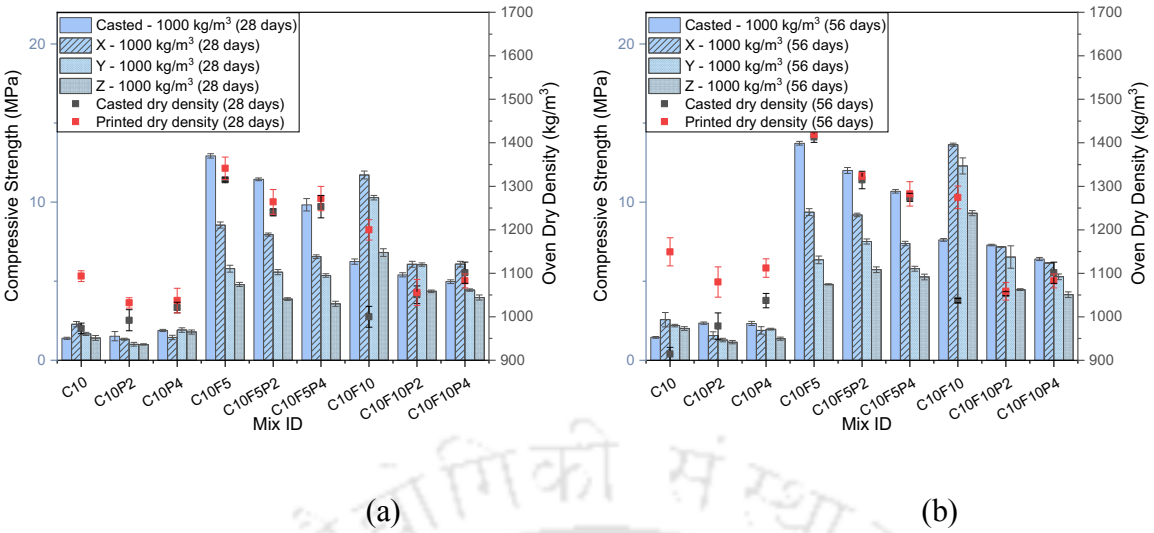

(a) (b)

Figure 5.14: Compressive strength of 3DP-FC (design density of 1000 kg/m^3).

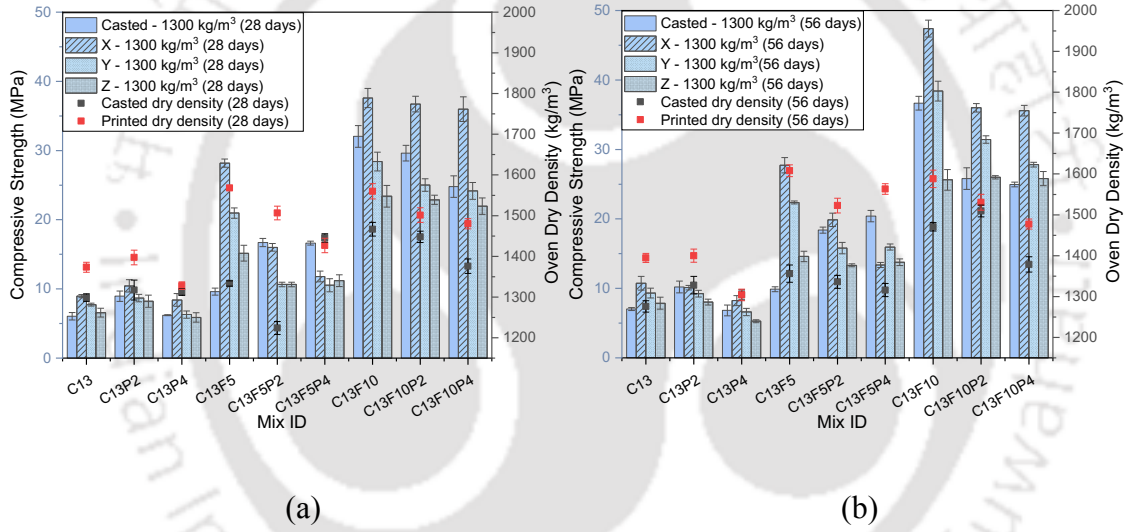

(a) (b)

Figure 5.15: Compressive strength of 3DP-FC (design density of 1300 kg/m^3).

Partial and complete replacement of sand with FA improved the compressive strength of mixes C13F5 and C13F10 with design density 1300 kg/m^3 by 176% and 284% respectively (for the printed samples). This can be attributed to the pozzolanic reaction and pore refinement resulting from addition of FA. Similar trend is observed in case of mixes with design density 1000 kg/m^3 as well. However, addition of PVA fibers to the mixes C13F5, C13F10, C10F5, and C10F10 reduced the compressive strength due to reduction of oven dry density resulting from reduction of bubble breakage. The above observation is contradictory to few studies reported in literature which stated increase in compressive strength due to enhanced bonding of fly ash matrix and fibre (Gandhi et al., 2023 and Singh et al., 2023). Although the proper bonding between the matrix and fibers are observed in

the microstructure (Figure 5.16(b)), dry density is the dominant parameter influencing the compressive strength. The low W/S ratios adopted for various mixes with fly ash in the present study could be attributed to the limited pozzolanic reaction and associated reduction in strength. Hence there is not much strength development noticed from 28 to 56 days for most of the mixes (except for C13F10) used in this study. These results are correlated with microstructural analysis in the section 5.4.9.

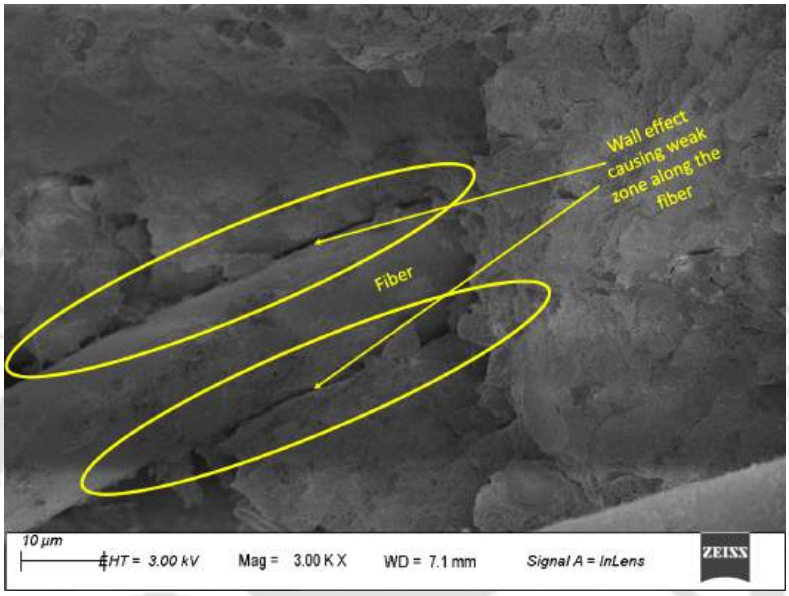

(a)

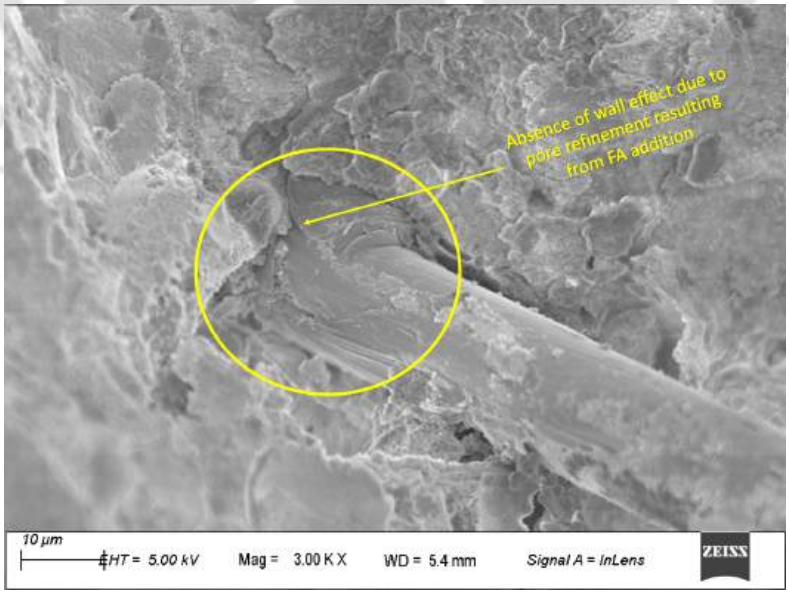

(b)

Figure 5.16: Typical FESEM images of the mixes (a) C13P4 (b) C13F10P4

Compressive anisotropicity of 3DP-FC (56 days) is presented in Figure 5.17. The base mixes C10 and C13 achieved an anisotropy of 0.25 and 0.30 respectively. Addition of fibers to base mixes increased the anisotropy by 10% and 54% for mixes C10P2 and C10P4 due to easier extrusion of paste when compared to fibers. Difference in extruding ability of paste and fibers resulted in the separation of fibers from the paste during the extrusion process. The above increment in anisotropy is more evident in low density mixes with higher dosage of the fibers. However, this behaviour is not observed in C13P2, since the mix could be extruded smoothly due to appropriate static yield stress of the paste. Moreover, the dependency of anisotropy on interlayer bond strength (as one of the factors) is already established in the literature by (Xiao et al., 2021). Bond strength reported in the Figure 5.20 follows trend opposite to anisotropy depicting the inverse proportionality. Furthermore, addition of FA as a filler replacement caused the increase in anisotropy of the 3DP-FC mixes for both partial and full replacement levels. The increase in anisotropy is about 184%, 56%, 113%, and 103% for C10F5, C10F10, C13F5, and C13F10 respectively when compared to base mixes of respective density. Although the bond strength properties are higher in 3DP-FC mixes with FA replacing sand, the bubble breakage created discrepancies in the mixture causing the higher anisotropy. Nonetheless, addition of PVA fibers to mixes with FA replacing sand reduced the anisotropy. This can also be attributed to the improvement of bond strength as evident in the Figure 5.20.

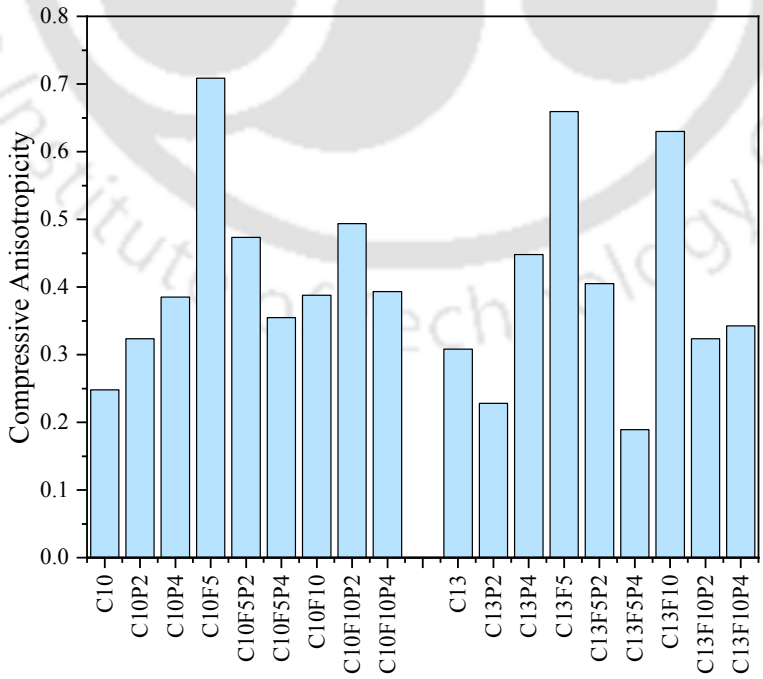

Figure 5.17: Compressive anisotropy of 3DP-FC specimens tested in 3 directions.

5.4.5.2 Flexural strength of 3DP-FC

Flexural strength of cast 3DP-FC specimens are less than printed specimens due to the higher oven dry densities of printed specimens caused by extrusion. This behaviour is similar to that of compressive strength results. Addition of PVA fibers showed an improvement in flexural strength of 100%, 255%, 5%, and 14% for the mixes C10P2, C10P4, C13P2, and C13P4 respectively when compared to the base mixes of the corresponding design densities (ref. Figure 5.18 and 5.19). This increase in flexural strength can be attributed to the tensile behaviour of the fibers used in mixes. Further, replacement of sand with FA resulted in improvement in flexural strength (at 56 days) of about 226%, 90%, 19%, and 37% for mixes C10F5, C10F10, C13F5, and C13F10 respectively when compared to the base mixes of the respective design densities. Nevertheless, the addition of fibers to mixes with FA replacing sand resulted in increment of flexural strength. This is due to the pore filling effect of the pozzolanic deposition on the pores generated by the fibers (Figure 5.16). This helped in increased flexural strength than the mixtures with sand and fibers. However, there is not much improvement in flexural strength beyond 28 days due to limited pozzolanic reaction (after 28 days) resulting from adoption of low W/S of the mixes.

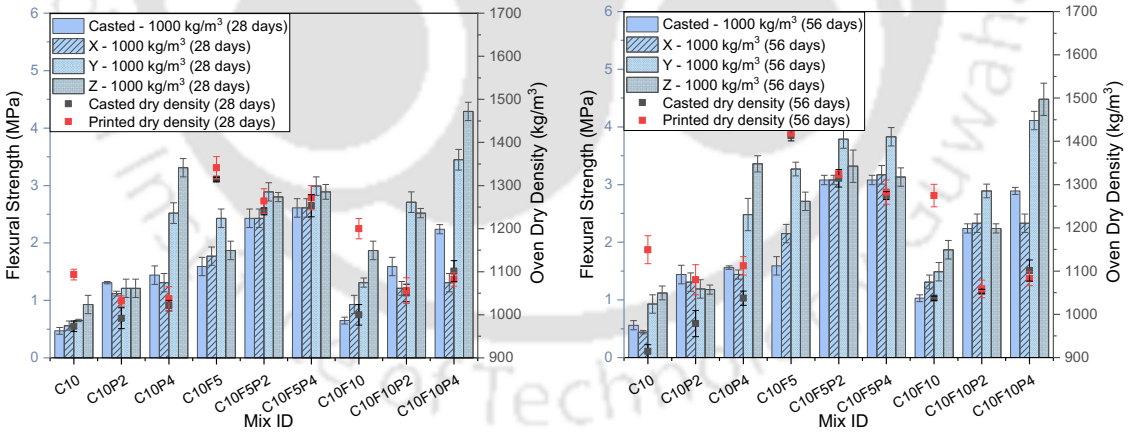

(a) (b)

Figure 5.18: Flexural strength of 3DP-FC (design density of 1000 kg/m^3).

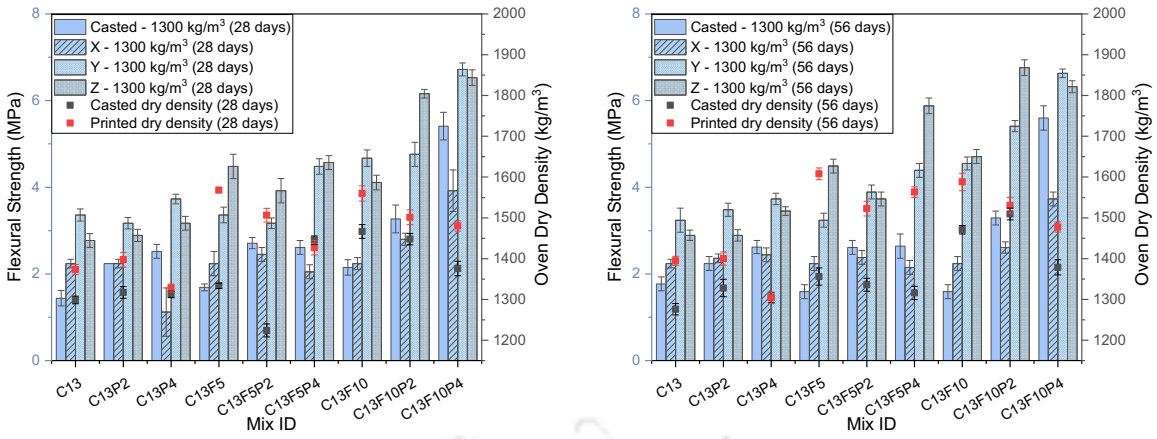

(a) (b)

Figure 5.19: Flexural strength of 3DP-FC (design density of 1300 kg/m^3).

5.4.5.3 Bond strength of 3DP-FC

Figure 5.20 shows the results of bond strength of 3DP-FC mixes. Base mixes C10 and C13 achieved bond strength of 0.45 MPa and 1.44 MPa respectively at 56 days. Addition of fibers improved the bond strength for mix C13P2 due to the contribution of fibers in enhancement of bridging effect between the layers. However, for mixes C10P2, C10P4, and C13P4, addition of fibers reduced the bond strength due to non-homogeneous distribution of fibers. Particularly for mix C10P2, even with low dosage of fibers, it is to be noted that the reduced amount of solids (when compared to higher density mixes) could be attributed to non-homogenous distribution of fibers. Further the addition of FA as a partial and full replacement caused the improvement in the bond strength due to strengthening of interface layer with additional pozzolanic CSH. Similarly, addition of fibers to mixes with FA replacing sand resulted in significant improvement in the bond strength due to the bridging effect except for C10F5P4 that could be due to diminished shape stability of the layer. Nonetheless, the bond strength showed insignificant improvement after 28 days due to limited pozzolanic reaction. FESEM images (Figure 5.28) indicate that the unreacted spherical particles of FA are abundant in the sand replaced with FA mixes confirming the limited pozzolanic reaction after 28 days.

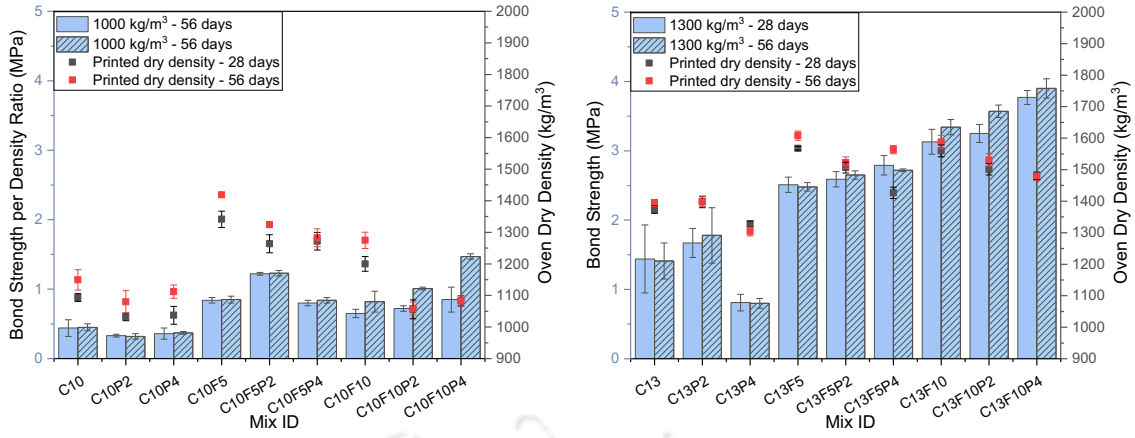

(a) (b)

Figure 5.20: Bond strength of 3DP-FC (design density of 1000 and 1300 kg/m^3).

5.4.6 Thermal properties of 3DP-FC

The results of thermal conductivity of 3DP-FC mixes are reported in Figure 5.21. The ranges of thermal conductivity of FC with design densities 1000 kg/m^3 and 1300 kg/m^3 (at 56 days) are 0.36-0.74 W/m.K and 0.50-0.91 W/mK respectively. Addition of PVA fibers reduced the thermal conductivity for all the mixes. The reduction is significant for C13P4 due to the reduction of oven dry density as well. Further, addition of FA increased the thermal conductivity value by 42%, 24%, and 21% for the mixes C10F5, C10F10, and C13F5, respectively when compared to respective control mixes of corresponding design densities. Partial replacement of sand with FA increased the densities due to bubble breakage and this in turn increased the conductivity values of 3DP-FC mixes. However, addition of PVA fibers to mixes with FA is found to reduce the conductivity values which is in line with the results reported earlier (Raj et al., 2019). These reductions in thermal conductivity can be attributed to reduction in the dry densities of 3DP-FC mixes.

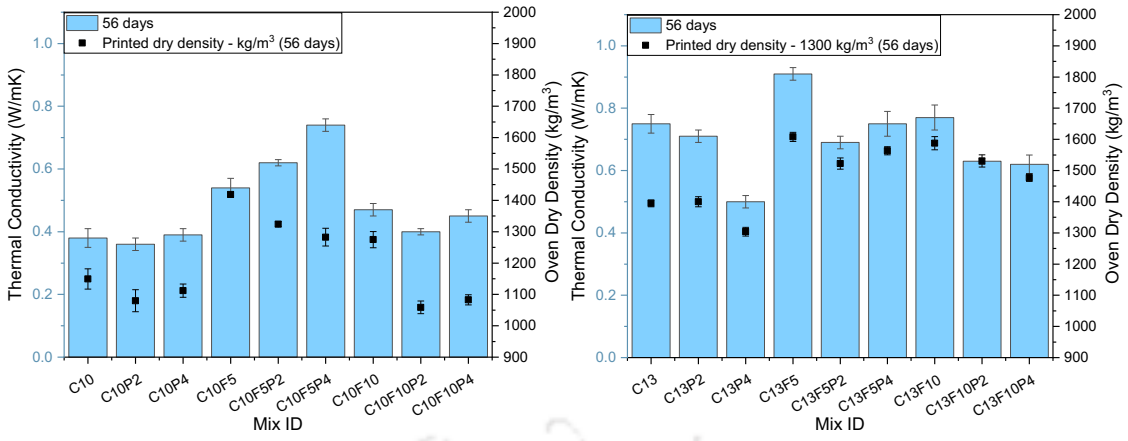

(a) (b)

Figure 5.21: Thermal Conductivity of 3DP-FC for design density of (a) 1000 kg/m^3 and (b) 1300 kg/m^3).

5.4.7 Water absorption of 3DP-FC

Density has significant impact on water absorption characteristics of 3DP-FC as observed from experimental results presented in Figure 5.22(a) and (b). Water absorption of the base mixes C10 and C13 is about 37% and 15% respectively. The results clearly indicate that an increase in foam content facilitates a greater permeation of air voids. In mixes with higher air content, the reduction in solid content, resulting in decreased inter-void thickness and closer proximity of air voids, enhances the likelihood of interconnection among entrained air voids (Yuan et al., 2021; Kamisetty et al., 2023; Raj et al., 2019). This led to the increase in water absorption behaviour of 3DP-FC with decrease in the density of the mixture. Further, addition of PVA fibers showed unsystematic behaviour in water absorption of 3DP-FC. These inconsistent results are common with the addition of fibers as there is no direct effect of fibers on water absorption (Gencel et al., 2021). Addition of FA as a sand replacement reduced the water absorption by nearly 49%, 56%, 54%, and 46% for the mixes C10F5, C10F10, C13F5, and C13F10 when compared to the corresponding base mixes, due to the bubble breakage. Nonetheless, fiber addition to sand replaced mixes (FA) has reduced the water absorption (except for C10F10P2) due to the pore refinement in the matrix surrounding the fiber as shown in Figure 5.16(b).

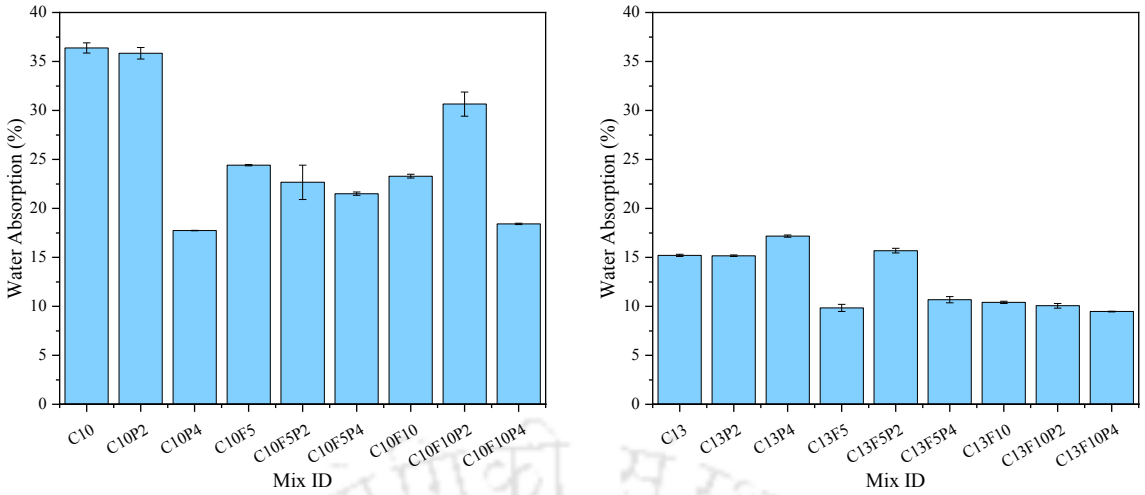

(a) (b)

Figure 5.22: Water absorption property of 3DP-FC for design density (a) 1000 kg/m^3 and (b) 1300 kg/m^3.

5.4.8 Sorption characteristics of 3DP-FC

Sorption characteristic is used as a potential measure for durability of the aerated concretes (Nambiar and Ramamurthy, 2007b). Figure 5.23 and 5.24 shows the results of sorptivity test conducted on the 3DP-FC mixes with design density 1000 and 1300 kg/m^3 respectively. The base mix C13 has higher sorption value than the C10 as presented in the Table 5.11 and 5.12. However, the sorption linear fit trend line of the base mix C10 exhibited correlation coefficient of 0.78 which is not acceptable as per ASTM C1585-20. But all the other mixes in this study are linear fitted with a correlation coefficient more than 0.98 satisfying ASTM standards. Further with the addition of PVA fibers, the interconnectivity of the bubbles has increased due to the additional pores formed along the fiber and the formation of networks by fiber with the air bubbles subsequently leading to higher sorptivity especially in the case of low density mixes (Gencel et al., 2021). With high dosage of PVA fibers the sorptivity is reduced and this can be attributed to the balling effect resulting from non-homogenous fiber distribution. Hence the effect of fiber network with the paste facilitating the capillary sorption is not realised in the above case.

Mixes having sand replaced with fly ash showed reduced Sorptivity in line with the results of water absorption. In case of 3DP-FC mixtures with design density 1300 kg/m^3, the sorptivity is reduced by 76%. This can be ascribed to the bubble breakage caused by fly

ash adsorption on to the bubbles resulting in reduction of sorptivity (Figure 5.23). Nonetheless, addition of PVA fibers to sand replaced mixes increased the sorptivity in contrary to the reduction in the water absorption as discussed in the earlier section. Hence more in depth studies are necessitated in this regard to understand the water permeation behaviour in the mixes with both fly ash and fibers.

Table 5.11: Sorptivity of 3DP-FC (of 1000 kg/m^3 density)

Design density	Mix ID	Sorption (mm/min$^{1/2}$)	SD (mm/min$^{1/2}$)	R^2
1000 kg/m^3	C10	0.130	0.023	0.780
	C10P2	0.276	0.025	0.983
	C10P4	0.190	0.003	0.991
	C10F5	0.267	0.021	0.995
	C10F5P2	0.220	0.011	0.985
	C10F5P4	0.157	0.004	0.992
	C10F10	0.382	0.025	0.986
	C10F10P2	0.445	0.017	0.992
	C10F10P4	0.202	0.004	0.993

Table 5.12: Sorptivity of 3DP-FC (of 1300 kg/m^3 density)

Design density	Mix ID	Sorption (mm/min$^{1/2}$)	SD (mm/min$^{1/2}$)	R^2
1300 kg/m^3	C13	0.221	0.037	0.800
	C13P2	0.253	0.007	0.992
	C13P4	0.178	0.005	0.992
	C13F5	0.048	0.001	0.993
	C13F5P2	0.124	0.004	0.989
	C13F5P4	0.075	0.002	0.995
	C13F10	0.042	0.0008	0.996
	C13F10P2	0.054	0.0009	0.997
	C13F10P4	0.053	0.001	0.990

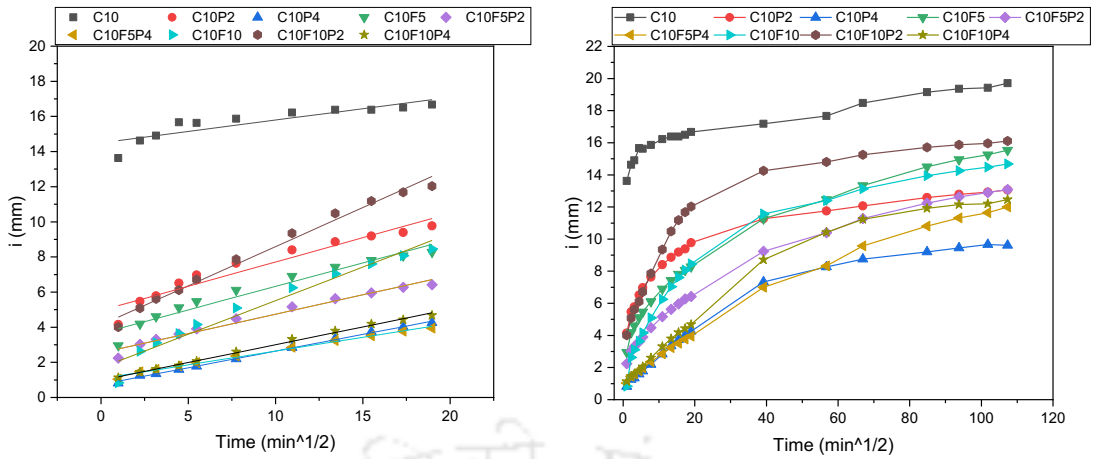

(a) (b)

Figure 5.23: Sorptivity of 3DP-FC for design density of 1000 kg/m^3 (a) Initial and (b) cumulative.

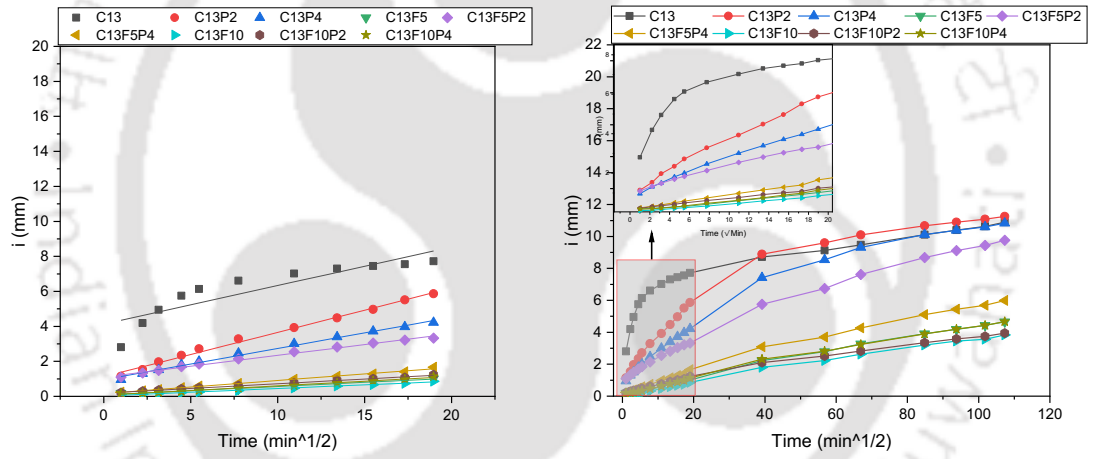

(a) (b)

Figure 5.24: Sorptivity of 3DP-FC for design density of 1300 kg/m^3 (a) Initial and (b) cumulative.

5.4.9 Chemical characteristics of 3DP-FC

Chemical characteristics of 3DP-FC are characterized using XRD, TGA, FESEM, and EDS analysis.

5.4.9.1 XRD analysis

X-ray diffractograms of 3DP-FC mixes for 1000 and 1300 kg/m^3 (at both 28 and 56 days) are shown in Figure 5.25 and 5.26. The mineralogical phases like ettringite (E), portlandite (P), quartz (Q), calcite (C), gypsum (G), and larnite (L) are identified in base mixes C10 and C13. Further, the addition of FA as partial and full replacement to sand resulted in the identification of new phase (i.e. mullite (M)) in C10F5, C10F10, C13F5, and C13F10 mixes. These replacements caused a reduction in the portlandite peaks, however, increased the quartz peaks showcasing the lime consuming pozzolanic reaction which densifies the microstructure. Semi-quantification is conducted for the mixes with FA replacing sand and reported in Figure 5.27. Table 5.13 shows the mineralogical phases identified along with RIR values obtained through semi-quantification analysis adopting RIR matrix flushing method. Semi-quantification analysis inferred that the quantum of mullite phase did not increase beyond 28 days depicting the limited pozzolanic reaction after 28 days. As mentioned earlier, adoption of low W/S ratio can be ascribed to limited pozzolanic reaction (Yu et al., 2015). Similarly, quantum of portlandite phase did not vary much beyond 28 days confirming the above inferred conclusion. However, the portlandite consumption was increased at 28 days by 37% and 40%, when replacement level of fly ash is increased from partial (C13F5 and C10F5) to full (C13F10 and C10F10).

Table 5.13: Phases identified in XRD analysis along with ICDD PDF card numbers.

Mineral phase	Card number	RIR	Phase angles (2θ)
E	01-072-0570	1.61	9.061^0, 15.728^0, 22.867^0
P	01-076-0570	3.56	34.194^0, 18.164^0, 47.340^0, 50.883^0
Q	01-082-0511	3.03	26.736^0, 21.069^0, 50.267^0
C	01-070-0095	2.09	29.624^0, 47.883^0, 48.887^0, 23.240^0
G	00-021-0816	1.70	31.127^0, 33.357^0
L	01-086-0399	1.26	32.470^0, 33.190^0
M	01-079-1276	0.75	26.203^0, 16.418^0, 35.236^0

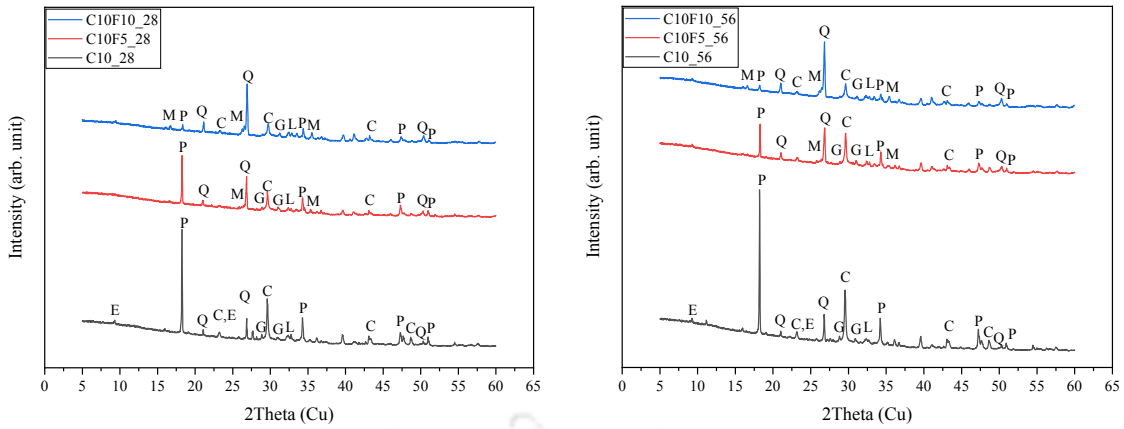

(a) (b)

Figure 5.25: X-ray diffractograms of 3DP-FC of design density 1000 kg/m^{3}measured at (a) 28 days, (b) 56 days.

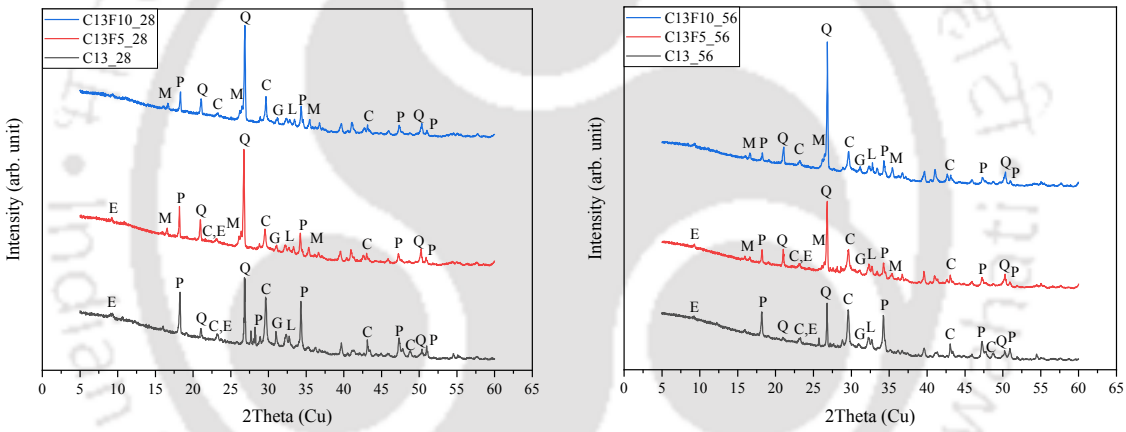

(a) (b)

Figure 5.26: X-ray diffractograms of 3DP-FC of design density 1300 kg/m^{3}measured at (a) 28 days, (b) 56 days.

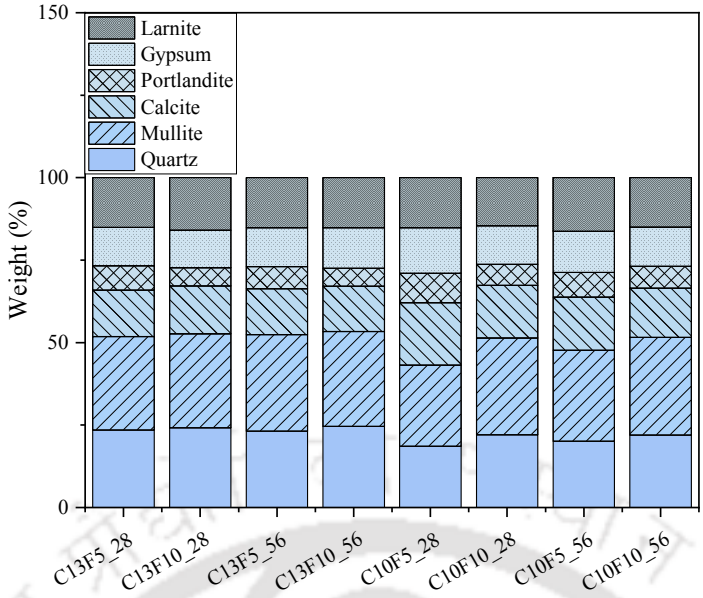

Figure 5.27: Semi-quantification of samples with FA replacing sand for both densities at 28 and 56 days.

5.4.9.2 FESEM analysis

Figure 5.28(a)-(l) shows FESEM images of all the 3DP-FC mixes. These images further confirms the XRD analysis results. Base mixes C10, and C13 shows the traces of CSH gel (in the form of reticular structure) and ettringite (in the form of needle structure) at both 28 and 56 days (Figure 5.28(a) and (b)). Furthermore, mixes with FA replacing sand (partial and full replacement) shows abundant presence of spherical unreacted and partially reacted FA particles for both the design densities of 1000 and 1300 kg/m^3 confirming the limited pozzolanic reaction after 28 days. This could be attributed to the low W/S ratios adopted in the mixes causing the unavailability of calcium dissolute (pore water) to react with FA (Fraay et al., 1989; Martin et al., 2017). Further, Figure 5.29(a) shows the availability of calcium hydroxide inside the entrained air void confirming the limited pozzolanic reaction. Nonetheless, fiber addition in 3DP-FC mixes is observed to assist in maintaining the bubble stability by supporting the pore walls and by forming network with the bubbles as shown Figure 5.29(c) and (d). On the other hand, coalescence and irregular pores are more evident in base mixes (Figure 5.29(b)).

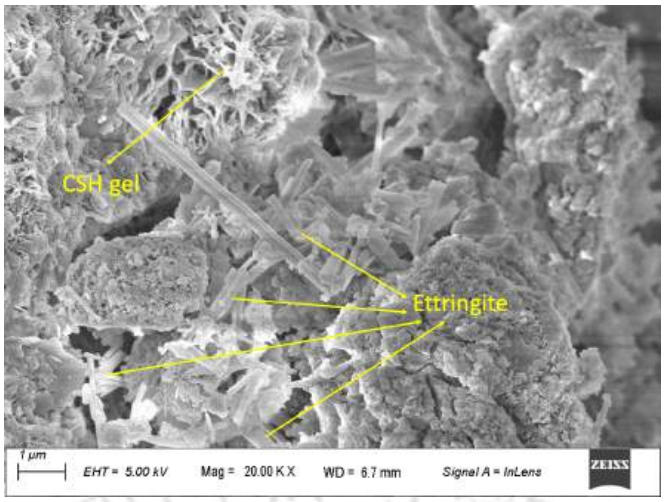

(a) C10_28days

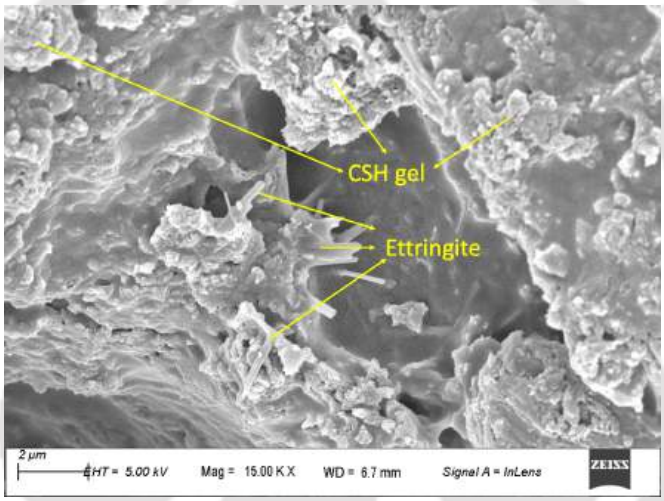

(b) C13_28days

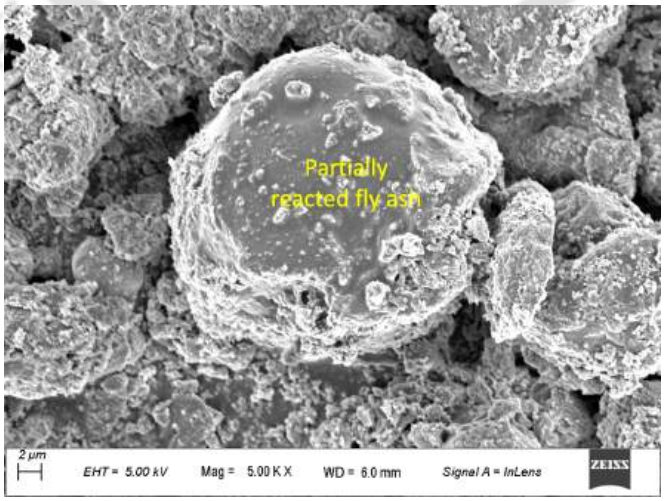

(c) C10F5_28days

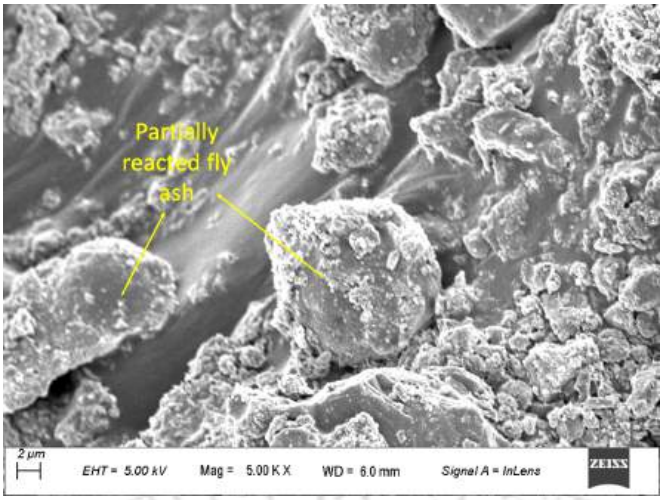

(d) C13F5_28days

(e) C10F10_28days

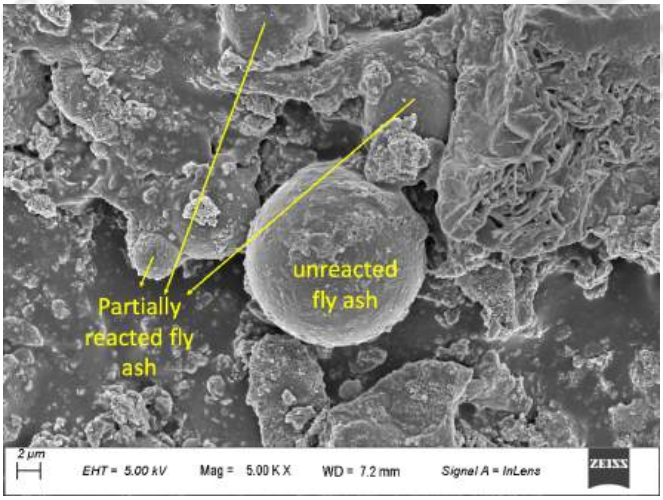

(f) C13F10_28days

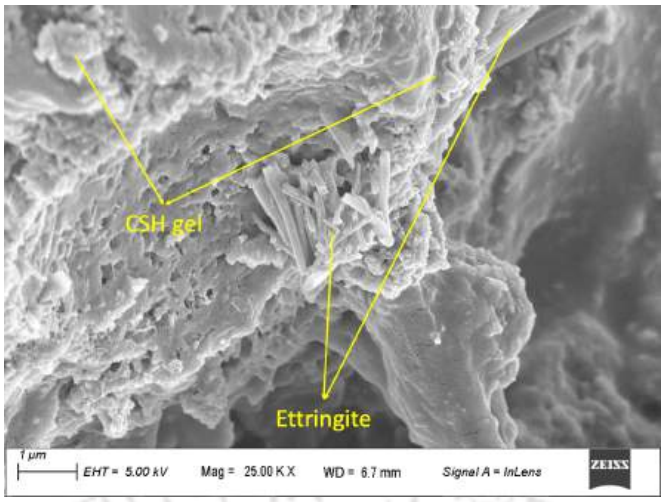

(g) C10_56days

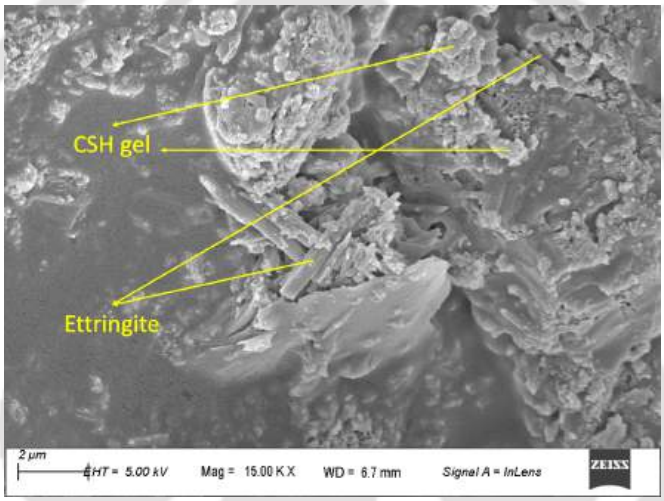

(h) C13_56days

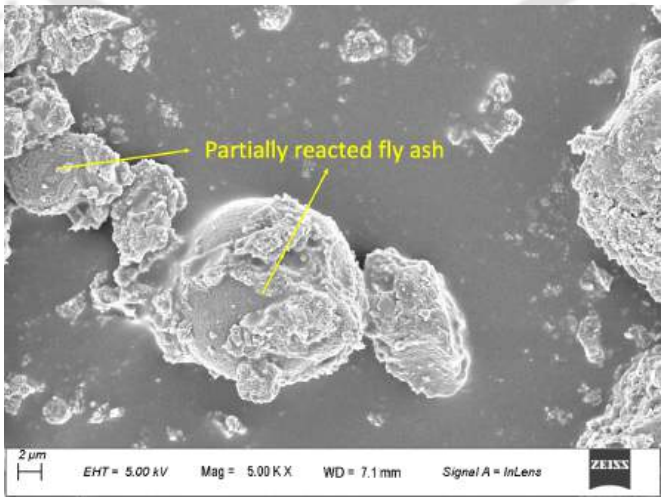

(i) C10F5_56days

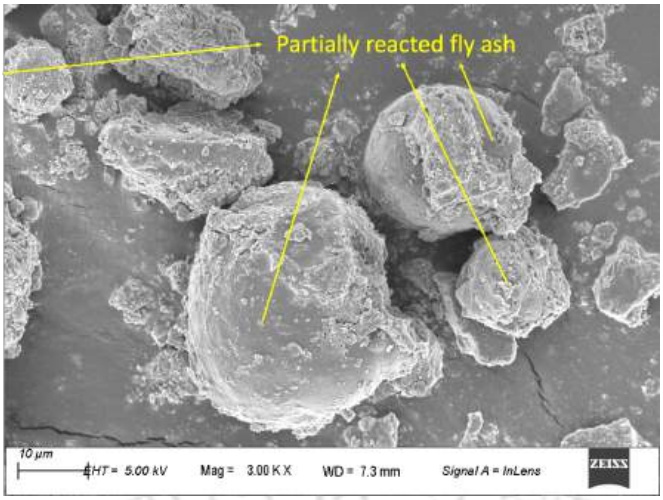

(j) C13F5_56days

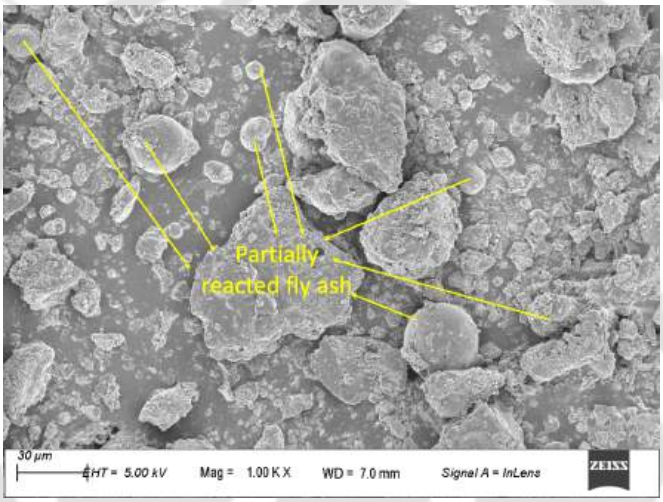

(k) C10F10_56days

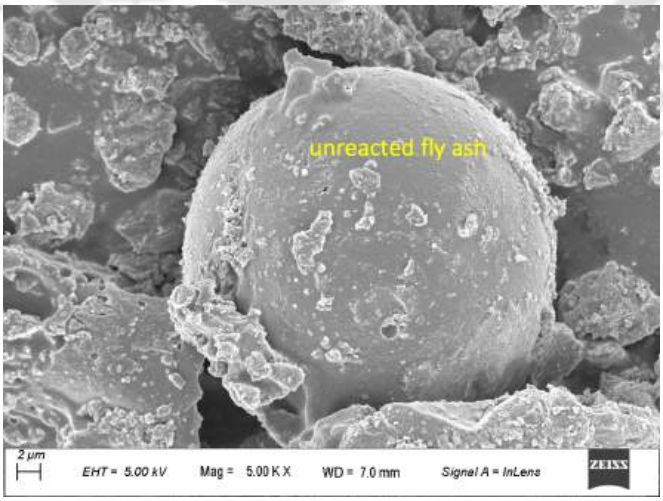

(l) C13F10_56days

Figure 5.28: FESEM images of 3DP-FC mixes.

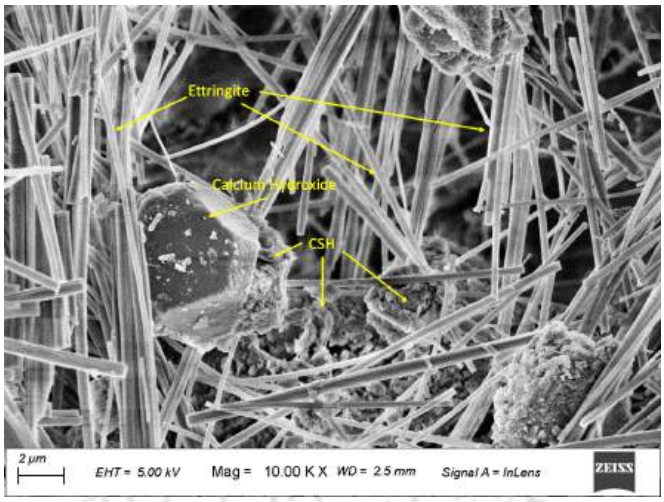
Ettringite
Calcium Hydroxide
CSH
2 µm
EHT = 5.00 kV
Mag = 10.00 K X
WD = 2.5 mm
Signal A = InLens
ZEISS

(a)

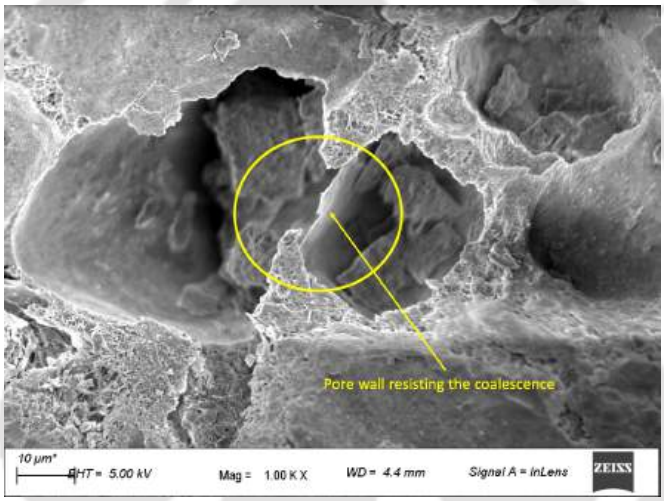
Pore wall resisting the coalescence
10 µm*
EHT = 5.00 kV
Mag = 1.00 K X
WD = 4.4 mm
Signal A = InLens
ZEISS

(b)

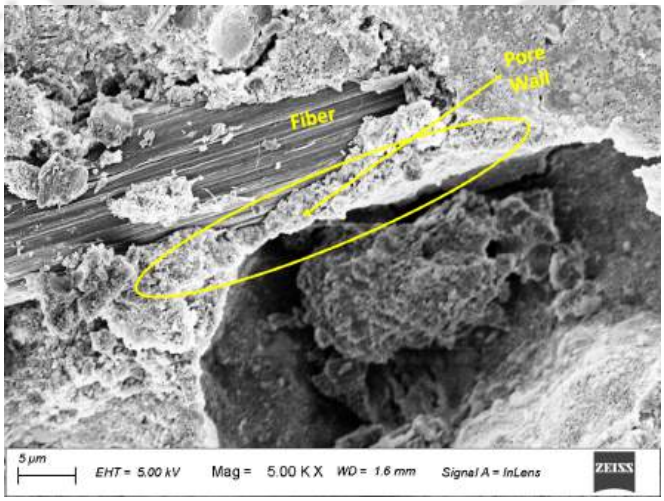
Pore Wall
Fiber
5 µm
EHT = 5.00 kV
Mag = 5.00 K X
WD = 1.6 mm
Signal A = InLens
ZEISS

(c)

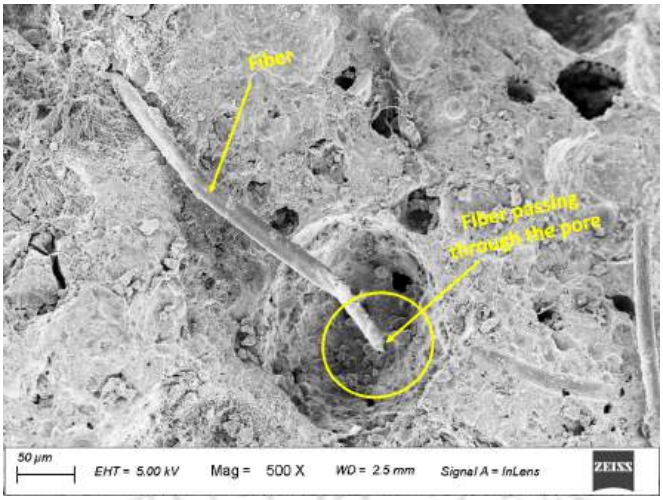

(d)

Figure 5.29: Typical FESEM images (at 56 days) showcasing (a) availability of calcium hydroxide indicating limited pozzolanic reaction (C13F5), (b) weak pore wall resisting the coalescence (C10F5), (c) fiber assisting the stability of the bubble(C13F10P2), (d) fiber connecting through the pores to form a network (C10P2).

5.4.9.3 Thermogravimetry analysis

Thermogravimetry analysis (TGA) is conducted for the 3DP-FC mixes (at 28 and 56 days) and the results are shown in the Figure 5.30 and 5.31. The mass loss (in percentage) from 105^0C to 400^0C represents the loss of bound water from CSH gel, aluminate hydrate, and ferro aluminate hydrate. Further, the mass loss from 400^0C to 480^0C represents the dehydration of portlandite phase present in the 3DP-FC. Nonetheless, the mass loss from 500^0C to 950^0C indicates the decarbonation of calcite phase resulting in the loss of mass as CO_2 gas (Jain and Pradhan, 2019). From Figure 5.30, it can be inferred that the addition of FA reduced the mass loss of portlandite in both design densities confirming the improvement of compressive strength results (due to pozzolanic activity). Similarly, decomposition of calcium carbonate is evident due to the FA addition confirming the pozzolanic reaction (Fraay et al., 1989). Further, results (Figure 5.31) of 56 days samples showed an insignificant improvement in the decomposition of (except for C10F5) depicting the limited pozzolanic reaction after 28 days supporting the mechanical results of the 3DP-FC presented in the section 5.4.5. The similar behaviour is observed for both design densities of 1000 and 1300 kg/m^3.

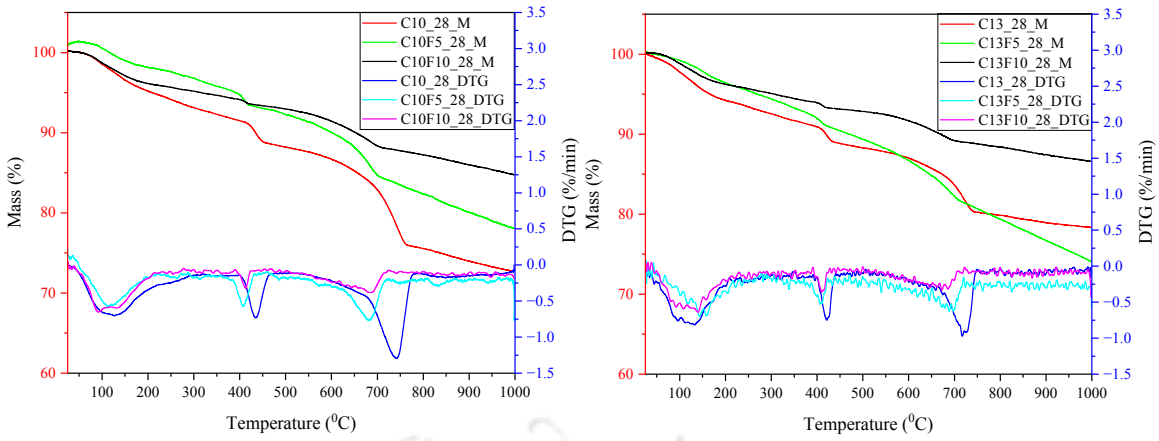

(a) (b)

Figure 5.30: Thermogravimetry analysis of 3DP-FC (at 28 days) with design densities (a) 1000 kg/m^3 and (b) 1300 kg/m^3.

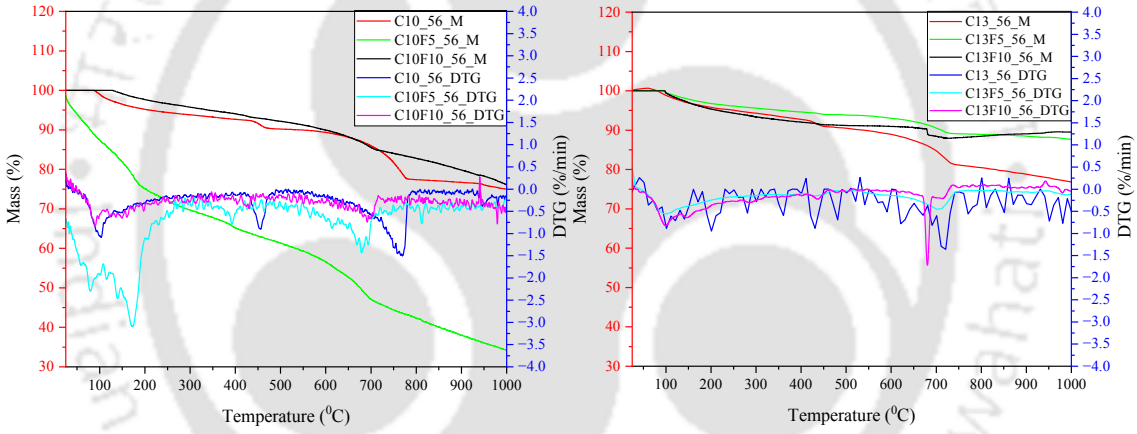

(a) (b)

Figure 5.31: Thermogravimetry analysis of 3DP-FC (at 56 days) with design densities (a) 1000 kg/m^3 and (b) 1300 kg/m^3.

5.4.9.4 Energy dispersive X-ray (EDX) analysis

EDX analysis conducted on 3DP-FC mixes are provided in the Figure 5.32 and 5.33 for both design densities 1000 and 1300 kg/m^3 (at 28 and 56 days). Ca/Si ratio of the mix C13 is higher than C10 showcasing its influence on the mechanical performance as reported literature (Kunther et al., 2017; Sahu and Gandhi 2021). Further, the mixes with sand replaced with fly ash (both in partial and full) exhibited reduction in the Ca/Si ratio by 35% and 52% for design density of 1300 kg/m^3 while it is 42% and 59% for design density of

1000 kg/m^3 respectively. These results are in line with the compressive strength results presented in the section 5.4.5.1. This reduction in Ca/Si ratios can be attributed to the pozzolanic reaction associated with the fly ash addition. Nonetheless, results of 56 days samples showed that the reduction Ca/Si ratios are insignificant when compared to the results of 28 days for both the design densities at partial and full replacement levels. This can be attributed to the limited pozzolanic reaction after 28 days that showed insignificant improvement in the mechanical performance of 3DP-FC mixes. It is worth noting that the variation of Ca/Si ratio between 28 and 56 days is less than 5% for both design density mixes (except for C13F5).

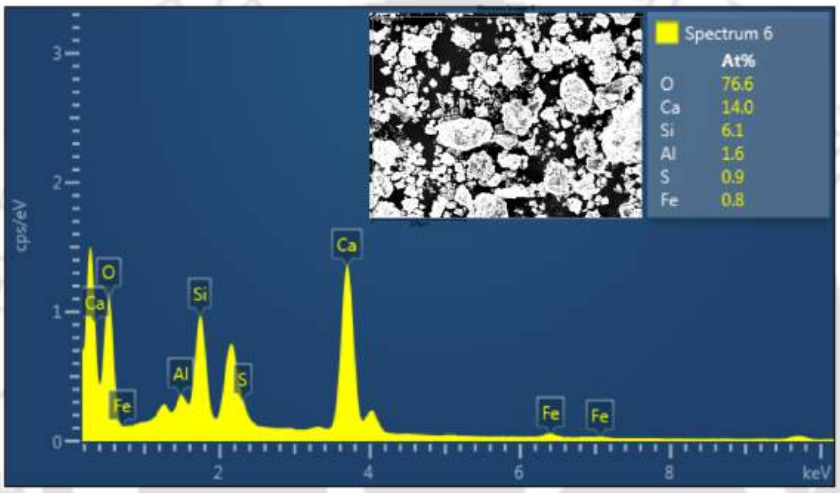

(a) C10_28days

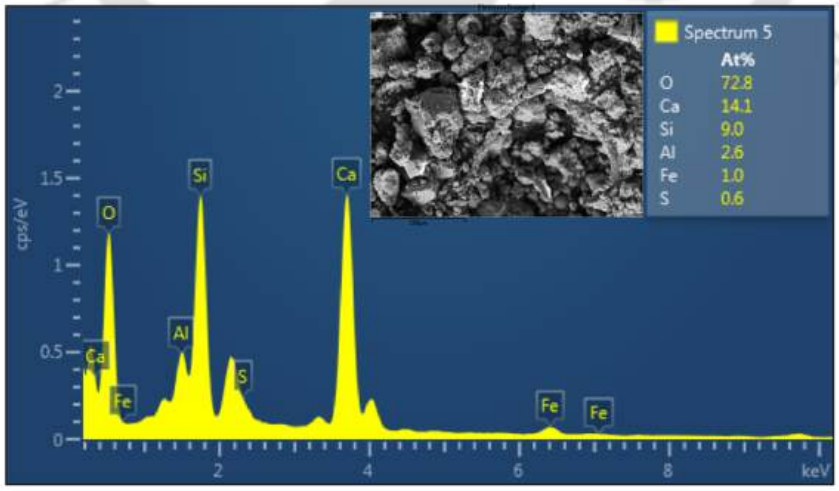

(b) C10F5_28days

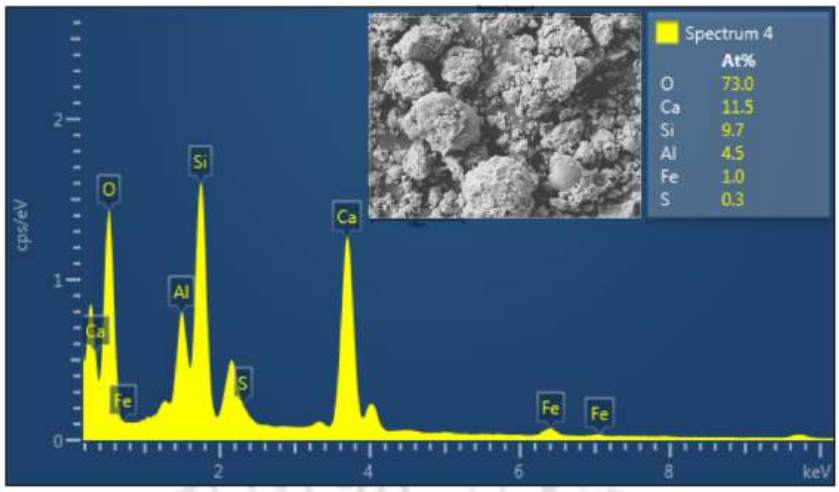

(c) C10F10_28days

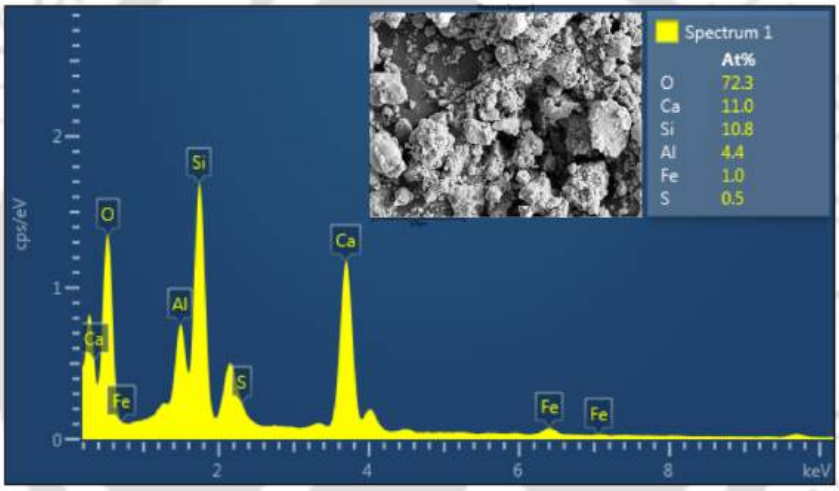

(d) C10_56days

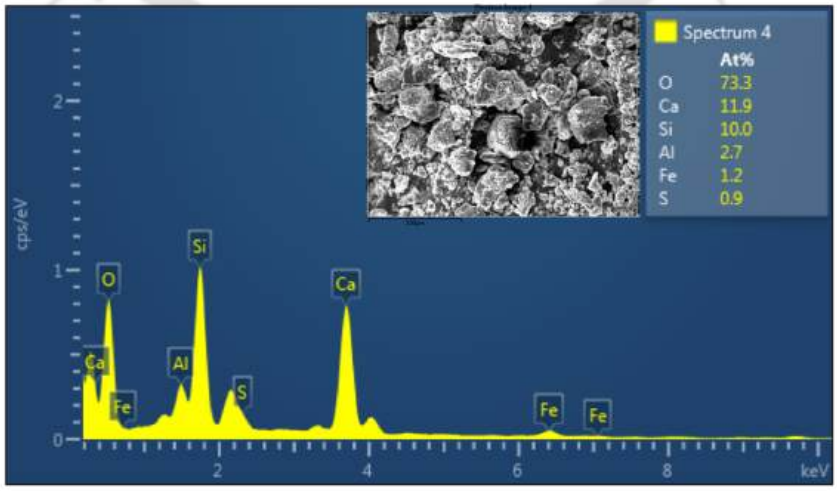

(e) C10F5_56days

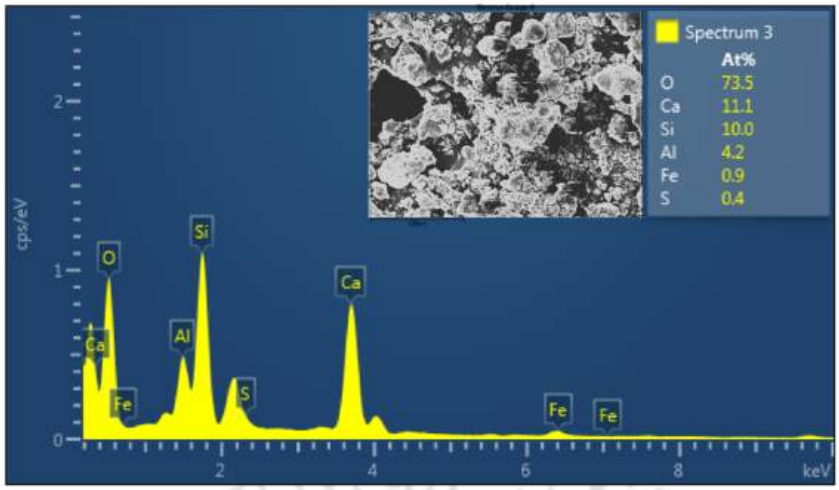

(f) C10F10_56days

Figure 5.32: EDX analysis of 3DP-FC with design density 1000 kg/m^3, (a) C10_28days, (b) C10F5_28days, (c) C10F10_28days, (d) C10_56days, (e) C10F5_56days, (f) C10F10_56days.

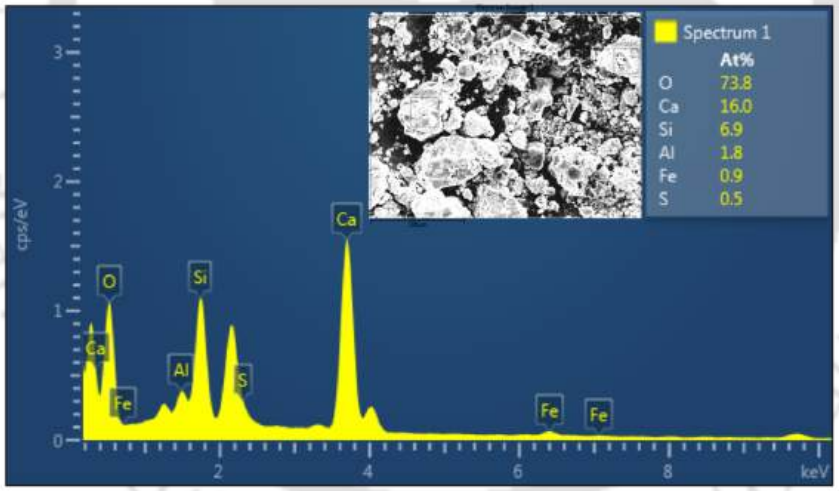

(a) C13_28days

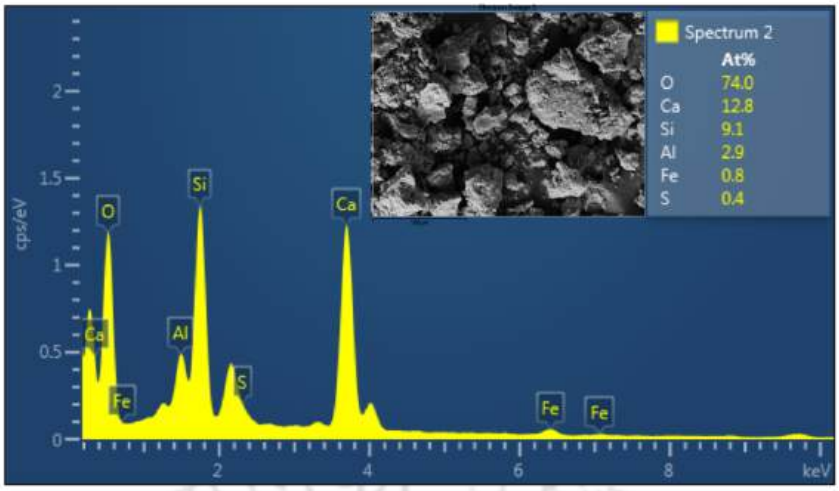

(b) C13F5_28days

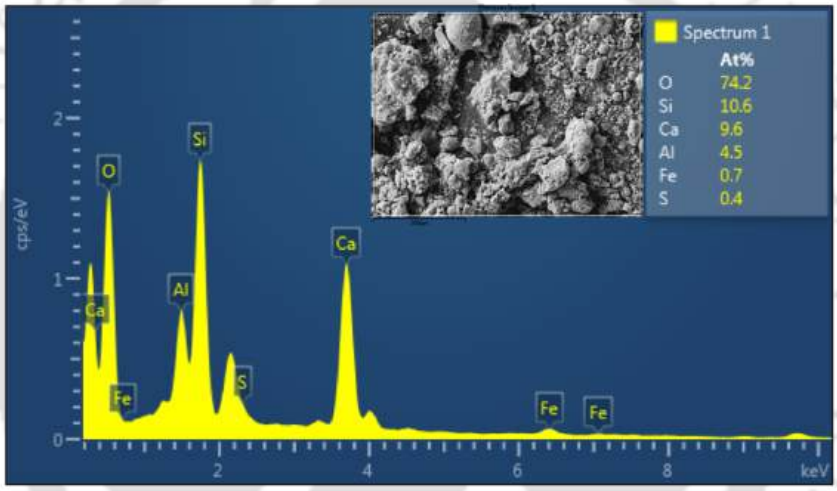

(c) C13F10_28days

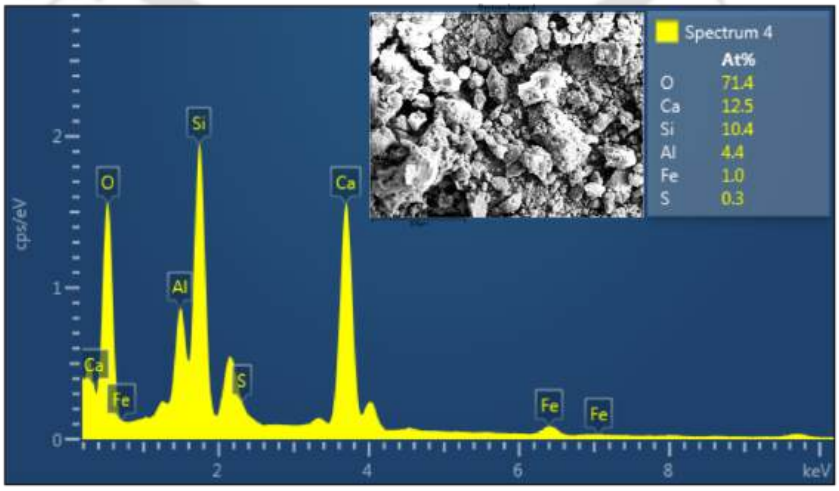

(d) C13_56days

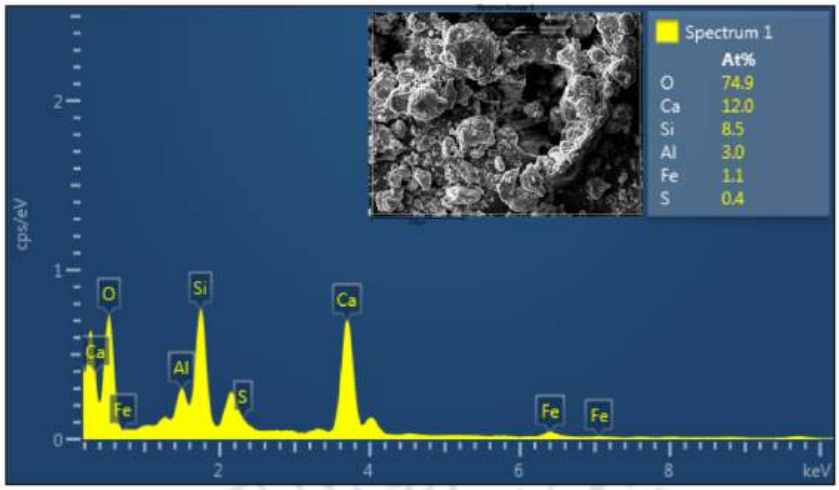

(e) C13F5_56days

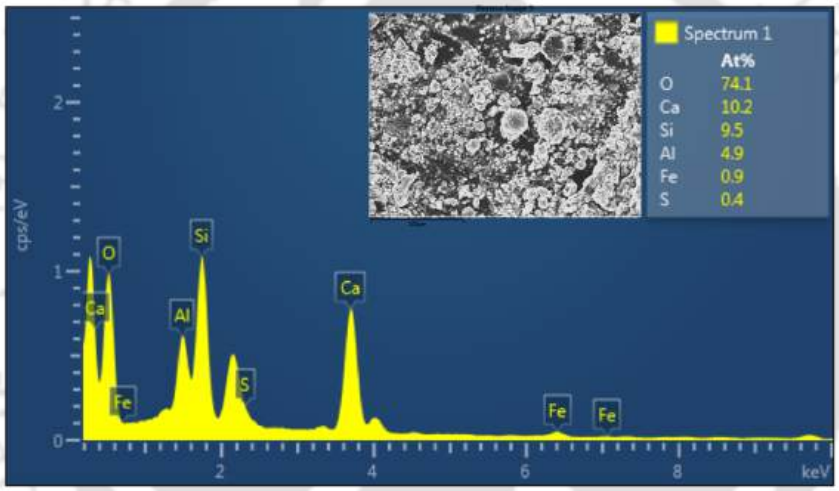

(f) C13F10_56days

Figure 5.33: EDX analysis of 3DP-FC with design density 1300 kg/m^3, (a) C13_28days, (b) C13F5_28days, (c) C13F10_28days, (d) C13_56days, (e) C13F5_56days, (f) C13F10_56days.

5.5 Summary

In this study, an attempt is made to improve the stability, rheology and mechanical properties of 3DP-FC through replacement of the sand with FA and addition of PVA fibers. Replacement of sand with FA and addition of PVA fibers has resulted in improvement of static yield stress due to the higher resistance offered to flow through cohesion and formation of networks by fibers. Although replacement of sand with FA enhanced the

buildability of 3PFC, but it is found to have negative effect on foam stability. Due to adoption of low W/S ratio to produce 3DP-FC it resulted in subsequent adsorption of water from foam bubble by FA particles, there by resulting in foam collapse and increase in dry density of the sample. However, addition of PVA fibers to mixes with FA replacing sand resulted in reduction of bubble breakage due to positive effect of formation of network with fibers. Further, the mechanical performance of 3DP-FC at 56 days indicate that the pozzolanic reaction is limited after 28 days. This is attributed to the low W/S ratio used for producing 3DP-FC mixture. It is worth noting that the anisotropicity of the 3DP-FC mixes showed opposite trend to the bond strength which states that with enhancing bond strength, the anisotropicity could be controlled. Additionally, mixes replaced sand with FA increased the thermal conductivity due to the bubble breakage. Besides, this is compensated by the addition of PVA fibers due to reduction in the dry densities of 3DP-FC mixes. Nevertheless, Density has significant impact on water absorption characteristics of 3DP-FC. It is due to the higher air content and the reduction in solid content, resulting in decreased inter-void thickness and closer proximity of air voids, enhanced the likelihood of interconnection among entrained air voids. Density has significant impact on water absorption characteristics of 3DP-FC as observed from experimental results. In mixes with higher air content, solid content is reduced, resulting in decreased inter-void thickness, enhancing the likelihood of interconnection among entrained air voids. Addition of FA as a sand replacement reduced absorption due to the bubble breakage. Nonetheless, fiber addition to sand replaced mixes has reduced the water absorption due to the pore refinement in the matrix surrounding the fiber.

भारतीय प्रौद्योगिकी संस्थान गुवाहाटी
Indian Institute of Technology Guwahati

Chapter 6

Conclusions

6.1 General

This section outlines the significant conclusions drawn from the research. Studies on foam concrete can be classified into two main sections:

1. Investigations on influence of surfactant characteristics on 3DP-FC
2. Synergistic effect of fly ash and polyvinyl alcohol fibers in improving rheology, stability and mechanical properties of 3D printable foam concrete

The experimental findings are grouped into these two sections, which pertain to the properties of the materials utilized and the range of parameters investigated. The conclusions drawn are specifically applicable to the laboratory-scale printer and the printing parameters used in this study. Additionally, these findings and tests were conducted at ambient room temperatures ranging from 25°C to 28°C, with an annual average relative humidity of 76%.

6.2 Conclusions of investigations on influence of surfactant characteristics on 3DP-FC

The aim of this study was to investigate the effects of surfactant characteristics on the extrudability and stability of 3DP-FC. Different tests on fresh properties, printability, and air void characterization were conducted for two surfactants (natural and synthetic-based) and with different foam stabilizers. The conclusions drawn from this study are as follows.

- An increase in the stabilizer concentration significantly increased the foam density and decreased the foam drainage for the surfactants. This improvement in foam behavior can be attributed to a significant increase in the viscosity of the surfactant solution owing to the increase in the stabilizer dosage.
- A surfactant solution with viscosity exceeding 5 mPa·s and surface tension lower than 31 mN/m could yield stable foam concrete with variations in the fresh density from the target densities within the ASTM- prescribed tolerance limits.

- The variation in the stabilizer concentration of the stable mixes did not significantly influence the fresh- state-related characteristics, such as slump, slump flow, and static yield stress. Similarly, the impact on the air void characteristics on 3DP-FC was minimal, unlike traditional foam concrete. The above trends indicate that the adopted stabilizers and their dosages are efficient, resulting in stable 3DP-FC mixes with appropriate rheological characteristics that enhance the bubble maintaining capacity.
- The foam volume of the mix significantly influenced the printability characteristics. Visual observation tests for extrudability and buildability showed that mixes with design density of 1300 kg/m^3 failed at the 13th layer, whereas failure occurred at 10th layer for the 1000 kg/m^3 mix.

6.3 Conclusions of synergistic effect of fly ash and polyvinyl alcohol fibers in improving rheology, stability and mechanical properties of 3d printable foam concrete

In this study, an attempt was made to improve the stability, rheology and mechanical properties of 3DP-FC through replacement of the sand with FA and addition of PVA fibers. The following are the significant conclusions drawn:

- Replacement of sand with FA and addition of PVA fibers has resulted in improvement of static yield stress due to the higher resistance offered to flow through cohesion and formation of networks by fibers.
- Although replacement of sand with FA enhanced the buildability of 3PFC, but it is found to have negative effect on foam stability. Due to adoption of low W/S ratio to produce 3DP-FC, it resulted in subsequent adsorption of water from foam bubble by FA particles, there by resulting in foam collapse and increase in dry density of the sample. However, addition of PVA fibers to mixes with FA replacing sand resulted in reduction of bubble breakage due to positive effect of formation of network with fibers.
- Addition of fiber to 3DP-FC mixes improved the flexural strength, but reduced the compressive strength due to the insufficient bonding between the fibers and matrix. Further, replacement of sand with FA improved the compressive and flexural strength, while improvement in compressive strength is noted to be dominant. Nonetheless, addition of fibers to mixes with sand replaced with FA perform better from flexural behavior perspective due to the tensile behavior of fibers dominating the composite

section in tension. While the compressive strength was reduced due to the reduced bubble breakage resulting in mixes with reduced density.

- Test results at 56 days indicate that the pozzolanic reaction is limited after 28 days. This was attributed to the low W/S ratio used for producing 3DP-FC. This conclusion was supported by XRD and FESEM analysis depicting the similar results.
- The correlation between the anisotropy and bond strength is evident from the results obtained. The trends of both the properties are inversely proportional to each other.
- Addition of PVA fibers reduced the thermal conductivity for all the mixes. But mixes replaced sand with FA increased the conductivity due to the bubble breakage. However, this was compensated by the addition of PVA fibers to mixes with FA due to reduction in the dry densities of 3DP-FC mixes.
- Density has significant impact on water absorption characteristics of 3DP-FC as observed from experimental results. In mixes with higher air content, solid content is reduced, resulting in decreased inter-void thickness, enhancing the likelihood of interconnection among entrained air voids. Addition of FA as a sand replacement reduced absorption due to the bubble breakage. Nonetheless, fiber addition to sand replaced mixes has reduced the water absorption due to the pore refinement in the matrix surrounding the fiber.

6.4 Scope for the future work

This study marks the preliminary stage of ongoing, comprehensive research into 3DP-FC. Subsequent long-term investigations can target specific areas to deepen the understanding of the material, ultimately enhancing its applicability and value within the construction industry. Following are the few research ideas that can be explored in the future:

- Investigations on developing low density FC mixtures suitable for 3DCP may be carried out. Given their significant contributions to various applications, these mixtures play a pivotal role in diverse frameworks.
- Studies on the development of 3DP-FC tailored for blast-mitigation structures, bullet traps, and other applications with a focus on rapid construction timelines can be explored.
- Conducting research on the life cycle analysis of 3DP-FC to assess its suitability for integration into large-scale applications is needed

- The existing printability models do not consider stability (a major issue in the 3DP-FC) that is potentially a major issue in the printability of foam concrete, that is to be considered as a parameter and new model could be developed.

References

ACI 523.3R-14, (2014). Guide for cellular concretes above 50 lb/ft^3 (800 kg/m^3). *American Concrete Institute.* https://books.google.co.in/books?id=-6mOoAEACAAJ

ACI 212.3R-16, (2016). Report on chemical admixtures for concrete. *American Concrete Institute.* https://books.google.co.in/books?id=WanUjwEACAAJ

Ahari, R. S., Erdem, T. K., and Ramyar, K. (2015). Thixotropy and structural breakdown properties of self consolidating concrete containing various supplementary cementitious materials. *Cement and Concrete Composites*, *59*, 26–37. https://doi.org/https://doi.org/10.1016/j.cemconcomp.2015.03.009

Akthar, F. K., and Evans, J. R. G. (2010). High porosity (> 90%) cementitious foams. *Cement and Concrete Research*, *40*(2), 352–358. https://doi.org/10.1016/j.cemconres.2009.10.012

Al Rashid, A., Khan, S. A., G. Al-Ghamdi, S., and Koç, M. (2020). Additive manufacturing: Technology, applications, markets, and opportunities for the built environment. *Automation in Construction*, *118*, 103268. https://doi.org/https://doi.org/10.1016/j.autcon.2020.103268

Alghamdi, H., Nair, S. A. O., and Neithalath, N. (2019). Insights into material design, extrusion rheology, and properties of 3D-printable alkali-activated fly ash-based binders. *Materials & Design*, *167*, 107634. https://doi.org/https://doi.org/10.1016/j.matdes.2019.107634

Alghamdi, H., and Neithalath, N. (2019). Synthesis and characterization of 3D-printable geopolymeric foams for thermally efficient building envelope materials. *Cement and Concrete Composites*, *104*(July), 103377. https://doi.org/10.1016/j.cemconcomp.2019.103377

Amran, M., Fediuk, R., Vatin, N., Lee, Y. H., Murali, G., Ozbakkaloglu, T., Klyuev, S., and Alabduljabber, H. (2020). Fibre-reinforced foamed concretes: A review. *Materials*, *13*(19), 1–36. https://doi.org/10.3390/ma13194323

Amran, Y. H. M., Farzadnia, N., and Ali, A. A. A. (2015). Properties and applications of foamed concrete; A review. *Construction and Building Materials*, *101*, 990–1005. https://doi.org/10.1016/j.conbuildmat.2015.10.112

Arunothayan, A. R., Nematollahi, B., Ranade, R., Bong, S. H., and Sanjayan, J. (2020). Development of 3D-printable ultra-high performance fiber-reinforced concrete for digital

construction. *Construction and Building Materials*, *257*, 119546. https://doi.org/10.1016/j.conbuildmat.2020.119546

Arunothayan, A. R., Nematollahi, B., Ranade, R., Bong, S. H., Sanjayan, J. G., and Khayat, K. H. (2021). Fiber orientation effects on ultra-high performance concrete formed by 3D printing. *Cement and Concrete Research*, *143*(February), 106384. https://doi.org/10.1016/j.cemconres.2021.106384

Arunothayan, A. R., Nematollahi, B., Ranade, R., Khayat, K. H., and Sanjayan, J. G. (2022). Digital fabrication of eco-friendly ultra-high performance fiber-reinforced concrete. *Cement and Concrete Composites*, *125*, 104281. https://doi.org/https://doi.org/10.1016/j.cemconcomp.2021.104281

ASTM C230/C230M-21., (2021). Standard specification for flow table for use in tests of hydraulic cement, *ASTM International, West Conshohocken, PA*, www.astm.org.

ASTM C457/C457M-16., (2016). Standard specification for flow table for use in tests of hydraulic cement, *ASTM International, West Conshohocken, PA*, www.astm.org.

ASTM C 796/C796M-19., (2019). Standard test method for foaming agents for use in producing cellular concrete using preformed foam, *ASTM International, West Conshohocken, PA,* www.astm.org.

ASTM C869/C869M-11., (2016). Standard specification for foaming agents used in making preformed foam for cellular concrete, *ASTM International, West Conshohocken, PA,* www.astm.org.

Barbosa, M. S., dos Anjos, M. A. S., Cabral, K. C., and Dias, L. S. (2022). Development of composites for 3D printing with reduced cement consumption. *Construction and Building Materials*, *341*, 127775. https://doi.org/https://doi.org/10.1016/j.conbuildmat.2022.127775

Bagheri, A., Samea, A. (2019). Effect of air content on rheology of foamed concrete. *Magazine of Concrete Research, 71(9),* 461-467. https://doi.org/10.1680/jmacr.17.00267

Bessaies-Bey, H., Khayat, K. H., Palacios, M., Schmidt, W., and Roussel, N. (2022). Viscosity modifying agents: Key components of advanced cement-based materials with adapted rheology. *Cement and Concrete Research*, *152*(October 2021), 106646. https://doi.org/10.1016/j.cemconres.2021.106646

Bhattacherjee, S., and Santhanam, M. (2020). Enhancing Buildability of 3D Printable Concrete by Spraying of Accelerating Admixture on Surface. In F. P. Bos, S. S. Lucas, R. J. M. Wolfs, and T. A. M. Salet (Eds.), *Second RILEM International Conference on Concrete*

and Digital Fabrication (pp. 13–22). Springer International Publishing. https://doi.org/10.1007/978-3-030-49916-7_2

Bhattacherjee, S., and Santhanam, M. (2022). Investigation on the effect of alkali-free aluminium sulfate based accelerator on the fresh properties of 3D printable concrete. *Cement and Concrete Composites*, *130*, 104521. https://doi.org/https://doi.org/10.1016/j.cemconcomp.2022.104521

Boddepalli, U., Gandhi, I. S. R., and Panda, B. (2023). Stability of three-dimensional printable foam concrete as function of surfactant characteristics. *Frontiers of Structural and Civil Engineering*, *17*(6), 935–947. https://doi.org/10.1007/s11709-023-0964-z

Breilly, D., Fadlallah, S., Froidevaux, V., Colas, A., and Allais, F. (2021). Origin and industrial applications of lignosulfonates with a focus on their use as superplasticizers in concrete. *Construction and Building Materials*, *301*, 124065. https://doi.org/10.1016/j.conbuildmat.2021.124065

Buswell, R. A., Leal de Silva, W. R., Jones, S. Z., and Dirrenberger, J. (2018). 3D printing using concrete extrusion: A roadmap for research. In *Cement and Concrete Research* (Vol. 112, Issue October 2017, pp. 37–49). Elsevier. https://doi.org/10.1016/j.cemconres.2018.05.006

Chatterji, S. (2003). Freezing of air-entrained cement-based materials and specific actions of air-entraining agents. *Cement and Concrete Composites*, *25*(7), 759–765. https://doi.org/https://doi.org/10.1016/S0958-9465(02)00099-9

Chaves Figueiredo, S., Romero Rodríguez, C., Ahmed, Z. Y., Bos, D. H., Xu, Y., Salet, T. M., Çopuroğlu, O., Schlangen, E., and Bos, F. P. (2019). An approach to develop printable strain hardening cementitious composites. *Materials & Design*, *169*(2019), 107651. https://doi.org/10.1016/j.matdes.2019.107651

Chen, M., Li, L., Wang, J., Huang, Y., Wang, S., Zhao, P., Lu, L., and Cheng, X. (2020d). Rheological parameters and building time of 3D printing sulphoaluminate cement paste modified by retarder and diatomite. *Construction and Building Materials*, *234*, 117391. https://doi.org/10.1016/j.conbuildmat.2019.117391

Chen, M., Liu, B., Li, L., Cao, L., Huang, Y., Wang, S., Zhao, P., Lu, L., and Cheng, X. (2020e). Rheological parameters, thixotropy and creep of 3D-printed calcium sulfoaluminate cement composites modified by bentonite. *Composites Part B: Engineering*, *186*(May 2019), 107821. https://doi.org/10.1016/j.compositesb.2020.107821

Chen, M., Yang, L., Zheng, Y., Huang, Y., Li, L., Zhao, P., Wang, S., Lu, L., and Cheng, X. (2020c). Yield stress and thixotropy control of 3D-printed calcium sulfoaluminate cement composites with metakaolin related to structural build-up. *Construction and Building Materials*, *252*, 119090. https://doi.org/https://doi.org/10.1016/j.conbuildmat.2020.119090

Chen, Y., Chaves Figueiredo, S., Li, Z., Chang, Z., Jansen, K., Çopuroğlu, O., and Schlangen, E. (2020a). Improving printability of limestone-calcined clay-based cementitious materials by using viscosity-modifying admixture. *Cement and Concrete Research*, *132*(November 2019), 106040. https://doi.org/10.1016/j.cemconres.2020.106040

Chen, Y., Chaves Figueiredo, S., Yalçinkaya, Ç., Çopuroğlu, O., Veer, F., and Schlangen, E. (2019a). The Effect of Viscosity-Modifying Admixture on the Extrudability of Limestone and Calcined Clay-Based Cementitious Material for Extrusion-Based 3D Concrete Printing. *Materials*, *12*(9), 1374. https://doi.org/10.3390/ma12091374

Chen, Y., He, S., Gan, Y., Çopuroğlu, O., Veer, F., and Schlangen, E. (2022). A review of printing strategies, sustainable cementitious materials and characterization methods in the context of extrusion-based 3D concrete printing. *Journal of Building Engineering*, *45*(November 2021), 103599. https://doi.org/10.1016/j.jobe.2021.103599

Chen, Y., Li, Z., Figueiredo, S. C., Çopuroğlu, O., Veer, F., and Schlangen, E. (2019b). Limestone and Calcined Clay-Based Sustainable Cementitious Materials for 3D Concrete Printing: A Fundamental Study of Extrudability and Early-Age Strength Development. *Applied Sciences (Switzerland)*, *9*(9). https://doi.org/10.3390/app9091809

Chen, Y., Romero Rodriguez, C., Li, Z., Chen, B., Çopuroğlu, O., and Schlangen, E. (2020b). Effect of different grade levels of calcined clays on fresh and hardened properties of ternary-blended cementitious materials for 3D printing. *Cement and Concrete Composites*, *114*(May). https://doi.org/10.1016/j.cemconcomp.2020.103708

Chica, L., and Alzate, A. (2019). Cellular concrete review: New trends for application in construction. *Construction and Building Materials*, *200*, 637–647. https://doi.org/10.1016/j.conbuildmat.2018.12.136

Cho, S. (2019, June). Mechanical evaluation of 3D printable nano-silica incorporated fibre-reinforced lightweight foam concrete. *Proceedings of the 10th International Conference on Fracture Mechanics of Concrete and Concrete Structures*. https://doi.org/10.21012/FC10.232696

Cho, S., Kruger, J., van Rooyen, A., and van Zijl, G. (2021). Rheology and application of buoyant foam concrete for digital fabrication. *Composites Part B: Engineering*, *215*(March), 108800. https://doi.org/10.1016/j.compositesb.2021.108800

Cho, S., Kruger, J., van Rooyen, A., Zeranka, S., and van Zijl, G. (2020). Rheology of 3D Printable Lightweight Foam Concrete Incorporating Nano-Silica. In V. Mechtcherine, K. Khayat, and E. Secrieru (Eds.), *Rheology and Processing of Construction Materials* (pp. 373–381). Springer International Publishing. https://doi.org/10.1007/978-3-030-22566-7_43

Cho, S., van Rooyen, A., Kearsley, E., and van Zijl, G. (2022). Foam stability of 3D printable foamed concrete. *Journal of Building Engineering*, *47*, 103884. https://doi.org/https://doi.org/10.1016/j.jobe.2021.103884

Collepardi, M. (2005). Admixtures - Enhancing Concrete Performance. In *Proceedings of the International Conference on Admixtures - Enhancing Concrete Performance*. Thomas Telford Ltd. https://doi.org/10.1680/aecp.34075

De Schutter, G., Lesage, K., Mechtcherine, V., Nerella, V. N., Habert, G., and Agusti-Juan, I. (2018). Vision of 3D printing with concrete — Technical, economic and environmental potentials. *Cement and Concrete Research*, *112*(August), 25–36. https://doi.org/10.1016/j.cemconres.2018.06.001

Dey, D., Srinivas, D., Boddepalli, U., Panda, B., Gandhi, I. S. R., and Sitharam, T. G. (2022). 3D printability of ternary Portland cement mixes containing fly ash and limestone. *Materials Today: Proceedings*, *70*, 195–200. https://doi.org/10.1016/j.matpr.2022.09.020

Dey, D., Srinivas, D., Panda, B., and Sitharam, T. G. (2023). *Processing of Cementitious Materials for 3D Concrete Printing* (pp. 283–291). Springer, Singapore. https://doi.org/10.1007/978-981-19-0561-2_26

Dey, D., Srinivas, D., Panda, B., Suraneni, P., and Sitharam, T. G. (2022). Use of industrial waste materials for 3D printing of sustainable concrete: A review. *Journal of Cleaner Production*, *340*, 130749. https://doi.org/https://doi.org/10.1016/j.jclepro.2022.130749

Dhandapani, Y., and Santhanam, M. (2020). Investigation on the microstructure-related characteristics to elucidate performance of composite cement with limestone-calcined clay combination. *Cement and Concrete Research*, *129*(October 2019), 105959. https://doi.org/10.1016/j.cemconres.2019.105959

Ding, T., Xiao, J., Zou, S., and Yu, J. (2021). Flexural properties of 3D printed fibre-reinforced concrete with recycled sand. *Construction and Building Materials*, *288*, 123077. https://doi.org/https://doi.org/10.1016/j.conbuildmat.2021.123077

Ding, T., Xiao, J., Zou, S., and Zhou, X. (2020). Anisotropic behavior in bending of 3D printed concrete reinforced with fibers. *Composite Structures*, *254*, 112808. https://doi.org/https://doi.org/10.1016/j.compstruct.2020.112808

Du Plessis, A., Babafemi, A. J., Paul, S. C., Panda, B., Tran, J. P., and Broeckhoven, C. (2021). Biomimicry for 3D concrete printing: A review and perspective. *Additive Manufacturing*, *38*, 101823. https://doi.org/https://doi.org/10.1016/j.addma.2020.101823

Ducoulombier, N., Carneau, P., Mesnil, R., Demont, L., Caron, J.-F., and Roussel, N. (2020). ``The Slug Test'': Inline Assessment of Yield Stress for Extrusion-Based Additive Manufacturing. In F. P. Bos, S. S. Lucas, R. J. M. Wolfs, and T. A. M. Salet (Eds.), *Second RILEM International Conference on Concrete and Digital Fabrication* (pp. 216–224). Springer International Publishing.

Ducoulombier, N., Mesnil, R., Carneau, P., Demont, L., Bessaies-Bey, H., Caron, J. F., and Roussel, N. (2021). The "Slugs-test" for extrusion-based additive manufacturing: Protocol, analysis and practical limits. *Cement and Concrete Composites*, *121*(March). https://doi.org/10.1016/j.cemconcomp.2021.104074

Dzuy, N. Q., and Boger, D. v. (2000). Yield Stress Measurement for Concentrated Suspensions. *Journal of Rheology*, *27*(4), 321. https://doi.org/10.1122/1.549709

Falliano, D., Domenico, D. De, Ricciardi, G., and Gugliandolo, E. (2018). *Mechanical Characterization of Extrudable Foamed Concrete : An Experimental Study*. *March*. https://doi.org/doi.org/10.5281/zenodo.1316103

Falliano, D., Domenico, D. De, Ricciardi, G., and Gugliandolo, E. (2020). 3D-printable lightweight foamed concrete and comparison with classical foamed concrete in terms of fresh state properties and mechanical strength. *Construction and Building Materials*, *254*, 119271. https://doi.org/10.1016/j.conbuildmat.2020.119271

Falliano, D., Gugliandolo, E., De Domenico, D., and Ricciardi, G. (2019a). Experimental Investigation on the Mechanical Strength and Thermal Conductivity of Extrudable Foamed Concrete and Preliminary Views on Its Potential Application in 3D Printed Multilayer Insulating Panels. In T. Wangler and R. J. Flatt (Eds.), *First RILEM International Conference on Concrete and Digital Fabrication -- Digital Concrete 2018* (pp. 277–286). Springer International Publishing.

Falliano, D., Parmigiani, S., Suarez-Riera, D., Ferro, G. A., and Restuccia, L. (2022). Stability, flexural behavior and compressive strength of ultra-lightweight fiber-reinforced foamed concrete with dry density lower than 100 kg/m3. *Journal of Building Engineering*, *51*, 104329. https://doi.org/10.1016/j.jobe.2022.104329

Falliano, D., Sciarrone, A., De Domenico, D., Maugeri, N., Longo, P., Gugliandolo, E., and Ricciardi, G. (2019b). Fiber-reinforced lightweight foamed concrete panels suitable for 3D printing applications. *IOP Conference Series: Materials Science and Engineering*, *615*(1). https://doi.org/10.1088/1757-899X/615/1/012018

Feys, D., and Khayat, K. H. (2017). Particle migration during concrete rheometry: How bad is it? *Materials and Structures*, *50*(2), 122. https://doi.org/10.1617/s11527-016-0992-4

Flatt, R., and Schober, I. (2012). Superplasticizers and the rheology of concrete. In N. B. T.-U. the R. of C. Roussel (Ed.), *Understanding the Rheology of Concrete* (pp. 144–208). Elsevier. https://doi.org/10.1533/9780857095282.2.144

Ford, S., and Despeisse, M. (2016). Additive manufacturing and sustainability: an exploratory study of the advantages and challenges. *Journal of Cleaner Production*, *137*, 1573–1587. https://doi.org/10.1016/j.jclepro.2016.04.150

Fraay, A. L. A., Bijen, J. M., and de Haan, Y. M. (1989). The reaction of fly ash in concrete a critical examination. *Cement and Concrete Research*, *19*(2), 235–246. https://doi.org/10.1016/0008-8846(89)90088-4

Francois Saucier, Michel Pigeon, and Patrick Plante. (1990). Air-void stability, Part III: Field tests of superplasticized concretes. *ACI Materials Journal*, *87*(1). https://doi.org/10.14359/2291

Gandhi, I. S. R., Boddepalli, U., Bisht, R., and Wagh, C. (2023). Impact of Addition of Fly Ash (as Sand Replacement) and Polypropylene Fibers on Energy Absorption Characteristics of Foam Concrete. *Advances in Civil Engineering Materials*, *12*(1), 20220131. https://doi.org/10.1520/ACEM20220131

Gao, Y., Hua, S., and Yue, H. (2023). Study on Preparation and Rheological Properties of 3D Printed Pre-Foaming Concrete. *Applied Sciences*, *13*(9), 5303. https://doi.org/10.3390/app13095303

Ge, Z., Yuan, H., Sun, R., Zhang, H., Wang, W., and Qi, H. (2020). Use of green calcium sulphoaluminate cement to prepare foamed concrete for road embankment: A feasibility study. *Construction and Building Materials*, *237*, 117791. https://doi.org/10.1016/j.conbuildmat.2019.117791

Gencel, O., Kazmi, S. M. S., Munir, M. J., Kaplan, G., Bayraktar, O. Y., Yarar, D. O., Karimipour, A., and Ahmad, M. R. (2021). Influence of bottom ash and polypropylene fibers on the physico-mechanical, durability and thermal performance of foam concrete: An experimental investigation. *Construction and Building Materials*, *306*(September), 124887. https://doi.org/10.1016/j.conbuildmat.2021.124887

Gosselin, C., Duballet, R., Roux, Ph., Gaudillière, N., Dirrenberger, J., and Morel, Ph. (2016). Large-scale 3D printing of ultra-high performance concrete – a new processing route for architects and builders. *Materials & Design*, *100*, 102–109. https://doi.org/https://doi.org/10.1016/j.matdes.2016.03.097

Hajimohammadi, A., Ngo, T., and Mendis, P. (2018). Enhancing the strength of pre-made foams for foam concrete applications. *Cement and Concrete Composites*, *87*, 164–171. https://doi.org/10.1016/j.cemconcomp.2017.12.014

Hamidi, F., and Aslani, F. (2019). Additive manufacturing of cementitious composites: Materials, methods, potentials, and challenges. *Construction and Building Materials*, *218*, 582–609. https://doi.org/https://doi.org/10.1016/j.conbuildmat.2019.05.140

Hekal, E. E., and Kishar, E. A. (1999). Effect of sodium salt of naphthalene-formaldehyde polycondensate on ettringite formation. *Cement and Concrete Research*, *29*(10), 1535–1540. https://doi.org/10.1016/S0008-8846(99)00110-6

Hou, S., Duan, Z., Xiao, J., and Ye, J. (2021). A review of 3D printed concrete: Performance requirements, testing measurements and mix design. *Construction and Building Materials*, *273*, 121745. https://doi.org/10.1016/j.conbuildmat.2020.121745

Huang, B., Nan, X., Fu, C., and Guo, T. (2021). Study of the bubble collapse mechanism and its influencing factors on stability under ultra-low surface tension. *Colloids and Surfaces A: Physicochemical and Engineering Aspects*, *618*, 126440. https://doi.org/10.1016/J.COLSURFA.2021.126440

Huang, F., Li, H., Yi, Z., Wang, Z., and Xie, Y. (2018). The rheological properties of self-compacting concrete containing superplasticizer and air-entraining agent. *Construction and Building Materials*, *166*, 833–838. https://doi.org/https://doi.org/10.1016/j.conbuildmat.2018.01.169

Huang, H., Yuan, Q., Deng, D., Peng, J., and Huang, Y. (2019). Effects of chemical and mineral admixtures on the foam indexes of cement-based materials. *Case Studies in Construction Materials*, *11*, e00232. https://doi.org/10.1016/j.cscm.2019.e00232

Ivanova, I., and Mechtcherine, V. (2020). Possibilities and challenges of constant shear rate test for evaluation of structural build-up rate of cementitious materials. *Cement and Concrete Research*, *130*(December 2019), 105974. https://doi.org/10.1016/j.cemconres.2020.105974

Jain, S., and Pradhan, B. (2019). Effect of cement type on hydration, microstructure and thermo-gravimetric behaviour of chloride admixed self-compacting concrete.

Construction and Building Materials, *212*, 304–316. https://doi.org/10.1016/j.conbuildmat.2019.04.001

Jayathilakage, R., Rajeev, P., and Sanjayan, J. (2020). Yield stress criteria to assess the buildability of 3D concrete printing. *Construction and Building Materials*, *240*, 117989. https://doi.org/10.1016/j.conbuildmat.2019.117989

Jeong, H., Han, S.-J., Choi, S.-H., Lee, Y., Yi, S., and Kim, K. (2019). Rheological Property Criteria for Buildable 3D Printing Concrete. *Materials*, *12*(4), 657. https://doi.org/10.3390/ma12040657

Jiao, D., De Schryver, R., Shi, C., and De Schutter, G. (2021). Thixotropic structural build-up of cement-based materials: A state-of-the-art review. *Cement and Concrete Composites*, *122*, 104152. https://doi.org/https://doi.org/10.1016/j.cemconcomp.2021.104152

Jiao, D., Shi, C., and De Schutter, G. (2022). Magneto-rheology control in 3D concrete printing: A rheological attempt. *Materials Letters*, *309*, 131374. https://doi.org/10.1016/j.matlet.2021.131374

Jones, M., and Mccarthy, A. (2005). Utilising unprocessed low-lime coal fly ash in foamed concrete. *Fuel*, *84*(11), 1398–1409. https://doi.org/10.1016/j.fuel.2004.09.030

Jones, M. R., Ozlutas, K., and Zheng, L. (2016). Stability and instability of foamed concrete. *Magazine of Concrete Research*, *68*(11), 542–549. https://doi.org/10.1680/macr.15.00097

Kamisetty, A., Gandhi, I. S. R., and Kumar, A. (2023). Combined effect of fly ash and fiber on spreadability, strength and water permeability of foam concrete. *Journal of Building Engineering*, 107607. https://doi.org/10.1016/j.jobe.2023.107607

Kashani, A., Ngo, T. D., Walkley, B., and Mendis, P. (2017). Thermal performance of calcium-rich alkali-activated materials: A microstructural and mechanical study. *Construction and Building Materials*, *153*, 225–237. https://doi.org/10.1016/j.conbuildmat.2017.07.119

Kazemian, A., Yuan, X., Cochran, E., and Khoshnevis, B. (2017). Cementitious materials for construction-scale 3D printing : Laboratory testing of fresh printing mixture. *Construction and Building Materials*, *145*, 639–647. https://doi.org/10.1016/j.conbuildmat.2017.04.015

Kearsley, E. P., and Wainwright, PJ. (2001). the Effect of fly ash content on the compressive strength development of concrete. *Cement and Concrete Research*, *31*(31), 105–112.

Khalil, N., Aouad, G., El Cheikh, K., and Rémond, S. (2017). Use of calcium sulfoaluminate cements for setting control of 3D-printing mortars. *Construction and Building Materials*, *157*, 382–391. https://doi.org/10.1016/j.conbuildmat.2017.09.109

Khan, M. A. (2020). Mix suitable for concrete 3D printing: A review. *Materials Today: Proceedings*, *32*, 831–837. https://doi.org/10.1016/j.matpr.2020.03.825

Khayat, K. H. (1998). Viscosity-enhancing admixtures for cement-based materials — An overview. *Cement and Concrete Composites*, *20*(2–3), 171–188. https://doi.org/10.1016/S0958-9465(98)80006-1

Khwairakpam, S., Gandhi, I. S. R., and Wagh, C. (2023). Investigations on Optimization of Extraction Process of Surfactant from Hingot Fruit (Balanites aegyptiaca) and Sesame Seed (Sesamum indicum) and Its Suitability in Foam Concrete Production. *Arabian Journal for Science and Engineering*. https://doi.org/10.1007/s13369-023-08098-9

Khwairakpam, S., and Ranjani Gandhi, I. S. (2020). Assessment of the potential of a naturally available foaming agent for use in the production of foam concrete. *Materials Today: Proceedings*, *32*, 896–903. https://doi.org/10.1016/j.matpr.2020.04.528

Kristombu Baduge, S., Navaratnam, S., Abu-Zidan, Y., McCormack, T., Nguyen, K., Mendis, P., Zhang, G., and Aye, L. (2021). Improving performance of additive manufactured (3D printed) concrete: A review on material mix design, processing, interlayer bonding, and reinforcing methods. *Structures*, *29*(August 2020), 1597–1609. https://doi.org/10.1016/j.istruc.2020.12.061

Kruger, J., Zeranka, S., and van Zijl, G. (2019a). 3D concrete printing: A lower bound analytical model for buildability performance quantification. *Automation in Construction*, *106*(June), 102904. https://doi.org/10.1016/j.autcon.2019.102904

Kruger, J., Zeranka, S., and van Zijl, G. (2019b). An ab initio approach for thixotropy characterisation of (nanoparticle-infused) 3D printable concrete. *Construction and Building Materials*, *224*, 372–386. https://doi.org/10.1016/j.conbuildmat.2019.07.078

Kruger, J., Zeranka, S., and Zijl, G. Van. (2020). A rheology-based quasi-static shape retention model for digitally fabricated concrete. *Construction and Building Materials*, *254*, 119241. https://doi.org/10.1016/j.conbuildmat.2020.119241

Kruger, P. J., van den Heever, M., Cho, S., Zeranka, S., and van Zijl, G. (2019). High-performance 3D printable concrete enhanced with nanomaterials. *Proceedings of the International Conference on Sustainable Materials, Systems and Structures*, *October*, 533–540.

Kunhanandan Nambiar, E. K., and Ramamurthy, K. (2008). Fresh State Characteristics of Foam Concrete. *Journal of Materials in Civil Engineering*, *20*(2), 111–117. https://doi.org/10.1061/(ASCE)0899-1561(2008)20:2(111)

Kunther, W., Ferreiro, S., and Skibsted, J. (2017). Influence of the Ca/Si ratio on the compressive strength of cementitious calcium–silicate–hydrate binders. *Journal of Materials Chemistry A*, *5*(33), 17401–17412. https://doi.org/10.1039/C7TA06104H

Le, T. T., Austin, S. A., Lim, S., Buswell, R. A., Gibb, A. G. F., and Thorpe, T. (2012). Mix design and fresh properties for high-performance printing concrete. *Materials and Structures*, *45*(8), 1221–1232. https://doi.org/10.1617/s11527-012-9828-z

Le, T. T., Austin, S. A., Lim, S., Buswell, R. A., Law, R., Gibb, A. G. F., and Thorpe, T. (2012). Hardened properties of high-performance printing concrete. *Cement and Concrete Research*, *42*(3), 558–566. https://doi.org/10.1016/j.cemconres.2011.12.003

Leal da Silva, W. R., Fryda, H., Bousseau, J.-N., Andreani, P.-A., and Andersen, T. J. (2020). Evaluation of Early-Age Concrete Structural Build-Up for 3D Concrete Printing by Oscillatory Rheometry. In *Advances in Intelligent Systems and Computing* (Vol. 975, pp. 35–47). https://doi.org/10.1007/978-3-030-20216-3_4

Leemann, A., and Winnefeld, F. (2007). The effect of viscosity modifying agents on mortar and concrete. *Cement and Concrete Composites*, *29*(5), 341–349. https://doi.org/10.1016/j.cemconcomp.2007.01.004

Li, X., Zhang, N., Yuan, J., Wang, X., Zhang, Y., Chen, F., and Zhang, Y. (2020). Preparation and microstructural characterization of a novel 3D printable building material composed of copper tailings and iron tailings. *Construction and Building Materials*, *249*, 118779. https://doi.org/10.1016/j.conbuildmat.2020.118779

Lim, S. K., Tan, C. S., Zhao, X., and Ling, T. C. (2015). Strength and toughness of lightweight foamed concrete with different sand grading. *KSCE Journal of Civil Engineering*, *19*(7), 2191–2197. https://doi.org/10.1007/s12205-014-0097-y

Liu, C., Wang, X., Chen, Y., Zhang, C., Ma, L., Deng, Z., Chen, C., Zhang, Y., Pan, J., and Banthia, N. (2021). Influence of hydroxypropyl methylcellulose and silica fume on stability, rheological properties, and printability of 3D printing foam concrete. *Cement and Concrete Composites*, *122*(May), 104158. https://doi.org/10.1016/j.cemconcomp.2021.104158

Liu, C., Xiong, Y., Chen, Y., Jia, L., Ma, L., Deng, Z., Wang, Z., Chen, C., Banthia, N., and Zhang, Y. (2022). Effect of sulphoaluminate cement on fresh and hardened properties of 3D printing foamed concrete. *Composites Part B: Engineering*, *232*, 109619. https://doi.org/10.1016/j.compositesb.2022.109619

Liu, J., Nguyen-Van, V., Panda, B., Fox, K., du Plessis, A., and Tran, P. (2021). Additive Manufacturing of Sustainable Construction Materials and Form-finding Structures: A

Review on Recent Progresses. *3D Printing and Additive Manufacturing*, *9*(1), 12–34. https://doi.org/10.1089/3dp.2020.0331

Liu, Z., Li, M., Weng, Y., Wong, T. N., and Tan, M. J. (2019). Mixture Design Approach to optimize the rheological properties of the material used in 3D cementitious material printing. *Construction and Building Materials*, *198*, 245–255. https://doi.org/10.1016/j.conbuildmat.2018.11.252

Long, W. J., Lin, C., Tao, J. L., Ye, T. H., and Fang, Y. (2021). Printability and particle packing of 3D-printable limestone calcined clay cement composites. *Construction and Building Materials*, *282*, 122647. https://doi.org/10.1016/j.conbuildmat.2021.122647

Lowke, D., Dini, E., Perrot, A., Weger, D., Gehlen, C., and Dillenburger, B. (2018). Particle-bed 3D printing in concrete construction – Possibilities and challenges. *Cement and Concrete Research*, *112*(May), 50–65. https://doi.org/10.1016/j.cemconres.2018.05.018

Lu, B., Qian, Y., Li, M., Weng, Y., Leong, K. F., Tan, M. J., and Qian, S. (2019). Designing spray-based 3D printable cementitious materials with fly ash cenosphere and air entraining agent. *Construction and Building Materials*, *211*, 1073–1084. https://doi.org/https://doi.org/10.1016/j.conbuildmat.2019.03.186

Ma, B., Peng, Y., Tan, H., Jian, S., Zhi, Z., Guo, Y., Qi, H., Zhang, T., and He, X. (2018). Effect of hydroxypropyl-methyl cellulose ether on rheology of cement paste plasticized by polycarboxylate superplasticizer. *Construction and Building Materials*, *160*, 341–350. https://doi.org/10.1016/j.conbuildmat.2017.11.010

Ma, G., Li, Z., and Wang, L. (2018). Printable properties of cementitious material containing copper tailings for extrusion based 3D printing. *Construction and Building Materials*, *162*, 613–627. https://doi.org/10.1016/j.conbuildmat.2017.12.051

Ma, G., and Wang, L. (2018). A critical review of preparation design and workability measurement of concrete material for largescale 3D printing. *Frontiers of Structural and Civil Engineering*, *12*(3), 382–400. https://doi.org/10.1007/s11709-017-0430-x

Marchon, D., Kawashima, S., Bessaies-Bey, H., Mantellato, S., and Ng, S. (2018). Hydration and rheology control of concrete for digital fabrication: Potential admixtures and cement chemistry. *Cement and Concrete Research*, *112*(December 2017), 96–110. https://doi.org/10.1016/j.cemconres.2018.05.014

Markin, Nerella, Schröfl, Guseynova, and Mechtcherine. (2019). Material Design and Performance Evaluation of Foam Concrete for Digital Fabrication. *Materials*, *12*(15), 2433. https://doi.org/10.3390/ma12152433

Markin, V., Krause, M., Otto, J., Schröfl, C., and Mechtcherine, V. (2021). 3D printing with foam concrete: from material design and testing to application and sustaintability. *Journal of Building Engineering*, 102870. https://doi.org/10.1016/j.jobe.2021.102870

Markin, V., Sahmenko, G., Nerella, V. N., Näther, M., and Mechtcherine, V. (2019). Investigations on the foam concrete production techniques suitable for 3D-printing with foam concrete. *IOP Conference Series: Materials Science and Engineering*, *660*(1), 012039. https://doi.org/10.1088/1757-899X/660/1/012039

Martin, L. H. J., Winnefeld, F., Tschopp, E., Müller, C. J., and Lothenbach, B. (2017). Influence of fly ash on the hydration of calcium sulfoaluminate cement. *Cement and Concrete Research*, *95*, 152–163. https://doi.org/10.1016/j.cemconres.2017.02.030

Mechtcherine, V., Bos, F. P., Perrot, A., da Silva, W. R. L., Nerella, V. N., Fataei, S., Wolfs, R. J. M., Sonebi, M., and Roussel, N. (2020). Extrusion-based additive manufacturing with cement-based materials – Production steps, processes, and their underlying physics: A review. In *Cement and Concrete Research* (Vol. 132, Issue March, p. 106037). Elsevier. https://doi.org/10.1016/j.cemconres.2020.106037

Menna, C., Mata-Falcón, J., Bos, F. P., Vantyghem, G., Ferrara, L., Asprone, D., Salet, T., and Kaufmann, W. (2020). Opportunities and challenges for structural engineering of digitally fabricated concrete. *Cement and Concrete Research*, *133*, 106079. https://doi.org/10.1016/j.cemconres.2020.106079

Mohan, M. K., Rahul, A. V., van Tittelboom, K., and de Schutter, G. (2021). Rheological and pumping behaviour of 3D printable cementitious materials with varying aggregate content. *Cement and Concrete Research*, *139*(September 2020), 106258. https://doi.org/10.1016/j.cemconres.2020.106258

Mohan, M. K., Rahul, A. V., De Schutter, G., and Van Tittelboom, K. (2021). Early age hydration, rheology and pumping characteristics of CSA cement-based 3D printable concrete. *Construction and Building Materials*, *275*, 122136. https://doi.org/10.1016/j.conbuildmat.2020.122136

Mohan, M. K., Rahul, A. V, Schutter, G. De, and Tittelboom, K. Van. (2021). Extrusion-based concrete 3D printing from a material perspective : A state-of-the-art review. *Cement and Concrete Composites*, *115*(June 2020), 103855. https://doi.org/10.1016/j.cemconcomp.2020.103855

Muthukrishnan, S., Kua, H. W., Yu, L. N., and Chung, J. K. H. (2020). Fresh Properties of Cementitious Materials Containing Rice Husk Ash for Construction 3D Printing. *Journal*

of Materials in Civil Engineering, *32*(8), 04020195. https://doi.org/10.1061/(ASCE)MT.1943-5533.0003230

Muthukrishnan, S., Ramakrishnan, S., and Sanjayan, J. (2021). Effect of alkali reactions on the rheology of one-part 3D printable geopolymer concrete. *Cement and Concrete Composites*, *116*(December 2020), 103899. https://doi.org/10.1016/j.cemconcomp.2020.103899

Nambiar, E. K. K., and Ramamurthy, K. (2006a). Influence of filler type on the properties of foam concrete. *Cement and Concrete Composites*, *28*(5), 475–480. https://doi.org/10.1016/j.cemconcomp.2005.12.001

Nambiar, E. K. K., and Ramamurthy, K. (2006b). Models relating mixture composition to the density and strength of foam concrete using response surface methodology. *Cement and Concrete Composites*, *28*(9), 752–760. https://doi.org/10.1016/j.cemconcomp.2006.06.001

Nambiar, E. K. K., and Ramamurthy, K. (2007a). Air-void characterisation of foam concrete. *Cement and Concrete Research*, *37*(2), 221–230. https://doi.org/10.1016/J.CEMCONRES.2006.10.009

Nambiar, E. K. K., and Ramamurthy, K. (2007b). Sorption characteristics of foam concrete. *Cement and Concrete Research*, *37*(9), 1341–1347. https://doi.org/10.1016/j.cemconres.2007.05.010

Nambiar, E. K. K., and Ramamurthy, K. (2009). Shrinkage Behavior of Foam Concrete. *Journal of Materials in Civil Engineering*, *21*(11), 631–636. https://doi.org/10.1061/(asce)0899-1561(2009)21:11(631)

Natanzi, A. S., and McNally, C. (2020). *Characterising Concrete Mixes for 3D Printing* (F. P. Bos, S. S. Lucas, R. J. M. Wolfs, and T. A. M. Salet, Eds.; pp. 83–92). Springer International Publishing. https://doi.org/10.1007/978-3-030-49916-7_9

Navarrete, I., Kurama, Y., Escalona, N., and Lopez, M. (2020). Impact of physical and physicochemical properties of supplementary cementitious materials on structural build-up of cement-based pastes. *Cement and Concrete Research*, *130*, 105994. https://doi.org/https://doi.org/10.1016/j.cemconres.2020.105994

Nerella, V. N., Beigh, M. A. B., Fataei, S., and Mechtcherine, V. (2019). Strain-based approach for measuring structural build-up of cement pastes in the context of digital construction. *Cement and Concrete Research*, *115*(August 2018), 530–544. https://doi.org/10.1016/j.cemconres.2018.08.003

Nerella, V. N., and Mechtcherine, V. (2018). Virtual Sliding Pipe Rheometer for estimating pumpability of concrete. *Construction and Building Materials*, *170*, 366–377. https://doi.org/10.1016/j.conbuildmat.2018.03.003

Nerella, V. N., Näther, M., Iqbal, A., Butler, M., and Mechtcherine, V. (2019). Inline quantification of extrudability of cementitious materials for digital construction. *Cement and Concrete Composites*, *95*(September 2018), 260–270. https://doi.org/10.1016/j.cemconcomp.2018.09.015

Nguyen, N. T., Bui, T.-T., and Bui, Q.-B. (2022). Fiber reinforced concrete for slabs without steel rebar reinforcement: Assessing the feasibility for 3D-printed individual houses. *Case Studies in Construction Materials*, *16*, e00950. https://doi.org/https://doi.org/10.1016/j.cscm.2022.e00950

Nguyen-Van, V., Nguyen-Xuan, H., Panda, B., and Tran, P. (2022). 3D concrete printing modelling of thin-walled structures. *Structures*, *39*, 496–511. https://doi.org/https://doi.org/10.1016/j.istruc.2022.03.049

Ogura, H., Nerella, V. N., and Mechtcherine, V. (2018). Developing and testing of Strain-Hardening Cement-Based Composites (SHCC) in the context of 3D-printing. *Materials*, *11*(8), 1–18. https://doi.org/10.3390/ma11081375

Othuman, M. A., and Wang, Y. C. (2011). Elevated-temperature thermal properties of lightweight foamed concrete. *Construction and Building Materials*, *25*(2), 705–716. https://doi.org/10.1016/j.conbuildmat.2010.07.016

Palacios, M., and Flatt, R. J. (2016). Working mechanism of viscosity-modifying admixtures. In *Science and Technology of Concrete Admixtures: Vol. i* (pp. 415–432). Elsevier Ltd. https://doi.org/10.1016/B978-0-08-100693-1.00020-5

Pan, T., Jiang, Y., and Ji, X. (2022). Interlayer bonding investigation of 3D printing cementitious materials with fluidity-retaining polycarboxylate superplasticizer and high-dispersion polycarboxylate superplasticizer. *Construction and Building Materials*, *330*, 127151. https://doi.org/https://doi.org/10.1016/j.conbuildmat.2022.127151

Panda, B., Lim, J. H., and Tan, M. J. (2019). Mechanical properties and deformation behaviour of early age concrete in the context of digital construction. *Composites Part B: Engineering*, *165*, 563–571. https://doi.org/10.1016/j.compositesb.2019.02.040

Panda, B., Noor Mohamed, N. A., Paul, S. C., Bhagath Singh, G., Tan, M. J., and Šavija, B. (2019). The Effect of Material Fresh Properties and Process Parameters on Buildability and Interlayer Adhesion of 3D Printed Concrete. *Materials*, *12*(13), 2149. https://doi.org/10.3390/ma12132149

Panda, B., Paul, S. C., and Tan, M. J. (2017). Anisotropic mechanical performance of 3D printed fiber reinforced sustainable construction material. *Materials Letters*, *209*, 146–149. https://doi.org/10.1016/j.matlet.2017.07.123

Panda, B., and Tan, M. J. (2018). Experimental study on mix proportion and fresh properties of fl y ash based geopolymer for 3D concrete printing. *Ceramics International*, *44*(9), 10258–10265. https://doi.org/10.1016/j.ceramint.2018.03.031

Panda, B., and Tan, M. J. (2019). Rheological behavior of high volume fly ash mixtures containing micro silica for digital construction application. *Materials Letters*, *237*, 348–351. https://doi.org/https://doi.org/10.1016/j.matlet.2018.11.131

Panda, B., Tay, Y. W. D., Paul, S. C., and Tan, M. J. (2018). Current challenges and future potential of 3D concrete printing. *Materialwissenschaft Und Werkstofftechnik*, *49*(5), 666–673. https://doi.org/https://doi.org/10.1002/mawe.201700279

Panda, B., and Tran, J. (2022). *Material Design, Additive Manufacturing, and Performance of Cement-Based Materials BT - Innovation in Construction: A Practical Guide to Transforming the Construction Industry* (S. H. Ghaffar, P. Mullett, E. Pei, and J. Roberts, Eds.; pp. 301–320). Springer International Publishing. https://doi.org/10.1007/978-3-030-95798-8_13

Panda, B., Unluer, C., and Tan, M. J. (2019). Extrusion and rheology characterization of geopolymer nanocomposites used in 3D printing. *Composites Part B: Engineering*, *176*(July), 107290. https://doi.org/10.1016/j.compositesb.2019.107290

Panesar, D. K. (2013). Cellular concrete properties and the effect of synthetic and protein foaming agents. *Construction and Building Materials*, *44*, 575–584. https://doi.org/10.1016/j.conbuildmat.2013.03.024

Papo, A., and Piani, L. (2004). Effect of various superplasticizers on the rheological properties of Portland cement pastes. *Cement and Concrete Research*, *34*(11), 2097–2101. https://doi.org/10.1016/j.cemconres.2004.03.017

Pasupathy, K., Ramakrishnan, S., and Sanjayan, J. (2022). Enhancing the properties of foam concrete 3D printing using porous aggregates. *Cement and Concrete Composites*, *133*, 104687. https://doi.org/10.1016/j.cemconcomp.2022.104687

Patural, L., Marchal, P., Govin, A., Grosseau, P., Ruot, B., and Devès, O. (2011). Cellulose ethers influence on water retention and consistency in cement-based mortars. *Cement and Concrete Research*, *41*(1), 46–55. https://doi.org/https://doi.org/10.1016/j.cemconres.2010.09.004

Paul, S. C., Tay, Y. W. D., Panda, B., and Tan, M. J. (2018). Fresh and hardened properties of 3D printable cementitious materials for building and construction. *Archives of Civil and Mechanical Engineering*, *18*(1), 311–319. https://doi.org/10.1016/j.acme.2017.02.008

Perrot, A., Rangeard, D., and Pierre, A. (2016). Structural built-up of cement-based materials used for 3D-printing extrusion techniques. *Materials and Structures*, *49*(4), 1213–1220. https://doi.org/10.1617/s11527-015-0571-0

Pham, L., Panda, B., and Tran, P. (2022). Fresh and hardened properties of 3D printable polymer-fibre-reinforced high-performance cementitious composite. *Advances in Cement Research*, *34*(2), 80–92. https://doi.org/10.1680/jadcr.20.00038

Pham, L., Tran, P., and Sanjayan, J. (2020). Steel fibres reinforced 3D printed concrete: Influence of fibre sizes on mechanical performance. *Construction and Building Materials*, *250*, 118785. https://doi.org/https://doi.org/10.1016/j.conbuildmat.2020.118785

Pj, K., Cho, S., Zeranka, S., and Gpag, V. Z. (2018). Multi-physics approach for improved thixotropy of cement-based materials for 3DPC. *1st International Conference on 3D Construction Printing (3DcP)*, *2018*(November), 26–28.

Plank, J., and Hirsch, C. (2007). Impact of zeta potential of early cement hydration phases on superplasticizer adsorption. *Cement and Concrete Research*, *37*(4), 537–542. https://doi.org/10.1016/j.cemconres.2007.01.007

Porter, M. (2013). *Handbook of surfactants*. https://books.google.com/books?hl=en&lr=&id=UX3SBwAAQBAJ&oi=fnd&pg=PA1&ots=F8VUOpjA1K&sig=gGoS378miOqJ2cIVcUIMxJmXZJ0

Pott, U., and Stephan, D. (2021). Penetration test as a fast method to determine yield stress and structural build-up for 3D printing of cementitious materials. *Cement and Concrete Composites*, *121*(April), 104066. https://doi.org/10.1016/j.cemconcomp.2021.104066

Qian, Y. (2021). Effect of polycarboxylate ether (PCE) superplasticizer on thixotropic structural build-up of fresh cement pastes over time. *Construction and Building Materials*, *291*, 123241. https://doi.org/10.1016/j.conbuildmat.2021.123241

Rahman, M. K., Baluch, M. H., and Malik, M. A. (2014). Thixotropic behavior of self compacting concrete with different mineral admixtures. *Construction and Building Materials*, *50*, 710–717. https://doi.org/https://doi.org/10.1016/j.conbuildmat.2013.10.025

Rahul, A. V, and Santhanam, M. (2020). Evaluating the printability of concretes containing lightweight coarse aggregates. *Cement and Concrete Composites*, *109*(February), 103570. https://doi.org/10.1016/j.cemconcomp.2020.103570

Rahul, A. V, Santhanam, M., Meena, H., and Ghani, Z. (2019). 3D printable concrete : Mixture design and test methods. *Cement and Concrete Composites*, *97*(March 2018), 13–23. https://doi.org/10.1016/j.cemconcomp.2018.12.014

Rahul, A. V, Sharma, A., and Santhanam, M. (2020). A desorptivity-based approach for the assessment of phase separation during extrusion of cementitious materials. *Cement and Concrete Composites*, *108*(July 2019), 103546. https://doi.org/10.1016/j.cemconcomp.2020.103546

Raj, A., Sathyan, D., and Mini, K. M. (2019). Physical and functional characteristics of foam concrete: A review. *Construction and Building Materials*, *221*, 787–799. https://doi.org/10.1016/j.conbuildmat.2019.06.052

Raj, B., Sathyan, D., Madhavan, M. K., and Raj, A. (2020). Mechanical and durability properties of hybrid fiber reinforced foam concrete. *Construction and Building Materials*, *245*, 118373. https://doi.org/10.1016/j.conbuildmat.2020.118373

Raj, S., Krishnan, J. M., and Ramamurthy, K. (2022). Influence of admixtures on the characteristics of aqueous foam produced using a synthetic surfactant. *Colloids and Surfaces A: Physicochemical and Engineering Aspects*, *643*, 128770. https://doi.org/10.1016/j.colsurfa.2022.128770

Ramamurthy, K., Kunhanandan Nambiar, E. K., and Indu Siva Ranjani, G. (2009). A classification of studies on properties of foam concrete. *Cement and Concrete Composites*, *31*(6), 388–396. https://doi.org/10.1016/j.cemconcomp.2009.04.006

Ranjani, G. I. S., and Ramamurthy, K. (2010). Analysis of the Foam Generated Using Surfactant Sodium Lauryl Sulfate. *International Journal of Concrete Structures and Materials*, *4*(1), 55–62. https://doi.org/10.4334/ijcsm.2010.4.1.055

Ranjani, I. S., and Ramamurthy, K. (2010). Relative assessment of density and stability of foam produced with four synthetic surfactants. *Materials and Structures*, *43*(10), 1317–1325. https://doi.org/10.1617/s11527-010-9582-z

Reiter, L. (2019). *Structural build-up for digital fabrication with concrete - materials, methods and processes* [ETH Zurich]. https://doi.org/10.3929/ethz-b-000456199

Roussel, N. (2018). Rheological requirements for printable concretes. In *Cement and Concrete Research* (Vol. 112, Issue May, pp. 76–85). Elsevier. https://doi.org/10.1016/j.cemconres.2018.04.005

Roussel, N., Ovarlez, G., Garrault, S., and Brumaud, C. (2012). The origins of thixotropy of fresh cement pastes. *Cement and Concrete Research*, *42*(1), 148–157. https://doi.org/10.1016/j.cemconres.2011.09.004

Rubin, A. P., Hasse, J. A., and Repette, W. L. (2021). The evaluation of rheological parameters of 3D printable concretes and the effect of accelerating admixture. *Construction and Building Materials*, *276*, 122221. https://doi.org/10.1016/j.conbuildmat.2020.122221

Sahu, S. S., and Gandhi, I. S. R. (2019). Evaluation of performance of foam produced with different methodologies for use in foam concrete production. *IOP Conference Series: Materials Science and Engineering*, *652*(1), 012050. https://doi.org/10.1088/1757-899X/652/1/012050

Sahu, S. S., and Gandhi, I. S. R. (2021). Studies on influence of characteristics of surfactant and foam on foam concrete behaviour. *Journal of Building Engineering*, *40*(February), 102333. https://doi.org/10.1016/j.jobe.2021.102333

Sahu, S. S., Gandhi, I. S. R., and Khwairakpam, S. (2018). State-of-the-Art Review on the Characteristics of Surfactants and Foam from Foam Concrete Perspective. *Journal of The Institution of Engineers (India): Series A*, *99*(2), 391–405. https://doi.org/10.1007/s40030-018-0288-5

Sahu, S. S., Ranjani Gandhi, I. S., Kumar, A., and Garg, S. (2021). Evaluation of Suitability of Carboxymethyl Cellulose in Performance Improvement of Sodium Lauryl Sulfate Foam and Compressive Strength of Foam Concrete. *Advances in Civil Engineering Materials*, *10*(1), 20200083. https://doi.org/10.1520/ACEM20200083

Salvini, V. R., Pandolfelli, V. C., and Bradt, R. C. (2012). Extension of Hasselman's thermal shock theory for crack/microstructure interactions in refractories. *Ceramics International*, *38*(7), 5369–5375. https://doi.org/10.1016/j.ceramint.2012.03.046

Sanjayan, J. G., Jayathilakage, R., and Rajeev, P. (2021). Vibration induced active rheology control for 3D concrete printing. *Cement and Concrete Research*, *140*(November 2020), 106293. https://doi.org/10.1016/j.cemconres.2020.106293

Scrivener, K., Martirena, F., Bishnoi, S., and Maity, S. (2018). Calcined clay limestone cements (LC3). *Cement and Concrete Research*, *114*(March 2017), 49–56. https://doi.org/10.1016/j.cemconres.2017.08.017

Selija, K., and Gandhi, I. S. R. (2022). Comprehensive investigation into the effect of the newly developed natural foaming agents and water to solids ratio on foam concrete behaviour. *Journal of Building Engineering*, *58*, 105042. https://doi.org/10.1016/j.jobe.2022.105042

Shahzad, Q., Wang, X., Wang, W., Wan, Y., Li, G., Ren, C., and Mao, Y. (2020). Coordinated adjustment and optimization of setting time, flowability, and mechanical strength for construction 3D printing material derived from solid waste. *Construction and Building*

Materials, *259*, 119854. https://doi.org/https://doi.org/10.1016/j.conbuildmat.2020.119854

Siddika, A., Mamun, Md. A. Al, Ferdous, W., Saha, A. K., and Alyousef, R. (2020). 3D-printed concrete: applications, performance, and challenges. In *Journal of Sustainable Cement-Based Materials* (Vol. 9, Issue 3, pp. 127–164). Taylor & Francis. https://doi.org/10.1080/21650373.2019.1705199

Singh Batra, S., Boddepalli, U., Gandhi, I. S. R., and Panda, B. (2023). Influence of various admixtures on energy absorption characteristics of foam concrete measured using one dimensional strain analysis test. *Materials Today: Proceedings*. https://doi.org/https://doi.org/10.1016/j.matpr.2023.03.685

Siva, M., Ramamurthy, K., and Dhamodharan, R. (2017). Development of a green foaming agent and its performance evaluation. *Cement and Concrete Composites*, *80*, 245–257. https://doi.org/10.1016/j.cemconcomp.2017.03.012

Soltan, D. G., and Li, V. C. (2018). A self-reinforced cementitious composite for building-scale 3D printing. *Cement and Concrete Composites*, *90*, 1–13. https://doi.org/10.1016/j.cemconcomp.2018.03.017

Srinivas, D., Dey, D., Panda, B., and Sitharam, T. G. (2022). Printability, Thermal and Compressive Strength Properties of Cementitious Materials: A Comparative Study with Silica Fume and Limestone. *Materials*, *15*(23), 8607. https://doi.org/10.3390/ma15238607

Suiker, A. S. J., Wolfs, R. J. M., Lucas, S. M., and Salet, T. A. M. (2020). Elastic buckling and plastic collapse during 3D concrete printing. *Cement and Concrete Research*, *135*(January), 106016. https://doi.org/10.1016/j.cemconres.2020.106016

Sukontasukkul, P., Panklum, K., Maho, B., Banthia, N., Jongvivatsakul, P., Imjai, T., Sata, V., Limkatanyu, S., and Chindaprasirt, P. (2022). Effect of synthetic microfiber and viscosity modifier agent on layer deformation, viscosity, and open time of cement mortar for 3D printing application. *Construction and Building Materials*, *319*, 126111. https://doi.org/https://doi.org/10.1016/j.conbuildmat.2021.126111

Sun, C., Xiang, J., Xu, M., He, Y., Tong, Z., and Cui, X. (2020). 3D extrusion free forming of geopolymer composites: Materials modification and processing optimization. *Journal of Cleaner Production*, *258*, 120986. https://doi.org/10.1016/j.jclepro.2020.120986

Sun, J., Aslani, F., Lu, J., Wang, L., Huang, Y., and Ma, G. (2021). Fibre-reinforced lightweight engineered cementitious composites for 3D concrete printing. *Ceramics International*, *47*(19), 27107–27121. https://doi.org/https://doi.org/10.1016/j.ceramint.2021.06.124

Sun, X., Zhou, J., Wang, Q., Shi, J., and Wang, H. (2022). PVA fibre reinforced high-strength cementitious composite for 3D printing: Mechanical properties and durability. *Additive Manufacturing*, *49*, 102500. https://doi.org/https://doi.org/10.1016/j.addma.2021.102500

Szwabowski, J., & Łaźniewska-Piekarczyk, B. (2008). The increase of air content in SCC mixes under the influence of carboxylate superplasticizer. *Cement Wapno Beton*, *4*, 205-215.

Tarhan, Y., and Şahin, R. (2021). Fresh and Rheological Performances of Air-Entrained 3D Printable Mortars. *Materials*, *14*(9), 2409. https://doi.org/10.3390/ma14092409

Tay, Y. W. D., Panda, B., Paul, S. C., Noor Mohamed, N. A., Tan, M. J., and Leong, K. F. (2017). 3D printing trends in building and construction industry: a review. *Virtual and Physical Prototyping*, *12*(3), 261–276. https://doi.org/10.1080/17452759.2017.1326724

Tay, Y. W. D., Qian, Y., and Tan, M. J. (2019). Printability region for 3D concrete printing using slump and slump flow test. *Composites Part B: Engineering*, *174*(February), 106968. https://doi.org/10.1016/j.compositesb.2019.106968

Tay, Y. W., Panda, B., Paul, S. C., Tan, M. J., Qian, S. Z., Leong, K. F., and Chua, C. K. (2016). Processing and Properties of Construction Materials for 3D Printing. *Materials Science Forum*, *861*, 177–181. https://doi.org/10.4028/www.scientific.net/MSF.861.177

Toutou, Z., Roussel, N., and Lanos, C. (2005). The squeezing test: a tool to identify firm cement-based material's rheological behaviour and evaluate their extrusion ability. *Cement and Concrete Research*, *35*(10), 1891–1899. https://doi.org/https://doi.org/10.1016/j.cemconres.2004.09.007

Tramontin Souza, M., Maia Ferreira, I., Guzi de Moraes, E., Senff, L., Arcaro, S., Castro Pessôa, J. R., J. Ribeiro, M., and Novaes de Oliveira, A. P. (2022). Role of chemical admixtures on 3D printed Portland cement: Assessing rheology and buildability. *Construction and Building Materials*, *314*(November 2021), 125666. https://doi.org/10.1016/j.conbuildmat.2021.125666

Tran, M. V, Cu, Y. T. H., and Le, C. V. H. (2021). Rheology and shrinkage of concrete using polypropylene fiber for 3D concrete printing. *Journal of Building Engineering*, *44*, 103400. https://doi.org/https://doi.org/10.1016/j.jobe.2021.103400

Vallurupalli, K., Farzadnia, N., and Khayat, K. H. (2021). Effect of flow behavior and process-induced variations on shape stability of 3D printed elements – A review. *Cement and Concrete Composites*, *118*(January), 103952. https://doi.org/10.1016/j.cemconcomp.2021.103952

Valore R. C. (1954). Cellular concretes part 2 physical properties. *ACI Journal Proceedings,* 50(6), 817-836. https://doi.org/10.14359/11795

Wagh, C. D., Indu Siva Ranjani, G., and Kamisetty, A. (2021). Thermal Properties of Foamed Concrete: A Review. *RILEM Bookseries*, *29*, 113–137. https://doi.org/10.1007/978-3-030-51485-3_9

Wagh, C. D., and Gandhi, I. S. R. (2024). Investigations on the performance of xanthan gum as a foam stabilizer and assessment of economic and environmental impacts of foam concrete production. *Journal of Building Engineering*, *82*, 108286. https://doi.org/10.1016/j.jobe.2023.108286

Wangler, T., Roussel, N., Bos, F. P., Salet, T. A. M., and Flatt, R. J. (2019). Digital Concrete: A Review. *Cement and Concrete Research*, *123*(June), 105780. https://doi.org/10.1016/j.cemconres.2019.105780

Wei, S., Yiqiang, C., Yunsheng, Z., and Jones, M. R. (2013). Characterization and simulation of microstructure and thermal properties of foamed concrete. *Construction and Building Materials*, *47*, 1278–1291. https://doi.org/10.1016/j.conbuildmat.2013.06.027

Weng, Y., Li, M., Tan, M. J., and Qian, S. (2018). Design 3D printing cementitious materials via Fuller Thompson theory and Marson-Percy model. *Construction and Building Materials*, *163*, 600–610. https://doi.org/https://doi.org/10.1016/j.conbuildmat.2017.12.112

Weng, Y., Lu, B., Li, M., Liu, Z., Tan, M. J., and Qian, S. (2018). Empirical models to predict rheological properties of fiber reinforced cementitious composites for 3D printing. *Construction and Building Materials*, *189*, 676–685. https://doi.org/https://doi.org/10.1016/j.conbuildmat.2018.09.039

Winnefeld, F., Becker, S., Pakusch, J., and Götz, T. (2007). Effects of the molecular architecture of comb-shaped superplasticizers on their performance in cementitious systems. *Cement and Concrete Composites*, *29*(4), 251–262. https://doi.org/10.1016/j.cemconcomp.2006.12.006

Wolfs, R. J. M., Bos, F. P., and Salet, T. A. M. (2018). Early age mechanical behaviour of 3D printed concrete : Numerical modelling and experimental testing. *Cement and Concrete Research*, *106*(May 2017), 103–116. https://doi.org/10.1016/j.cemconres.2018.02.001

Wolfs, R. J. M., Bos, F. P., and Salet, T. A. M. (2019). Triaxial compression testing on early age concrete for numerical analysis of 3D concrete printing. *Cement and Concrete Composites*, *104*(June), 103344. https://doi.org/10.1016/j.cemconcomp.2019.103344

Wu, P., Wang, J., and Wang, X. (2016). A critical review of the use of 3-D printing in the construction industry. *Automation in Construction*, *68*, 21–31. https://doi.org/10.1016/j.autcon.2016.04.005

Wu, Y., Liu, C., Liu, H., Zhang, Z., He, C., Liu, S., Zhang, R., Wang, Y., and Bai, G. (2021). Study on the rheology and buildability of 3D printed concrete with recycled coarse aggregates. *Journal of Building Engineering*, *42*, 103030. https://doi.org/https://doi.org/10.1016/j.jobe.2021.103030

Yang, X., Liu, J., Li, H., Xu, L., Ren, Q., and Li, L. (2019). Effect of triethanolamine hydrochloride on the performance of cement paste. *Construction and Building Materials*, *200*, 218–225. https://doi.org/10.1016/j.conbuildmat.2018.12.124

Yang, Y., Wu, C., Liu, Z., Li, J., Yang, T., and Jiang, X. (2022). Characteristics of 3D-printing ultra-high performance fibre-reinforced concrete under impact loading. *International Journal of Impact Engineering*, *164*, 104205. https://doi.org/https://doi.org/10.1016/j.ijimpeng.2022.104205

Yang, Y., Wu, C., Liu, Z., Wang, H., and Ren, Q. (2022). Mechanical anisotropy of ultra-high performance fibre-reinforced concrete for 3D printing. *Cement and Concrete Composites*, *125*, 104310. https://doi.org/https://doi.org/10.1016/j.cemconcomp.2021.104310

Yang, Y., Wu, C., Liu, Z., and Zhang, H. (2022). 3D-printing ultra-high performance fiber-reinforced concrete under triaxial confining loads. *Additive Manufacturing*, *50*, 102568. https://doi.org/https://doi.org/10.1016/j.addma.2021.102568

Yilmaz, V. T., and Glasser, F. P. (1989). Influence of sulphonated melamine formaldehyde superplasticizer on cement hydration and microstructure. *Advances in Cement Research*, *2*(7), 111–119. https://doi.org/10.1680/adcr.1989.2.7.111

Yoris-Nobile, A. I., Lizasoain-Arteaga, E., Slebi-Acevedo, C. J., Blanco-Fernandez, E., Alonso-Cañon, S., Indacoechea-Vega, I., and Castro-Fresno, D. (2022). Life cycle assessment (LCA) and multi-criteria decision-making (MCDM) analysis to determine the performance of 3D printed cement mortars and geopolymers. *Journal of Sustainable Cement-Based Materials*, 1–18. https://doi.org/10.1080/21650373.2022.2099479

Yuan, Q., Li, Z., Zhou, D., Huang, T., Huang, H., Jiao, D., and Shi, C. (2019). A feasible method for measuring the buildability of fresh 3D printing mortar. *Construction and Building Materials*, *227*, 116600. https://doi.org/https://doi.org/10.1016/j.conbuildmat.2019.07.326

Zhang, C., Hou, Z., Chen, C., Zhang, Y., Mechtcherine, V., and Sun, Z. (2019). Design of 3D printable concrete based on the relationship between flowability of cement paste and

optimum aggregate content. *Cement and Concrete Composites*, *104*(April), 103406. https://doi.org/10.1016/j.cemconcomp.2019.103406

Zhang, D.-W., Wang, D., Lin, X.-Q., and Zhang, T. (2018). The study of the structure rebuilding and yield stress of 3D printing geopolymer pastes. *Construction and Building Materials*, *184*, 575–580. https://doi.org/https://doi.org/10.1016/j.conbuildmat.2018.06.233

Zhang, J., Gao, X., and Yu, L. (2020). Improvement of viscosity-modifying agents on air-void system of vibrated concrete. *Construction and Building Materials*, *239*, 117843. https://doi.org/10.1016/j.conbuildmat.2019.117843

Zhang, X., and Han, J. (2000). The effect of ultra-fine admixture on the rheological property of cement paste. *Cement and Concrete Research*, *30*(5), 827–830. https://doi.org/https://doi.org/10.1016/S0008-8846(00)00236-2

Zhang, Y., Zhang, Y., Liu, G., Yang, Y., Wu, M., and Pang, B. (2018). Fresh properties of a novel 3D printing concrete ink. *Construction and Building Materials*, *174*, 263–271. https://doi.org/10.1016/j.conbuildmat.2018.04.115

Zhang, Y., Zhang, Y., She, W., Yang, L., Liu, G., and Yang, Y. (2019). Rheological and harden properties of the high-thixotropy 3D printing concrete. *Construction and Building Materials*, *201*, 278–285. https://doi.org/10.1016/j.conbuildmat.2018.12.061

Zhang, Y., Zhang, Y., Yang, L., Liu, G., and Du, H. (2022). Evaluation of aggregates, fibers and voids distribution in 3D printed concrete. *Journal of Sustainable Cement-Based Materials*, 1–14. https://doi.org/10.1080/21650373.2022.2113168

Zhu, B., Nematollahi, B., Pan, J., Zhang, Y., Zhou, Z., and Zhang, Y. (2021). 3D concrete printing of permanent formwork for concrete column construction. *Cement and Concrete Composites*, *121*, 104039. https://doi.org/https://doi.org/10.1016/j.cemconcomp.2021.104039

Zhu, B., Pan, J., Nematollahi, B., Zhou, Z., Zhang, Y., and Sanjayan, J. (2019). Development of 3D printable engineered cementitious composites with ultra-high tensile ductility for digital construction. *Materials & Design*, *181*, 108088. https://doi.org/https://doi.org/10.1016/j.matdes.2019.108088

Zhu, H., Chen, L., Xu, J., and Han, Q. (2020). Experimental study on performance improvement of anionic surfactant foaming agent by xanthan gum. *Construction and Building Materials*, *230*, 116993. https://doi.org/10.1016/j.conbuildmat.2019.116993

Zou, S., Xiao, J., Ding, T., Duan, Z., and Zhang, Q. (2021). Printability and advantages of 3D printing mortar with 100% recycled sand. *Construction and Building Materials*, *273*, 121699. https://doi.org/https://doi.org/10.1016/j.conbuildmat.2020.121699

Zou, S., Xiao, J., Duan, Z., Ding, T., and Hou, S. (2021). On rheology of mortar with recycled fine aggregate for 3D printing. *Construction and Building Materials*, *311*, 125312. https://doi.org/https://doi.org/10.1016/j.conbuildmat.2021.125312

भारतीय प्रौद्योगिकी संस्थान गुवाहाटी
Indian Institute of Technology Guwahati

Publications

Publications from PhD thesis:

International Journals:

1. **U. Boddepalli**, B. Panda, and I. S. R. Gandhi (2023), "Rheology and printability of Portland cement based materials: A review," J. Sustain. Cem.-Based Mater., vol. 12, No. 7, 789-807. Doi: http://dx.doi.org/10.1080/21650373.2022.2119620.
2. **U. Boddepalli**, I. S. R. Gandhi, and B. Panda, (2023), "Stability of 3D printable foam concrete as a function of surfactant characteristics," Front. Struct. Civ. Eng., vol. 17, No. 6, 935-947. Doi: https://doi.org/10.1007/s11709-023-0964-z.
3. **U. Boddepalli**, I. S. R. Gandhi, and B. Panda, (2024), "Synergistic Effect of Fly Ash and Polyvinyl Alcohol Fibers in Improving Stability, Rheology, and Mechanical Properties of 3D Printable Foam Concrete", Consrt. Build. Mater., vol. 429, 136464, Doi: https://doi.org/10.1016/j.conbuildmat.2024.136464.

Book Chapters:

1. **U. Boddepalli**, I. S. R. Gandhi, and B. Panda, (2024) "State-of-the-art Review on Foam Concrete: properties and new trends of applications in infrastructure", Sustainable Materials in Civil Infrastructure, 1, 3-24, ISBN: 9780443161421. Doi: 10.1016/B978-0-443-16142-1.00001-X
2. **U. Boddepalli**, B. Panda, and I. S. R. Gandhi, (2023) "Influence of Water to Solids Ratio on Stability, printability, and Mechanical properties of 3D Printable Foam concrete", Construction 3D Printing, 165-173, Doi: https://doi.org/10.1007/978-3-031-64269-2_21

Patents:

1. **U. Boddepalli**, I. S. R. Gandhi and B. Panda, "Compositions for 3D Printable Foam Concrete Structures", Application filed on 01-11-2023. (Application number: 202331074446)

International Conferences:

1. **U. Boddepalli**, B. Panda, and I. S. R. Gandhi, "Influence of Water to Solids Ratio on Stability, printability, and Mechanical properties of 3D Printable Foam concrete", 4th

International Conference on 3D Construction Printing held at NTU Singapore, July 19-21, 2023. **(Presenter)**

Achievements:

1. Awarded with Prime Minister's Research Fellowship in the lateral entry category for the 6th cycle in December 2020.
2. Pre-finalists in a competition conducted by TATA Steel named "Material Next 4.0" held in April 2023. In which we have cleared 2 rounds to reach a development phase (a prototype need to be developed to within two months with the given funding).
3. Delivered a webinar on "Rheology of 3D printable concrete" at VR Siddhartha Engineering College, Andhra Pradesh, organised by ICI VRSEC.

Other Publications:

International Journals:

1. I. S. R. Gandhi, **U. Boddepalli**, R. Bisht, and C. Wagh, (2023) "Impact of Addition of Fly Ash (as sand replacement) and Polypropylene Fibers on Energy Absorption Characteristics of Foam Concrete," Adv. Civ. Eng., vol. 12, No. 1, 127-144. Doi: https://doi.org/10.1520/ACEM20220131.
2. D. Dey, D. Srinivas, **U. Boddepalli**, B. Panda, I. S. R. Gandhi, and T. G. Sitharam, (2022) "3D Printability of Ternary Portland Cement Mixes Containing Fly ash and Limestone," Mater. Today: Proc., vol. 70, 195-200. Doi: https://doi.org/10.1016/j.matpr.2022.09.020.
3. S. S. Batra, **U. Boddepalli**, I. S. R. Gandhi, and B. Panda, (2023) "Influence of Various Admixtures on Energy Absorption Characteristics of Foam Concrete Measured using One-dimensional Strain Analysis Test", Mater. Today: Proc., Doi: https://doi.org/10.1016/j.matpr.2023.03.685.
4. P. Gulia, S. Dogra, A. Gupta, **U. Boddepalli,** D. Srinivas, I. S. R. Gandhi, and B. Panda, (2024) "Building a Metamaterial Wall with Gosper Curve", J. Build. Eng., (submitted).

Book Chapters:

1. D. Srinivas, **U. Boddepalli**, D. Dey, B. Panda, I. S. R. Gandhi, and T. G. Sitharam, (2024) "Development of outdoor furniture using 3D concrete Printing," Springer nature. (Accepted)

International Conferences:

1. D. Srinivas, **U. Boddepalli**, D. Dey, B. Panda, I. S. R. Gandhi, and T. G. Sitharam, "Development of outdoor furniture using 3D concrete Printing," North East Research Conclave held at Indian Institute of Technology, Guwahati, India, May 20-22, 2022. **(Presenter)**

Poster Presentations:

1. S.B.F. Warsi, **U. Boddepalli**, D. Srinivas, D. Dey, B. Choaudhary, B. Panda, T. G. Sitharam, and I. S. R. Gandhi, "Development of outdoor furniture using 3D concrete Printing" North East Research Conclave held at Indian Institute of Technology, Guwahati, India, May 20-22, 2022.
2. **U. Boddepalli**, S.B.F. Warsi, D. Srinivas, D. Dey, B. Choaudhary, B. Panda, T. G. Sitharam, and I. S. R. Gandhi, "Development of 3D Printed Structures at IIT Guwahati" presented among the selected projects at G20 summit in February, 2023. Organised by IIT Guwahati.

Workshops:

1. Attended an international workshop on 3D Concrete Printing conducted by IIT Madras, IIT Hyderabad, and Arizona State University, held at IIT Madras, March 17-18, 2023.

Achievements:

1. Won the best paper award in the 2nd International Conference on Construction Materials and Structures, December 2022 held at NIT Calicut. Organized by NIT Calicut, Purdue University, Virginia Tech, University of Bath, Monash University, UNSW Sydney, and BITS Pilani.
2. Won the best exhibitors award in the "Innovation for the future" category in the North-East Research Conclave (NERC) held at IIT Guwahati on May 20-22, 2022.